R-08-74

Towards a new generation of flow and transport models for the Äspö Hard Rock Laboratory

Main results from the project Äspömodels 2005

Urban Svensson (editor), CFE

Patrik Vidstrand, Bergab

Ivars Neretnieks, KTH

Bill Wallin, Geokema

May 2008

SKB

Towards a new generation of flow and transport models for the Äspö Hard Rock Laboratory

Main results from the project Äspömodels 2005

Urban Svensson (editor), CFE

Patrik Vidstrand, Bergab

Ivars Neretnieks, KTH

Bill Wallin, Geokema

May 2008

Abstract

This report constitutes the outcome of a project called "Äspömodels 2005". The main objective of the project has been to provide a first step towards a new generation of numerical models of flow and transport, for the Äspö HRL.

In order to achieve this goal, work has been carried out along three parallel lines; discussion of basic concepts, compilation and analysis of data and model applications. A number of subtasks are reported as appendices in the report. In fact, these appendices represent the main achievements of the project: an analysis of fracture properties, compilation of isotope and chemical data, dispersion and mixing in fractured rocks and model results.

The conclusion of the project is that significant contributions to a new generation of Äspö models have been obtained. It has further been demonstrated that working numerical simulations are up and running. Recommendations are provided for the continued work.

Sammanfattning

Föreliggande rapport utgör en dokumentation av ett projekt som benämnts "Äspömodeller 2005". Det huvudsakliga målet med projektet har varit att etablera en ny generation av numeriska modeller, för flöde och transport, med tillämpning på Äspö och Äspötunneln.

För att uppnå detta har projektet genomförts efter tre huvudlinjer; diskussioner av grundläggande koncept, datasammanställningar (med analys) och modelluppsättningar. Ett antal delprojekt har definierats och genomförts; dessa redovisas som sex appendix i rapporten. Dessa appendix representerar vad som åstadkommits i projektet: analys av sprickegenskaper, sammanställning av isotop och kemi data, diskussion av processer som genererar dispersion och blandning i spricksystem och modellresultat.

Slutsatsen av projektet är att ett antal väsentliga bidrag till en ny generation modeller har levererats. Modelluppsättningar som ger realistiska resultat har visats, dock återstår validering av modellerna. Projektet ger även rekommendationer för det fortsatta arbetet.

Contents

1   Introduction

1.1   Background

As a general background to the project one may quote the following sentences from the Äspö HRL Status report (IPR-03-27):

Natural barriers

At the Äspö HRL experiments are performed at conditions that are expected to prevail at repository depth. The experiments are related to the rock, its properties, and in situ environmental conditions. The goals are to increase the scientific knowledge of the safety margins of the deep repository and provide data for performance and safety assessments and thereby clearly present the role of the geosphere for the barrier functions: isolation, retardation and dilution. Tests of models for groundwater flow, radionuclide migration and chemical/biological processes are one of the main purposes of the Äspö HRL. The programme includes projects with the aim to evaluate the usefulness and reliability of different models and to develop and test methods for determination of parameters required as input to the models.

The project is a sub-task of "Natural barriers" and the sentences thus also give the directions for the project. In a particular we note the part "Test of models for groundwater flow".

A first generation of flow models for Äspö HRL was set up 1997/98 /Svensson 1997ab, 1999/ using the code PHOENICS and 2001 the code DarcyTools was used to simulate the conditions around the Prototype Repository /Svensson 2001a/. This was actually the very first application of DarcyTools and the code has developed substantially after 2001. The development of DarcyTools V3.0, was one element in the formulation of the project plan for the present project; it was decided that this code should be used for what we may call "the second generation of Äspö models".

Another corner stone of the project plan is the "compilation of data". The data base available for Äspö HRL is unique both in term of size and quality and is certainly a challenge to a modelling project. It is outside the scope of the present project to carry out new measurements; instead "data mining" and compilations suitable for the model set-ups will be in focus.

Finally the project plan suggests that the conceptual models of flow and transport in a sparsely fractured granite should be discussed and evaluated. All numerical simulation models entail a large number of ideas and assumptions that can not be proved in a scientific sense. It is essential that these are clearly explained and scrutinized. In the project the concepts embodied in DarcyTools are discussed and evaluated and, when possible, related to measurements and conditions at Äspö HRL.

1.2   Objectives

From the above we can summarize the following project objectives:

- Discuss and evaluate conceptual models for flow and transport in a sparsely fractured granite.
- Compile data relevant for the simulation tasks (fracture properties, chemistry, boundary conditions, etc).
- Set up numerical simulations based on the code DarcyTools V3.0.

1.3 Approach

In order to achieve the goals, the project has been advanced along three parallel lines:

- *Discussion of concepts*: at each project meeting a special topic (examples: Dispersion in fractured rocks, development of various chemical species over 10,000 years, fracture properties, salinity effects, etc) has been selected as a seminar topic. The project participants have given their views, followed by an open discussion. No attempt to conclude the discussions has been made.

- *Compilation of data.* Subtasks have been defined, carried out and documented.

- *Model set-ups*. The development of DarcyTools V3.0 has been carried out during the same period as the project has lasted. It is hence only during the last year of the project, that realistic simulations have been possible. However, a first set of model set-ups has been carried out and documented.

1.4 Outline of report

The main body of the project documentation is given by six appendices. An extended summary of these is included in the main part of the report, which also includes an introduction (this part), a section on confidence building, a discussion section and some concluding remarks.

2 Main Result

2.1 Introduction

The understanding of the present day hydrogeological conditions at Äspö needs to be based on a historical perspective, including at least the last 10,000 years (i.e. since the last inland ice). A good illustration of this statement is the fact that water from the last glaciation (or older) has been found at a depth of a few hundred metres at Äspö. This fact needs to be considered, for example, when the fracture system is characterized in mathematical terms (power laws, transmissivity models, etc). In order to store water for 10,000 years, the fracture network needs to include large pockets, or dead-end systems, of fairly stagnant water. If the network is too dense the fresh water infiltrating from above (precipitation) will wash out the glacial water.

This example illustrates many aspects of the present project; we look for chemical evidence that can constrain hydrogeological models, the historical development of the site is always in focus, exchange and dispersion of water in fracture systems is a key issue and we have the ambition to include the understanding of the processes and the site in numerical simulation models.

The rest of this section is devoted to summaries of the subtasks carried out in the project. By keeping the general picture outlined above in mind, it will be clear that all parts fit the general objectives.

2.2 Model specifications – empirical estimates of fracture and fracture zone properties

With the development of discrete fracture descriptions in numerical models it has become an enhanced topic to be able to parameterise unique features. Each fracture and fracture zone within a model domain needs to be assigned a geometrical description as well as properties. The geometrical descriptions used in these simulations are based on interpretations of statistics in different scales.

For the largest structures (on the kilometre scale) the Geological Structural model of deterministic deformation zones Laxemar v1.2 constitutes the basis for the more conductive skeleton of structures. In our simulations high, medium, as well as low confidence (of occurrence) structures, from the Geological Structural model are included, see Figure 2-1.

In order to capture the defined large scale structures from the GeoMod project /Berglund et al. 2003/ at the Äspö HRL two local larger structures, ZAS0004A0 and ZAS0007A0 in the size between 0.5 and 1 kilometre were incorporated. All properties on common larger structures between the Geological Structural model Laxemar v1.2 and the GeoMod model were set to correspond with the GeoMod specifications in order to fit known Äspö HRL properties /Berglund et al. 2003, Vidstrand 2003/.

All structures smaller than 0.5 kilometre are stochastically generated and based on local DFN statistics. Fracture statistics from Äspö HRL (Magnor 2005, pers. comm.) and earlier modelling experiences /Svensson 1999/ was used to establish three different fracture sets, two sub-vertical and one sub-horizontal fracture sets.
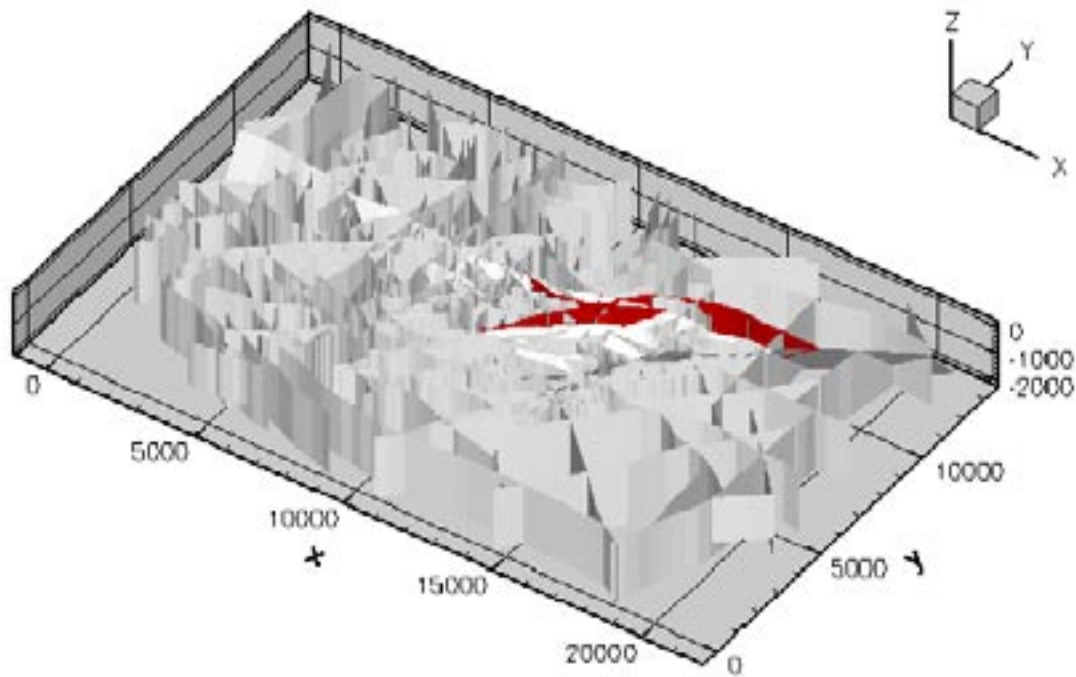
Figure 2-1. *The used Geological Structural model of deterministic deformation zones. The zones in red colour are part of the local geological structure model of Äspö.*

The stochastic fractures are, in DT30, generated in accordance with a power law governing the fractures size. The largest fracture size used is specified based on the smallest structure scale used, in our simulation 500 metres. This since we make the assumption that all larger fracture zones have been specified in the deterministic deformation zone model and that the power law relationship yields a continuous fracture set between the stochastic and deterministic informa-tion. The smallest fracture size is specified in accordance with the grid size. In our 10,000 years simulations the grid size yields a smallest fracture size of 50 metres; in the tunnel simulations the discretisation close to the tunnel is much smaller and fractures down to 20 metres are generated.

As a part of this study a compilation on local Äspö HRL properties for different scales were per-formed. This compilation is based on the assumption that there exist a relationship between the fracture properties and the fracture size (length), see Figure 2-2. The available data at the Äspö HRL consists of values of aperture, transmissivity, and storativity. With respect to the fracture size only indicative information is available and relationships have hence been established based on known properties and estimates on size.

It was decided to distinguish between unique fractures and structures composed of a cluster of fractures. No knowledge on a size of structures where such distinction could be made is known to the authors; however it was decided to have a cut-off size of 100 metres.

In Appendix A detailed model specifications along with the data analyses performed is reported.
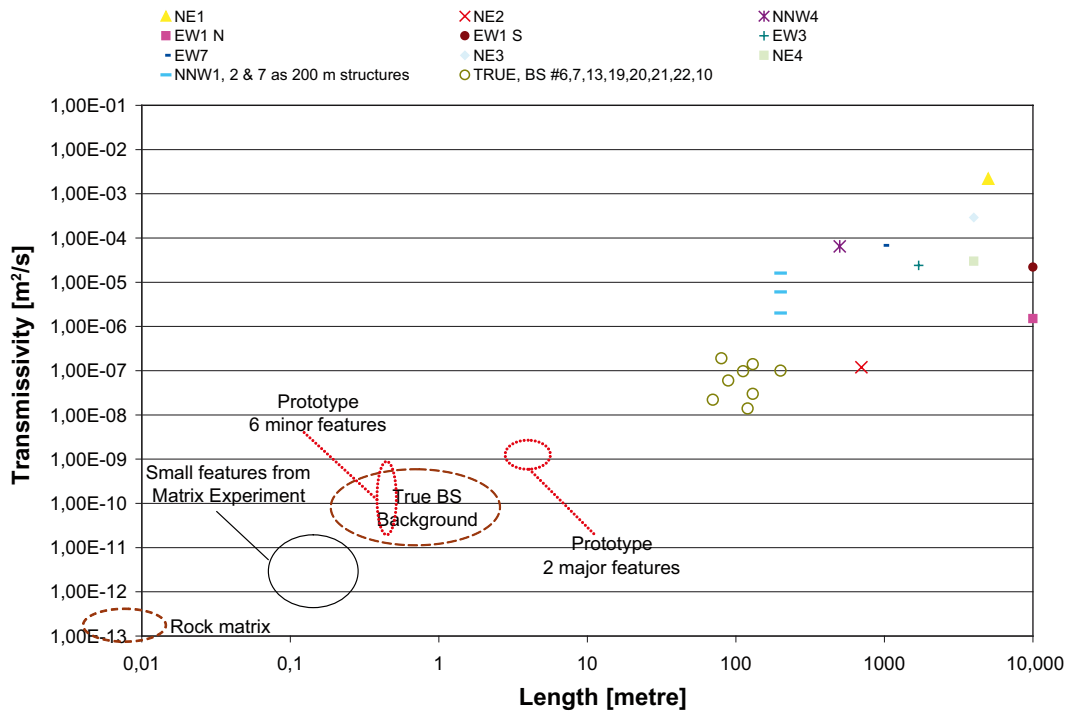
10

Figure 2-2. *Compilation of transmissivity values for unique fractures and their length. Circumference illustrations indicate the possible location of the feature based on extracted constrains in characterisation information.*

2.3 Isotope and chemical evidence from groundwater and fracture fillings in the basement at Äspö and Laxemar

The development of the groundwater system in the crystalline basement rocks at Äspö is used for constructing credible scenarios of possible future hydrologic changes that could occur within the time frame of concern for nuclear deposits. Accordingly, the objective of this study was to make an assessment of potential utilization of data in order to attain a better understanding of the paleohydrology at the site and to provide valuable information for groundwater modeling. Chemical and isotopic data have been used to delineate the different waters involved in the groundwater system over the last 10,000 years.

The origin and evolution of brackish-to-saline groundwaters are reflected in the present day water situation as well as recorded in the fracture fillings. A key task in this study has been to find strong evidences for where and when these different water types occur in the basement rock, and hence, their relation to penetration depth, maximum age and origin.

The major findings and the results from this study are presented as summaries in the appendices. Four different groundwaters are identified in the present day groundwater system, which reflect the post-glacial development at Äspö; those are *Glacial water, Meteoric water, Marine water* and *Brine water*.

Remnants of *Glacial water*, defined by its chemistry and negative isotopic signature is found at 1,040 m depth in Laxemar (KLX02) and documented at a depth between 400 and 840 m at Äspö. Glacial and run-off glacial water have a minimum age of about 14,000 BP.

Meteoric water at Laxemar is found at a depth of 1,000 m and at Äspö at a depth of 100–150 m. These findings are supported by the REE chemistry of calcite fracture fillings and strontium isotopes in both groundwater and fracture fillings. Present day meteoric water is found at Äspö at 100 m depth and pockets of tritium free waters are located up to 200 m depth.

Groundwater with marine signature is presently found to a depth of 500 m and recorded in calcite fracture fillings at 640 m at Äspö. The isotope signatures, REE chemistry as well as the mineralogical features in the calcite fracture fillings, support these findings. The *Marine water* now found is interpreted as old Littorina water with an age between 9,500 and 3,500 years at Äspö. The dissolved salt is typically marine in its origin.

The *Brine water* at Äspö is developed at depth of 1,100–1,200 m and deeper at Laxemar and observed in the groundwater component. The chlorine is dated at 1 million years old. There is evidence of Brine water at 1,000 m depth at Laxemar in calcite fracture fluid inclusions and by $^{87}Sr/^{86}Sr$. The salt is interpreted to be dissolved salts from the basement rocks and/or evaporates.

In conclusion, a sequence of events during the postglacial period is reflected in the groundwater chemistry and isotopic signatures. All four types of waters are developed at present at Äspö and documented at various depths by the variation in chemistry and isotopes in the calcite fracture filling. The comparison between the fracture fillings and the groundwater provide a record of spatial information. The groundwater ages are still uncertain, however, it is possible to delineate relative ages between the different waters residing now at Äspö, where Brine water is the oldest. Glacial water is introduced early in the basement rocks, followed by Marine waters and postglacial precipitation as Meteoric water.

2.4 Dispersion and mixing in fractured rocks

Old salt water in deep lying fractured rock systems will be displaced by fresh intruding rainwater. The old water is present in the fractures and fracture zones of the rock and, more importantly, also in the micropores of the rock matrix itself. The latter water volume may be 20 to 100 times larger than the water volume in the flowing fractures. It is deemed that the freshwater circulation started mainly at the end of the last ice age some 5,000 to 10,000 years ago. Old salt water has been found at depth and fresh water in the shallower parts of the rock. However, very complex salt profiles are present because there are large variations of hydraulic transmissivity in the fractures and fractures zones that make up a very complex 3 dimensional network of flowpaths with varying lengths and hydraulic properties. It is thought that the observed salt profiles could be used to validate the hydrologic and transport models that are used in performance assessment.

Appendix C describes the different displacement and mixing processes that take place in flowing fractured systems and attempts to quantify their importance in PA time and distance scales.

The higher density of saltwater will tend to stabilize the saltwater at depth. The less dense freshwater will choose paths closer to the surface unless the hydraulic gradient is large enough to overcome the density difference. Mixing will occur between salt and freshwater over the joint interface. The mixing is caused by molecular diffusion, which is a slow process. Stagnant water in the micropores of the rock matrix will also contribute to the change of the salt content and density of the flowing water. The complex network structure can also have a very large impact on where fresh and salt water boundaries could be located at present.

There is much more water in the matrix pores than there is flowing water in the fractures. Mixing due to molecular diffusion in the matrix of the rock blocks is the by far dominating mixing process between salt and fresh water. This will considerably delay the washing out of the saltwater. In inflow areas scoping calculations suggest that matrix pores in blocks smaller than a few metres will have been depleted of their original salt whereas blocks larger than 10 metres still can have considerable salt concentrations in their interior, see Figure 2-3.

Sample calculations on the effects of different mixing processes are presented. Taylor dispersion, diffusional mixing between streams with different velocities and mixing due to subsurface tidal waves, although probably present, are overshadowed by matrix diffusion effects.
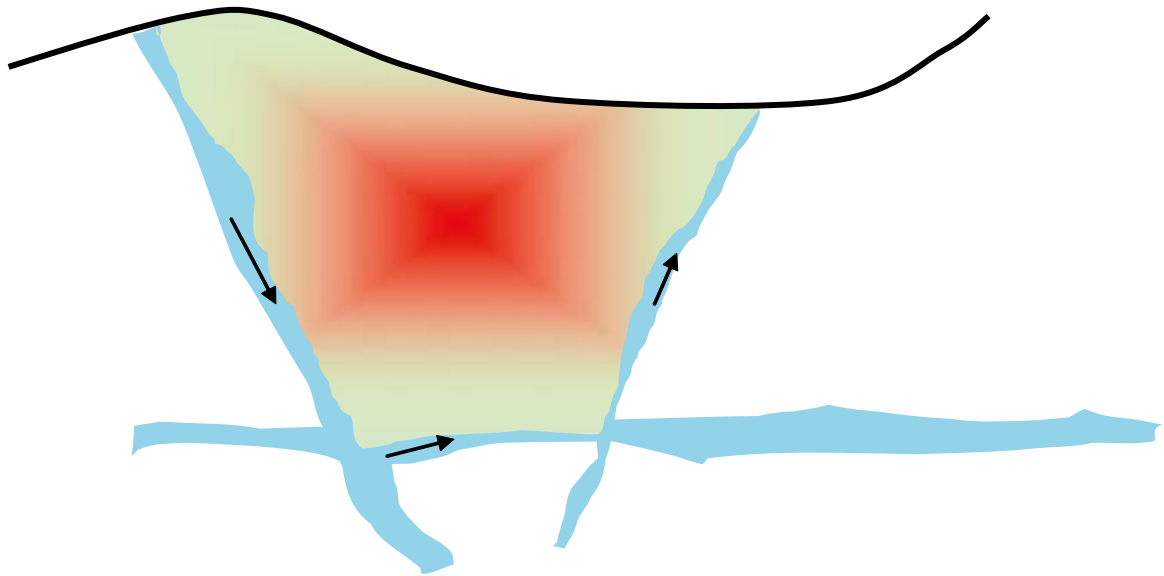
Figure 2-3. *Water in highly conductive fracture zones may contain freshwater while large rock masses at shallower depths may contain saltwater.*

2.5   DarcyTools V3.0, basic concepts

Modelling flow and transport in a sparsely fractured granite introduces a number of concepts and assumptions. When assessing the credibility of a computer code, it is essential that these are clearly defined and described. Here the concepts, assumptions and methods of the code DarcyTools, which is currently developed for the Swedish Nuclear Waste Management Company (SKB AB), are described. The situation considered is outlined in Figure 2-4; essentially it is a fracture network contained in some domain with a length scale, L.

In the present version of DarcyTools it is assumed that "*the number of fractures in a certain length interval follows a power law*". This assumption is well supported by field data and also offers some distinct advantages in model formulations.

Numerical models normally discretize space in some way. DarcyTools is a finite-volume code and the domain in Figure 2-4 is meshed to consist of a large number of cells. Typically a grid of 10^6 cells is used. The next assumption introduced is related to this grid and can be stated as follows: "*in a sparsely fractured granite, flow is assumed to be distributed on relatively few flow channels, that are due to large scale fractures and zones. It is assumed that all essential flow channels are due to fractures and zones that are larger than the smallest cell size*". If this cell size, Δ, is 0.01 L this is thus the lower limit for water-carrying fractures.
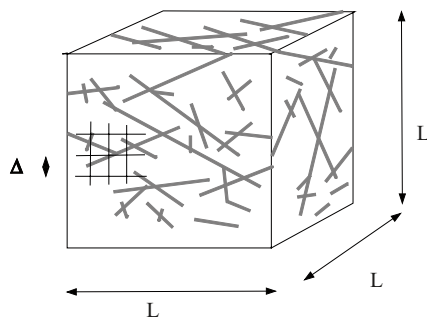

Figure 2-4. *Situation considered.*

Next we will discuss how the resolved fractures (i.e. larger than the cell size) are represented on the grid. In the present context we will simply assume that a fracture, or a zone, can be described as a plane rectangular feature with a certain thickness and properties (conductivity, porosity, storativity, etc). The following concept is then used: "*a fracture contributes to the grid value of a variable by an amount which is equal to the intersecting volume times the value of the variable in question. Contributions from all fractures that intersect the cell are added and the sum is divided by the volume of the cell*". As an example, see Figure 2-5, we may think of porosity; the intersecting volume times the porosity gives a contribution to the free space of the cell. It can be shown that this method gives accurate results for flow, transport (advection/diffusion equation) and particle tracking. Some early examples can be found in /Svensson 2001bc/.

Fractures smaller than the grid size, Δ, are, as discussed above, assumed to contribute negligible to the flow rate, but are assumed to be essential for dispersion and retention, when dealing with transport. A subgrid model, FRAME (FRActal scaling laws and Multirate Equations), has been developed to handle these processes. FRAME rests on a number of concepts and assumptions of which the most essential are:

Fractures smaller than the cell size are assumed to be filled with stagnant water (immobile volumes) and exchange matter with the flowing water (mobile volumes) by diffusion only.

Subgrid fractures are assumed to follow a power-law (same as for resolved fractures).

All immobile volumes can be represented by a set of boxes(or storage volumes), each with its own length scale, volume and effective diffusion coefficient.

In Figure 2-6 the subgrid model is illustrated. The multi rate diffusion technique /Haggerty and Gorelick 1995/ provides an efficient way to handle this problem computationally.

The computational grid can be characterized as an "object based adaptive cartesian grid". The objects may be tunnels, boreholes, fracture zones, etc and the grid can be generated with conditions related to these objects. One may, for example, state that tunnel walls should be resolved with a cell size of 1 metre. Figure 2-7 illustrates this kind of grid. The resulting linear system of equations is solved with an unstructured multigrid solver called MIGAL. Further details can be found in Appendix D.
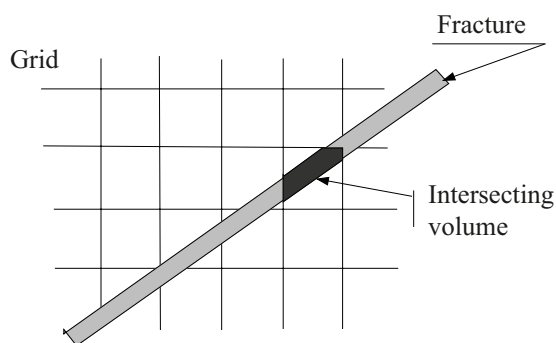

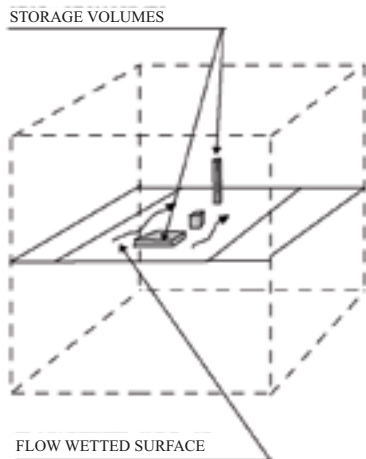**Figure 2-5.** *Intersecting volume concept.*

STORAGE VOLUMES

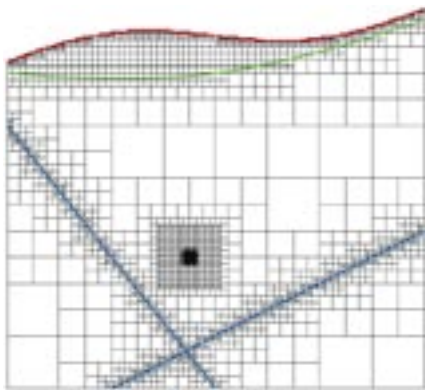FLOW WETTED SURFACE

Figure 2-6. *Subgrid model.*

Figure 2-7. *The adaptive Cartesian grid.*

2.6 Groundwater flow simulations of the last 10,000 years – evolution of water types since the last de-glaciation

The purpose of the regional modelling is to simulate the evolution of the groundwater chemistry (simplified into mixing of different water types) since the last deglaciation (approximately 10,000 years). The performed simulations are only a first set and further calibration simulations are needed.

The different water types are introduced as initial water types (Glacial, Mixed, and Brine) found at different depth within the model domain. Glacial water type is found down to 500 metres depth; between 500 and 1,500 metres depth sits Mixed water type and below that the Brine is found.

During the transient simulations different water types (with different salinity) are introduced on the top boundary. Initially the entire model domain is covered by the Baltic Ice Lake containing Glacial/fresh water. With time the water level decreases and land is exposed. Exposed land is subjected to Rain water (meteoric), the development of the Baltic Sea goes through phases of Glacial, Yoldia, Glacial (Ancylus), Litorina, and Baltic (present-day water type).

The transient development of the sea level /Påsse 1996/ and the salinity in the Baltic (ref) are found as graphs in Appendix E. A summary of flow boundary conditions is given by Table 2-1.

Table 2-1. Flow and pressure boundary conditions.

Boundary	Condition
Top BC	Fixed head at ground surface or at sea elevation.
Lateral and Bottom BC	No flow.

The results of our 10,000 years simulations are in agreement with results presented by e.g. /Follin et al. 2004/.

The top boundary with fixed head influences the results. Figure 2-8 illustrates the present-day distribution of Rain water at –450 metres (below sea level); deep penetration of Rain water is found beneath areas belonging to local summits. However, also the regional flow from the groundwater divide along the western border towards the Baltic Sea constitutes a significant factor for deep penetration of the Rain water. The Rain water penetrates down to approximately 1 kilometre beneath summits. This initial deep saline waters (Mixed) has however remained an isolated volume pushed down some at certain areas as well as lifted some at other areas; but for most of the model domain this water type sits unaffected.

Figure 2-9 illustrates the remains of the initial Glacial water found at depth in some few, mainly discharge, areas; however the majority of the Glacial waters is found in the bedrock beneath the Baltic Sea. Here, the glacial water is found at all depths however contained within block of less permeable rock domains within the bedrock (the rock mass).
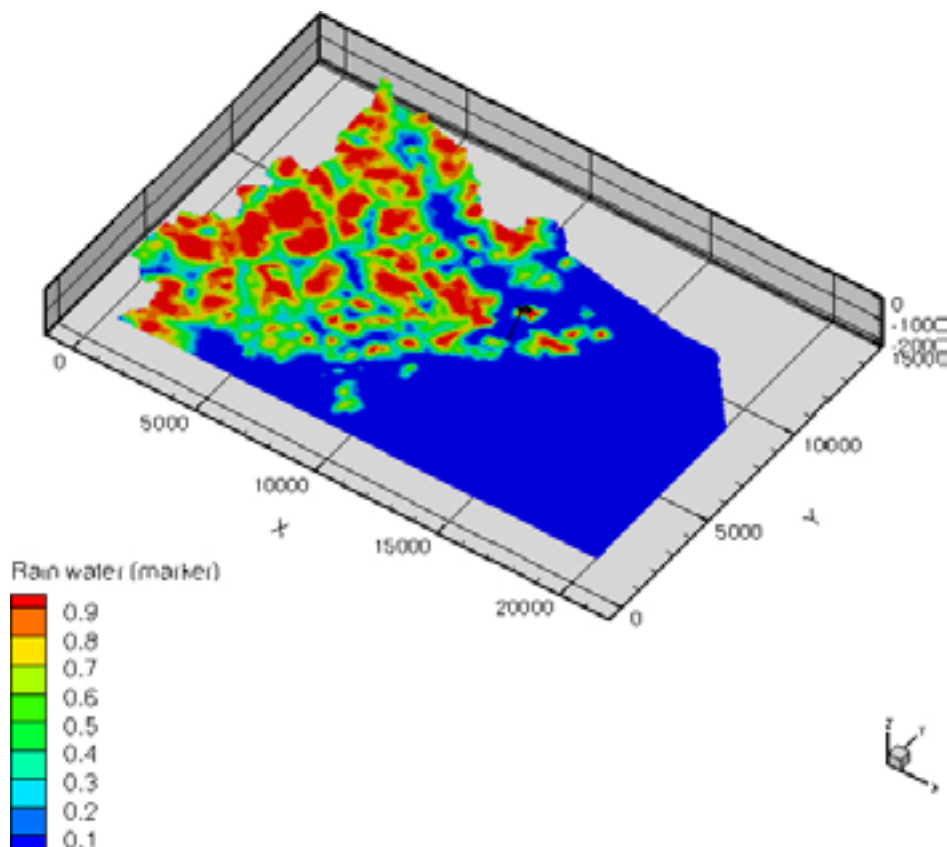

Figure 2-8. *Distribution of rain water (meteoric) after the entire simulation on a plane at the –450 metres elevation. The sea level stands at present day level and the rain has replaced the glacial water under the entire ground surface. Effects of the topography are observed through less penetration depth in regions of low lands acting as discharge area for the rain water and vice versa for the high summits. The Äspö HRL tunnel is illustrated in the figure, the simulation however has not included the tunnel.*
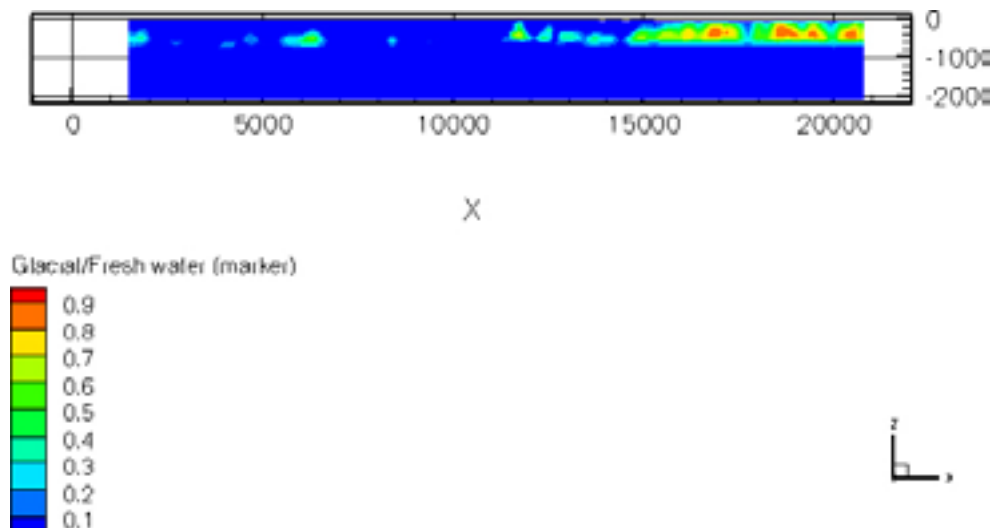
Figure 2-9. The distribution of the glacial water after the entire simulation on a plane along a transect at the y-coordinate of 8,000 metres, west – east. Below the exposed main land only small pockets of residual glacial water is trapped within blocks of rock mass. Out in the Baltic Sea far from the recharge areas little has happened with the residual glacial water during the last 3,000 years.

The 10,000 years simulations, still only a first set performed with little calibration work done, have proved to be a satisfying set-up with plausible results. The obtained final results can serve as initial conditions for a tunnel simulation.

2.7 Groundwater flow simulations of the Äspö HRL – Regional steady-state situation due to the Äspö HRL

The tunnel model is incorporated in the regional model of Äspö. However, in order to simulate the effects of the tunnel the discretisation within the model domain incorporates cell sizes of the regional scale of 128 metres in cube down to 1 metre in cube cell size along the tunnel walls.

The recharge is specified within the model; and a surface hydrology representation of rivers as lines of high permeability and a more permeable surface layer.

First a semi-steady-state without the tunnel was established. Starting in this situation the tunnel is introduced, with a step-wise approach – through a successively increasing tunnel wall permeability – so that the full draw-down effect with a tunnel wall permeability of approximately $1 \cdot 10^{-15}$ m^2, is approached after a couple of simulations.

The main results after the semi-steady-state simulation without the tunnel is well in agreement with the regional 10,000 year simulations. However, as illustrated in Figure 2-10 the Rain water in the regional tunnel simulations does not penetrate as deep as it does in the regional 10,000 year simulation. The top boundary conditions between the two models are the main difference. In the tunnel simulation the top boundary condition is governed by recharge, see Table 2-2, and a surface hydrology representation as compared to the fixed head condition in the regional 10,000 year simulations.

The simulations are on an early state model with no calibration performed; also all the known hydraulic conductors along the tunnel have not been introduced in the performed simulations. Therefore the results on drawdowns and flow are not presently comparable with known information from the Äspö HRL.
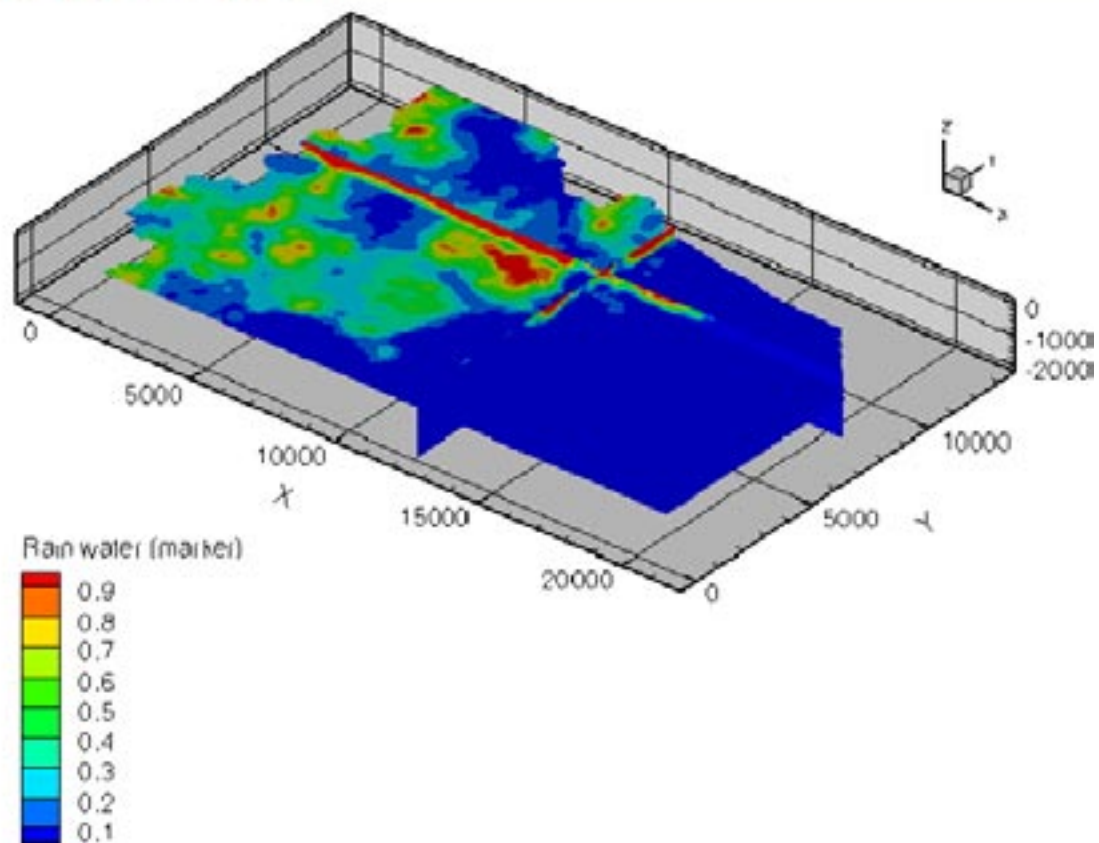
Figure 2-10. Distribution of Rain water in steady-state at the –450 metre elevation before the tunnel is introduced. The results seem plausible and reflect the known information both in the archipelago and on the main land. The deeper penetration of Rain water around the location (10000;7000) represents the Laxemar region which is a bit more elevated than are the surroundings to the south, north, and east.

Table 2-2. Flow, salinity, and pressure boundary conditions.

Boundary	Condition
Top BC	Recharge 165 mm/year
Western lateral BC, down to –500	Fixed head 3 metres below ground surface
	Salinity fixed to zero
Sea BC	Fixed head at sea level
	Salinity fixed to 0.73%
All other lateral BC	No flow
Bottom BC at –2,100	No flow
	Salinity fixed at 10%

The up-coning of deep saline waters is also not as profound in the simulations as it is known to be at the Äspö HRL. These results are not presently validated but the discrepancy with up-coning salinity values is believed due to the relatively strong depth-dependency on properties used in the simulations.

The novel features in DarcyTools v3.0, for example the unstructured grid approach, enable very detailed simulations around the tunnel even within a large regional model. Figure 2-11 illustrates some detailed draw-down at the Äspö HRL in the region around the Prototype Repository.
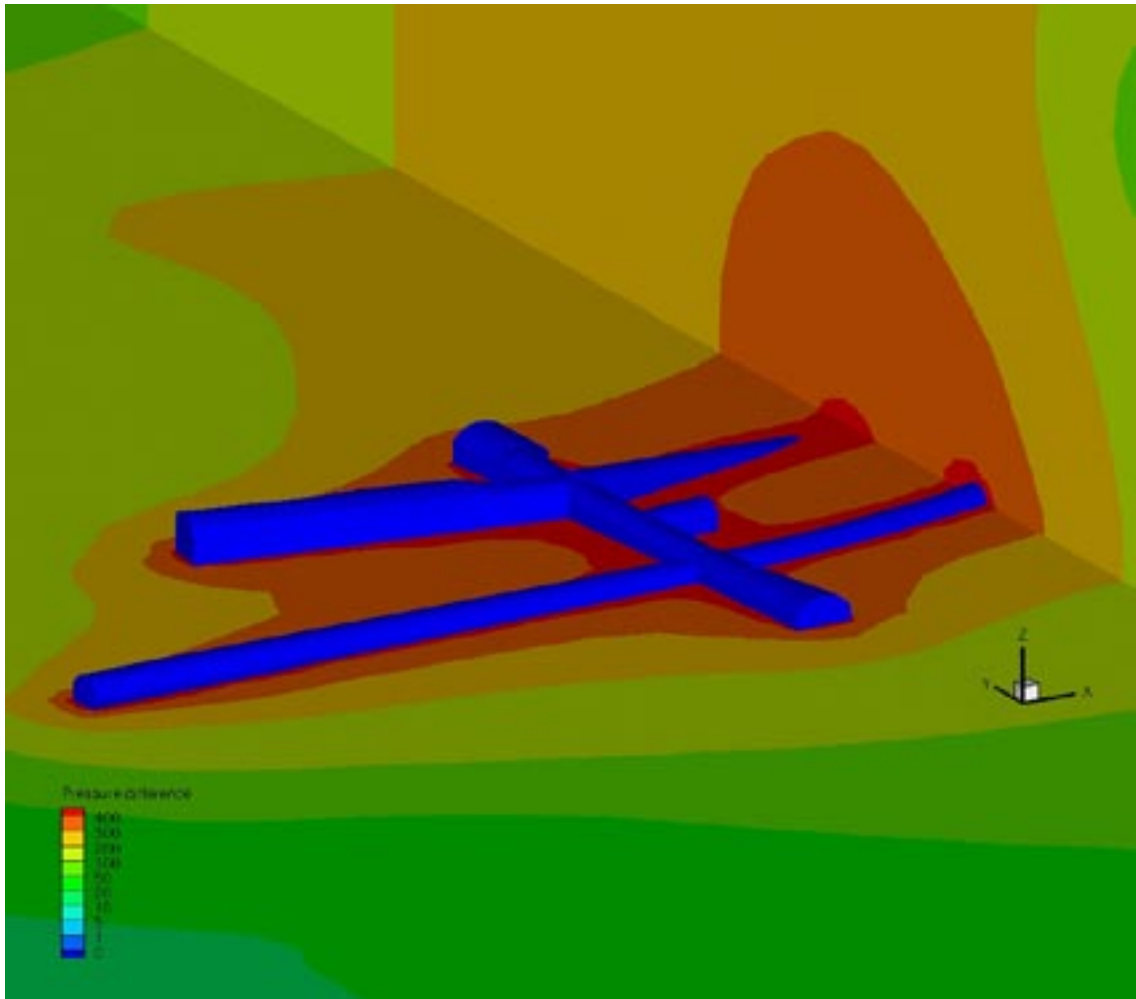
Figure 2-11. *Close-up details of the pressure difference in metres of fresh water head that results when the tunnel is introduced and the model is simulated to a steady-state situation. The illustrated differences are on the –450 metre elevation. The large drawdown is concentrated close to the tunnel construction and the pressure increases fast when moving away from the tunnel. As seen the pressure increase some 300 metres of fresh water head only in tens of metres from the tunnel wall.*

2.8 Concluding remarks

These summaries of subtasks quite well represent the bulk of the work carried out in the project; for a full account the reader is pointed to the Appendices. Work remains to introduce some results into the model set-ups and we thus consider some of the appendices as building blocks to be fully utilized in further work.

3   Confidence building

3.1   Introduction

The credibility of a computer code, or a certain application of the code, depends on a number of things, from the degree of code verification to the knowledge and attitude of the modeller.

The analysis of such aspects of a simulation is often called "an uncertainty analysis" and when one tries to systematically reduce these uncertainties one may call this process "confidence building".

When it comes to simulation of the flow and transport in fractured rocks, it is generally accepted that the main uncertainty is due to the fracture network. We still do not know enough about topics like "channelling in fracture planes", "mixing at fracture intersections", "matrix diffusion", etc. In other flow simulations, for example simulation of turbulent flows, it may be the mathematical model that is the weakest point. For the present work we do believe that the basic mathematical model, i.e. the Darcy law, is adequate; instead it is the "flow anatomy" that constitutes the main uncertainty.

A brief review of the literature shows that the topic *confidence building* is being increasingly discussed. We will start by giving an account of these general aspects of confidence building and then discuss the models for the Äspö site in light of these general guidelines.

3.2   Some definitions

During the last twenty years CFD (Computational Fluid Dynamics) has become a standard simulation tool in most engineering problems dealing with groundwater flow and transport. This development has been driven by readily available software packages and the significant increase in affordable computer speed and memory capacity. CFD is however not a simple technique to use; generally speaking a basic understanding of several subjects like fluid mechanics, numerical analysis and computer software programming is required. For groundwater modelling an understanding of geohydrology is of course also needed. The following main sources of errors and uncertainties in groundwater simulations can be identified:

- **Mathematical model.** The mathematical model does not describe the real flow exactly. For example, in textbooks the approximations inherent in the Darcy equation are often analysed and listed. Another often used approximation is that the water is incompressible.

- **Discretisation.** Numerical solutions are performed on a grid in space and time. The difference between the solution on this grid and the exact solution of the modelled equations is called the discretisation error.

- **Convergence and round-off errors.** Typically a CFD simulation involves iterative procedures. Convergence errors occur because these iterations are stopped by a certain criteria before they are completed. Round-off errors are due to the limited number of digits when a number is stored in the computer memory.

- **Application uncertainties.** This includes uncertainties about the geometry of the domain (for example a fracture network), boundary conditions, fluid properties, etc.

- **Code errors.** It is difficult to get software "bug-free".

- **User errors.** These are the errors that result from mistakes or carelessness by the user.

More points could have been listed (errors in postprocessing, interpretation of results, etc) but the list given probably gives the most important ones. In this context it may be of interest to note the following definitions:

Error: A recognisable deficiency that is not due to lack of knowledge.
Uncertainty: A potential deficiency that is due to lack of knowledge.

As the present report deals with flow and transport in a fractured rock, one should view the points given from this perspective. The significance of the different points may still vary depending on the modelling approach chosen and the problem studied. Here we concern ourselves with a fracture network, as represented in a continuum model. All of the above discussed errors and uncertainties may still be relevant to consider and it is not easy, in the author's view, to neglect (or set priority to) any of the points. For the modelling approach chosen it is however expected that the "quality" of a simulation is strongly dependent on how well the fracture network is represented in the continuum model. The fracture network is however only partly known (geometry, properties, etc) and we therefore need to consider the uncertainty introduced.

The question whether a computer code is credible or not and methods to answer this question are given in a recent issue of the AIAA journal /AIAA 1998/. Based on the papers presented, Table 3-1 has been created. The table is an attempt to illustrate the actions involved in the confidence building process. A few comments to the table:

- The order (from top to bottom) is essential. It is not possible to achieve certification without having demonstrated verification and validation.

- There is a consensus in the literature about the definitions of verification and validation. Additional steps and actions in the confidence building are still open to discussion.

- Some authors emphasise that it is important to distinguish between confidence building in a computer code and in a specific application. Related to this issue is the concept "fitness for purpose". It is for example of little value to have a very accurate numerical solution if the algorithm is so slow that the code is impractical for its intended use.

Table 3-1. Processes and actions involved in confidence building.

	Process	Definition	Action
C O N F I D E N C E B U I L D I N G	Verification	Demonstrate that the equations are solved correctly.	Comparison with analytical solutions and other models.
	Validation	Demonstrate that the right equations are solved.	Comparison with measurements (laboratory and field data).
	Certification	Assess whether the right things are done and whether they are done right.	Evaluate software construction and working procedures.
	More (QA-systems, wide range of applications, publications in international journals, etc).		

3.3 The Äspö models

With reference to Table 3-1, we can assume that the first step, i.e Verification, has been completed. About 25 verification cases, mostly comparisons with analytical solutions, have been completed and will be documented in the general documentation of DarcyTools V3.0.

The second step Validation is much more complicated, as it is linked to the conceptual assumptions of the code, i.e. "are the right equations solved?". During the discussion of the conceptual models it has, as an example, been questioned if the subgrid model FRAME is adequate. Presently FRAME is based on the multirate diffusion model and advective transport is hence not explicitly accounted for. The word "adequate" was used above, which links to the criterion "fitness for purpose". Perhaps FRAME neglects a physical process that can be important at some scales, but is still fit for its purpose. The intended use of the models thus needs to be clearly stated. For the Äspö HRL one can identify the following key applications:

- Provide a synthesis of as much relevant information as possible, i.e. field data, concepts, conservation laws, etc. Such a model can be used as a test bench for further tests of hydrogeological hypotheses and sub models.

- Predict the outcome of future experiments, so called scoping calculations.

- Predict the impact of various activities like construction works and experiments.

In order to be "fit for its purpose" the new models should be tailored to these key areas of application. The validation step should also be executed with the applications in mind. The following steps are suggested:

- The fracture network (intensity, anisotrophy, properties, deterministic zones, etc). A model that is based of a fracture network that fulfils a number of criteria is probably the most important step in a model set-up (easier said than done, though).

- Simulate the drawdown due to the Äspö HRL. At this step one should pay special attention to the fracture property specifications and the HPF (High Permeability Features) statistics available at the site.

- Comparisons with chemical data, including the salinity field.

The third step in Table 3-1 can be reformulated to say "is everything done in a scientifically defendable way?" When it comes to the documentation and working procedures of DarcyTools, this question has been evaluated by SKB and the answer was "yes". It is of course equally important that the validation and application to Äspö HRL apply sound working procedures.

3.4 Concluding remarks

By applying the principles outlined it is believed that credible Äspö models will result. In this project it has been stressed that the basic concepts of flow and transport in fractured rocks should always be in focus. However, for the next step of the work, we probably need to "accept what we have in the code" and let the discussion of basic concepts continue in some other forum.

4 Discussion

The models of the Äspö HRL presented in this report are not the first, and hopefully not the last, models of the site. In order to bring the present work into context, we will make a brief review of some related work. The objective is to find guidelines for the continued work and this will be done by a number of explicit recommendation statements.

The SKB site investigations are presently in an intensive phase of compilation of field data and modelling. The Laxemar site is close to Äspö HRL and the work done at this site needs to be considered. It is for example worth nothing that the regional scale (roughly $100 \times 150 \times 2$ km^3) used for the Laxemar site is probably also relevant for Äspö. Thus, the work on the lineaments, surface hydrology, etc should be evaluated and perhaps even directly "imported" to the Äspö models. In the regional model a number of sub domains, with respect to the fracture network, have been defined. Perhaps one should consider Äspö as such a sub domain, which has to be characterized by the modelling team at Äspö HRL, embedded in the same regional model as the one developed in the site investigations.

Recommendation: Strive to confirm to the regional model developed for the Laxemar site. Consider Äspö as a sub domain in accordance with the strategy used in the site investigation.

Earlier Äspö models (for example /Svensson 1997b/) may also provide a perspective on the present work and the continued development; "What can we do better?", "What can we make use of?", etc. In terms of modelling techniques, several major developments have been carried out during the last ten years; to mention a few:

- Grid system. The adaptive Cartesian grid allows a seamless resolution from the regional scale to the details of tunnels and deposition holes. The need for embedded grids, transfer of boundary conditions, etc is thus eliminated.

- FRAME. In the earlier models no exchange with the matrix was accounted for. Further, storage of salt and "water types" for long time periods can now, by FRAME, be achieved in a realistic way.

- Numerical techniques and computer capacity. Faster equation solver and readily available computer power have increased the maximum number of grid cells that can be employed.

These and other developments have resulted in significantly more efficient tools, as compared to earlier models.

Recommendation: Utilize all recent technical developments (including visualization tools) the best possible way.

Field data. The credibility of a numerical model will by most people be judged from comparisons with field data. The Äspö HRL has a unique data base both in the term of quantity and quality. Compared to the situation ten years ago, the data base is now larger and more readily accessible. In the present project some data mining has been carried out (Appendices A and B) and these results will be valuable in the continued work. More work on the geological structure model, for example an explicit account of all large fractures that cross the tunnel, is already anticipated. The objective of this discussion section is to provide a context for the continued work. With respect to field data the context is that "the best possible data bases are available and should be utilized". For the model development it is useful to distinguish between data used as input, for example properties of deterministic zones, and data used for validation, for example comparisons with chemical data.

Recommendation: The data base at Äspö HRL provides a very good foundation for model development and validation. For the development part we recommend that all aspects of the fracture network should be in focus, while the first validation should concern the drawdown due to the tunnel and comparisons with chemical data (including salinity).

As a final remark, it should be emphasized that these recommendations are given with the expected use of the models (see Section 3.3) in mind. It has further been assumed that the code DarcyTools V3.0 will be used in the continued work.

Water type analysis has been used in the present project as a means to compare model simulations and chemical observations. A first evaluation of these comparisons indicates that the general picture (fresh water down to 1 km depth at Laxemar, pockets of Glacial water, etc) from the simulation model fits the present conceptual model of the development since the last glaciation. Also the prescribed initial salinity profile seems to develop into the present day distribution in a plausible way. However, it is anticipated that the comprehensive compilation of isotope and chemical evidence carried out in this project (Appendix B) ought to be utilized further.

Recommendation: Continue the comparisons between water type distributions, as given by the simulation models and evaluated from field data. Chemistry provides the only way to support the long-term simulations.

Boundary conditions determine to a large extent most simulation results. The top boundary conditions usually receive most attention, while simpler assumptions (like a zero flux condition) are used for the vertical and bottom boundaries. Within the project it has been discussed if a zero flux condition, combined with a fixed salinity level, is appropriate for the bottom boundary. Considering the terrestrial heating, one may question if this transport is by pure conduction or if advection is also contributing; if so the zero flux condition at the lower boundary can be questioned.

Recommendation: Evaluate if the zero flux condition at the bottom boundary of the simulation domain can be justified.

5   Conclusions

The achievements of the project can be summarized as follows:

- *Discussions of the basic concepts* of flow and transport in sparsely fractured granites have been carried out. The participants of these discussions have found it valuable to learn about, and discuss, the different topics addressed. The discussions of conceptual issues have resulted in various updates of the numerical models. One example is the transmissivity-length relation which now has two parts, one for "single opening fractures" and another for "fracture zones consisting of many fractures". Another example is the discussions on "advective effects on the sub grid scale". In the continued work, the computational grid will be constructed to resolve the network to smaller scales. With smaller cell sizes, it is believed that the advective effects will be better captured.

- *Compilation of data.* The compilation of data for fracture properties (Appendix A) will be an essential part of the continued modelling work. Equally important are the "hard facts from chemistry" (Appendix B), that will provide boundaries for acceptable results, during the calibration phase.

- *Model set-ups.* The two set ups for the Äspö site should be considered as starting points for further work. It has been shown that the models are working from a technical point of view, but more work on calibration and use of site data is required. The project has provided some recommendations about the continued work and also how credibility of the new models can be achieved.

It is hoped that these achievements do provide a first step towards a new generation of Äspö models. The continued work on the model development will be directed by the Äspö HRL and the calibration will hence be carried out with good access to data bases and general knowledge of the site.

6   References

AIAA Journal, 1998. Special issue, Vol. 36, No. 5, May 1998.

Berglund J, Curtis P, Eliasson T, Olsson T, Starzec P, Tullborg E-L, 2003. Äspö Hard Rock Laboratory. Update of the geological model 2002. SKB IPR-03-34, Svensk Kärnbränslehantering AB.

Follin S, Stigsson M, Berglund S, Svensson U, 2004. Variable-density groundwater flow simulations and particle tracking – numerical modelling using DarcyTools. Preliminary site description of the Simpevarp area – version 1.1. SKB R-04-65, Svensk Kärnbränslehantering AB.

Haggerty R, Gorelick S M, 1995. Multiple-rate mass transfer for modelling diffusion and surface reactions in media with pore-scale heterogeneity. Water Resour. Res, 31 (10), pp 2383–2400.

Påsse T, 1996. A mathematical model of the shore level displacement in Fennoscandia. SKB TR-96-24, Svensk Kärnbränslehantering AB.

Svensson U, 1997a. A regional analysis of groundwater flow and salinity distribution in the Äspö area. SKB TR-97-09, Svensk Kärnbränslehantering AB.

Svensson U, 1997b. A site scale analysis of groundwater flow and salinity distribution in the Äspö area. SKB TR-97-17, Svensk Kärnbränslehantering AB.

Svensson U, 1999. A laboratory scale analysis of groundwater flow and salinity distribution in the Äspö area. SKB TR-99-24, Svensk Kärnbränslehantering AB.

Svensson U, 2001a. Äspö Hard Rock Laboratory. Prototype Repository. Groundwater flow, pressure and salinity distributions around the Prototype Repository. Continuum model No 1. SKB IPR-01-40, Svensk Kärnbränslehantering AB.

Svensson U, 2001b. A continuum representation of fracture networks. Part I: Method and basic test cases. Journal of Hydrology, 250, pp 170–186.

Svensson U, 2001c. A continuum representation of fracture networks. Part II: Application to the Äspö Hard Rock Laboratory. Journal of Hydrology, 250, pp 187–205.

Vidstrand P, 2003. Äspö Hard Rock Laboratory. Update of the hydrogeological model 2002. SKB IPR-03-35, Svensk Kärnbränslehantering AB.

Model specifications

Empirical estimates of fracture and fracture zone properties

Patrik Vidstrand, Bergab

August 2007

Contents

1   Introduction

This appendix describes the data and trends that are the basis while establishing input parameters and trends used in the performed simulations. For detailed information on used notations see /Rhén et al. 2003/.

The first two chapters present the geological information on geological structures and fractures along with our used interpretations of this data.

With the development of discrete fracture descriptions in numerical models it has become an enhanced topic to be able to parameterise unique features. Each fracture needs to be assigned a geometrical description, a transmissivity, a storativity, and a transport aperture. Additionally it may be necessary to assign in-fracture variation and information on the fractures connectivity with other fractures as well as with the rock matrix that may affect sorption and reactions observed in transportation issues.

This appendix does not intend to provide a complete scientific background for the used assumptions and proposed relationships. It does however compile information from the Äspö HRL site in relation with the permeable structure's length.

In order to, at least to some degree, validate the compiled information a brief comparison with more international data is presented along with some necessary introduction to the issues of concern.

2   The geological structural model

The basis of the used deterministic deformation zones is the geological structural model of deterministic deformation zones Laxemar v1.2[1] /SKB 2006/.

The geological structural model of Laxemar is described at a larger scale than is the local geological structural model of Äspö established within the GeoMod project /Berglund et al. 2003/. In regard to structures the geological structural model Laxemar v1.2 incorporate the same features with the exception of the local Äspö structures ZAS0004A0 (NE2) and ZAS0007A0 (NW1). In cooperation with the POM geological modelling team these two local structures were incorporated[2].

In regard of geological thicknesses of the geological structures the size of some of the structures from the geological structural model Laxemar v1.2 that are also a part of the local geological structure model of Äspö needed to be adjusted in order to fit known Äspö characteristics. All used structures have within DarcyTools been assigned the recommended hydraulic width from the GeoMod project /Vidstrand 2003/. The used width is assigned for the entire structure and not only over the local Äspö scale.

Of the modelled geological structures not all have been assigned a known transmissivity value (normally based on the geometric mean of some measurement values) /SKB 2006/. All of the structures in the local geological structure model of Äspö have been assigned known transmissivity values from the GeoMod model /Vidstrand 2003/.
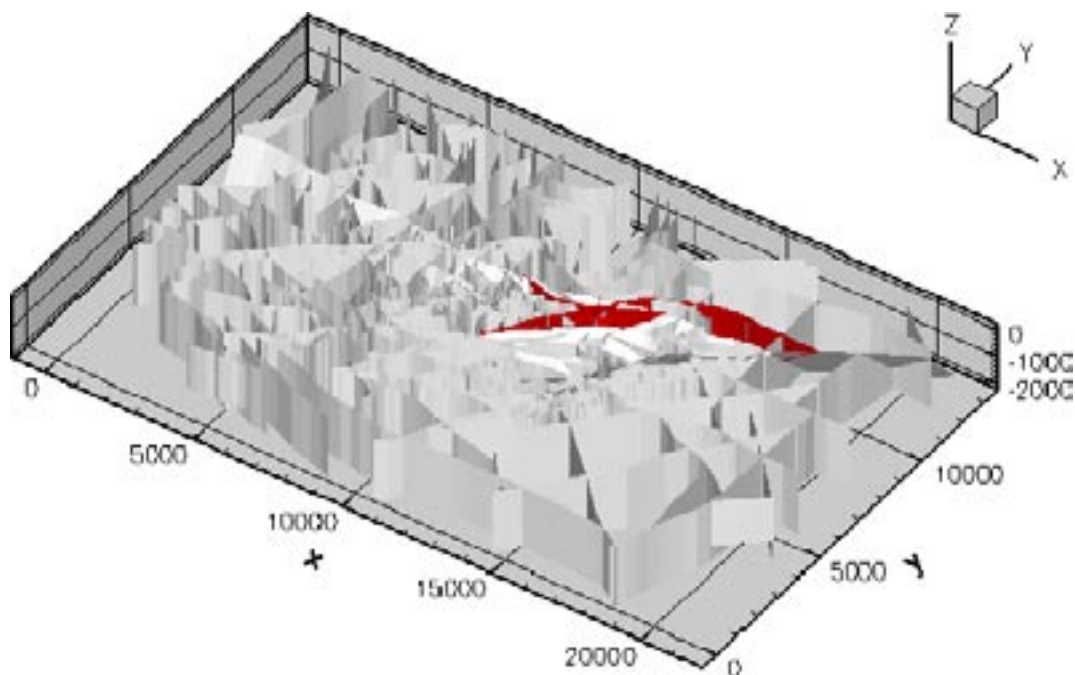

Figure A-1. The used geological structural model of deterministic deformation zones. The zones in red colour are part of the local geological structure model of Äspö. The illustrated coordinate system is the one used in the simulations and (0;0) relates to (1539000;6360000) in RT90.

---

[1] LX_V1.2.2_HYDRO_DZ (available in SIMONE).

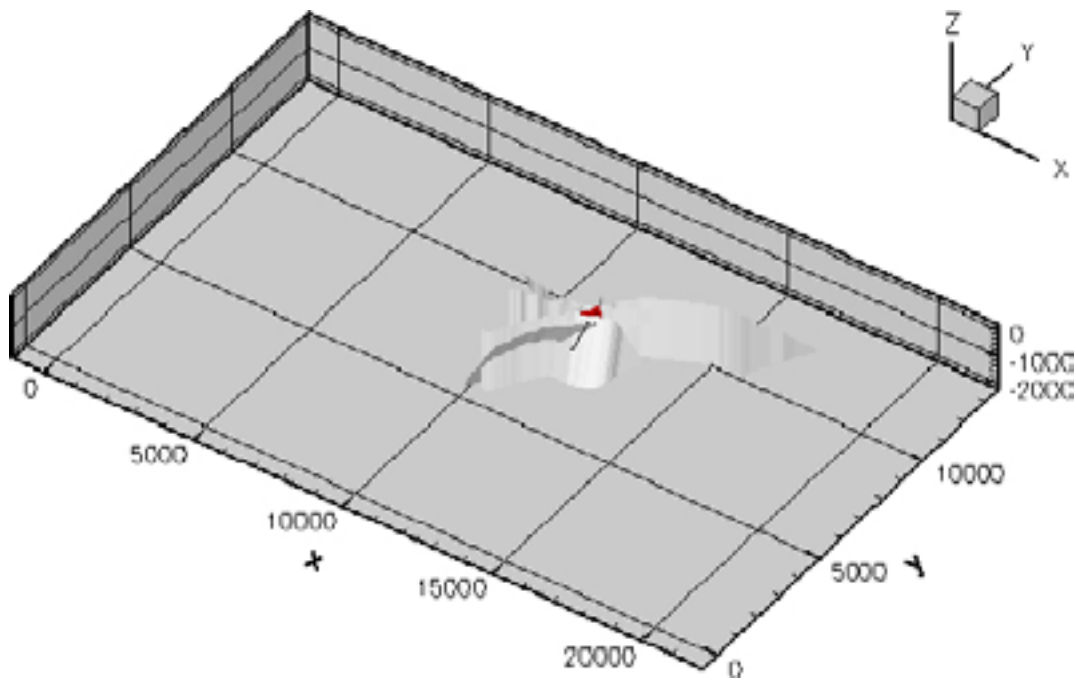[2] LX_V1.2.2_HYDRO_DZ_PV (available in SIMONE).

Figure A-2. *The parts of the Geological Structural model of deterministic deformation zones that refers to the local geological structure model of Äspö. The zones in red colour are the two smaller scale structures (NE2 and NW1) that have been incorporated. The illustrated coordinate system is the one used in the simulations and (0;0) relates to (1539000;6360000) in RT90. The Äspö tunnel is illustrated as a black line-feature.*
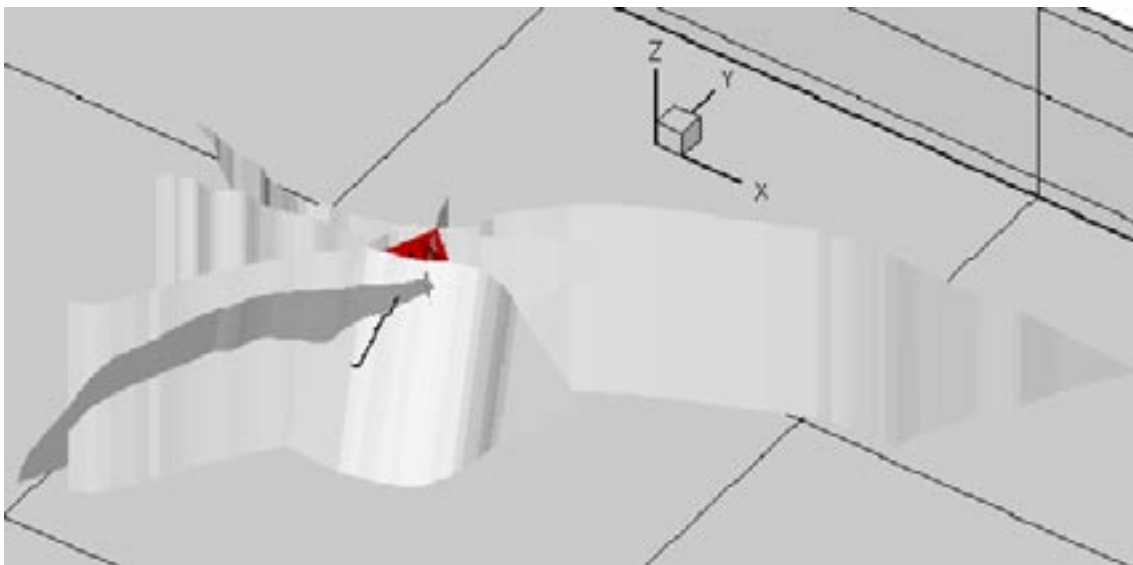

Figure A-3. *Zoomed in on the parts of the geological structural model of deterministic deformation zones that refers to the local geological structure model of Äspö. The zones in red colour are the two smaller scale structures (NE2 and NW1) that have been incorporated.*

38

Table A-1. The local geological structure model properties (transmissivity and width) /Vidstrand 2003/.

HCD	Idcode	Transmissivity Geometric mean [m²/s]	Width [m]
EW1a	ZAS0001A0	$5.2 \cdot 10^{-7}$	20
EW1b	ZAS0001B0	$1.2 \cdot 10^{-5}$	20
NE2	ZAS0004A0	$1.2 \cdot 10^{-7}$	10
NNW4	ZAS0005A0	$6.5 \cdot 10^{-5}$	10
NW1	ZAS0007A0	$5.0 \cdot 10^{-6}$	10
EW3	ZAS0003A0	$1.7 \cdot 10^{-5}$	10
NE1	ZAS0002A0	$2.2 \cdot 10^{-4}$	10
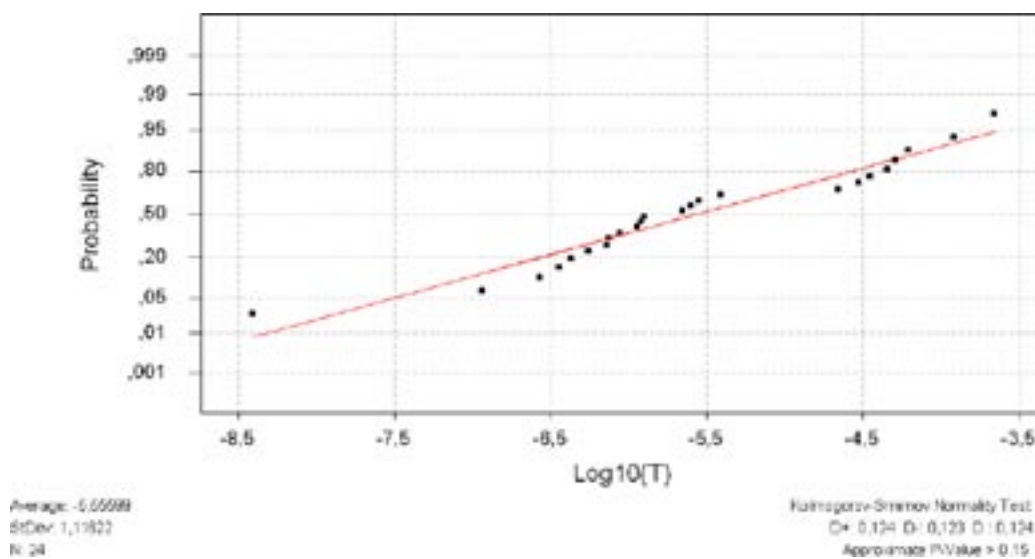
Figure A-4. *Normality test on the known structure transmissivity values.*

The geometrical mean of these known transmissivity values is $2.8 \cdot 10^{-6}$ m²/s, and the standard deviation in logarithmic scale is 1.1 (see Figure A-4). The recommendations from the POM modelling team is however to use a transmissivity value of $1.2 \cdot 10^{-5}$ m²/s (Rhén 2005, personal communications) for the unknown transmissivity values. This latter value has been assigned to all structures with un-known transmissivity.

All zones are created with a series of triangulated planes. These planes are assigned stochastic properties of a lognormal distribution based on the assigned transmissivity value and its related standard deviation along with an assigned depth-dependency trend. For all zones a maximum value of $3.0 \cdot 10^{-4}$ m²/s and a minimum value of $1.0 \cdot 10^{-7}$ m²/s have been assessed. Used standard deviations and assigned transmissivity values are based either on local Äspö HRL information /Vidstrand 2003/ or the recommendations from the site investigations /SKB 2006/.

In the DarcyTool set up a general depth dependency is assigned on bedrock properties (e.g. porosity, hydraulic conductivity). For the hydraulic conductivity the decrease is with a factor 10 for every 400 metres and porosity and specific storage decrease with a factor 10 for every 800 metres. These numbers are in agreement with the recommended depth trends suggested by the site investigation programmes /SKB 2006/.
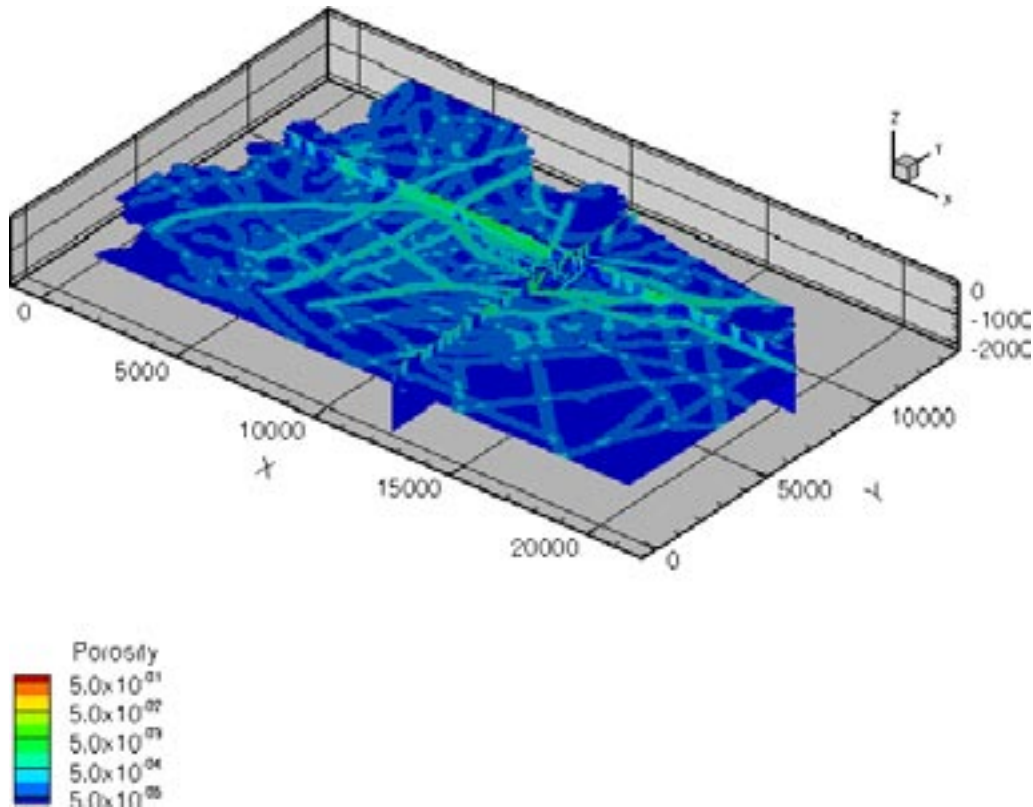
Figure A-5. *Illustration of the porosity field in the model domain.*

Table A-2. Depth dependency as specified for the hydraulic conductivity.

Depth interval [metres] Metres below ground	Hydraulic conductivity [m/s] Equation of depth dependency
0–1	$K = 5 \cdot 10^{-3} \cdot 10^{-\frac{depth}{3}}$
11–20	$K = 1 \cdot 10^{-6}$
20–	$K = K_{DT} \cdot 10^{-\frac{depth}{400}}$, $K \geq 1 \cdot 10^{-10}$
	K_{DT} = Based on established fracture network.

The structures have been assigned a storativity and transport aperture with the herein (cf to relevant chapters in this appendix) recommended relationships. However, in the simulations a storativity of zero has been used.

One important difference between the local geological structure model of Äspö established in the GeoMod project and the local model from the Äspö97 model /Rhén et al. 1997/ (is the omission of the NNW structures (NNW7, NNW1, and NNW2) that crosses the tunnel spiral in the Äspö97 model. Also an important note is that the NW1 structure in the local model of GeoMod is not the same structure as the NW1 structure in the Äspö97 model. In fact the NW1 structure from the GeoMod project is one of two newly defined deformation zones in the tunnel region. The other zone (NEHQ3) is however not found to be hydraulically active neither as a conductor nor as a barrier.

3 The DFN model

The DFN statistics at Äspö HRL are different from the DFN statistics at the Laxemar subarea /Berglund et al. 2003, especially on the southern part of Äspö the predominance of the steep northwesterly fracture set seems to be a local phenomena, except for some minor localities at the Laxemar. The local statistics is used for the simulations presented herein, even though the used regional model domain has the same scale as the Laxemar models, since the main purpose of the performed simulations is to update the Äspö HRL models. By using local Äspö HRL data the accuracy of the model results are believed better representing the Äspö site.

The DFN statistics govern the stochastic fracture network on the scales smaller than the geological structural model. For the performed simulations the local geological structure model of Äspö compromises structures down to the scale of 500 metres length. It is believed that all structures larger than 500 metres are known on the Äspö HRL, therefore only stochastic fractures shorter than 500 metres are generated; this in order to keep the amount of larger structures correct. The POM site hydrogeological models generate stochastic fractures smaller than 1,000 metres /e.g. Follin et al. 2004/; this discrepancy is likely to make the blocks of rock mass in our numerical model somewhat tighter than their equals in the POM site hydrogeological models.

The different fracture sets and their intensity are in our simulations are partly based on local Äspö HRL information; but also on earlier work at Äspö HRL /e.g. Svensson 1999, Stigsson et al. 2001/.

Based on the statistic presented above (Figure A-6, Figure A-7, and Figure A-8) and earlier modelling experiences /e.g. Svensson 1999, Stigsson et al. 2001/ it was decided to use three different sets, two sub-vertical and one sub-horizontal fracture sets. As clearly seen in Figure A-8 for the fractures with leakage the WNW striking fracture set is dominating. The other two sets (the NNE striking and the sub-horizontal) seem equally important however, experiences have shown that the vertical set is more water conductive compared to the horizontal /e.g. Svensson 1999/.

The fracture set statistics (Table A-3 and Table A-4) are described with conventions for the normal vector to the fracture plane described for pole orientations on a lower hemisphere coordinate projection. The fractures within a fracture sets are assumed to belong to a Fisher distribution with a spread (dispersion) around the mean pole value.
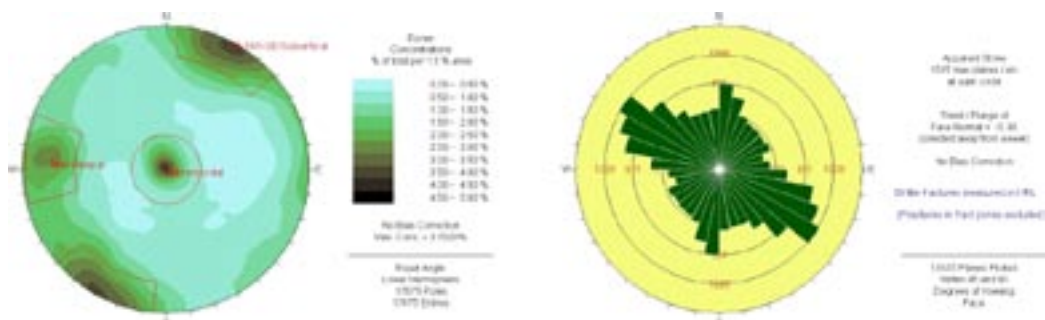

Figure A-6. *All brittle fractures from Äspö HRL tunnel wall mapping (TMS database), compiled by SKB /Magnor 2005/.*
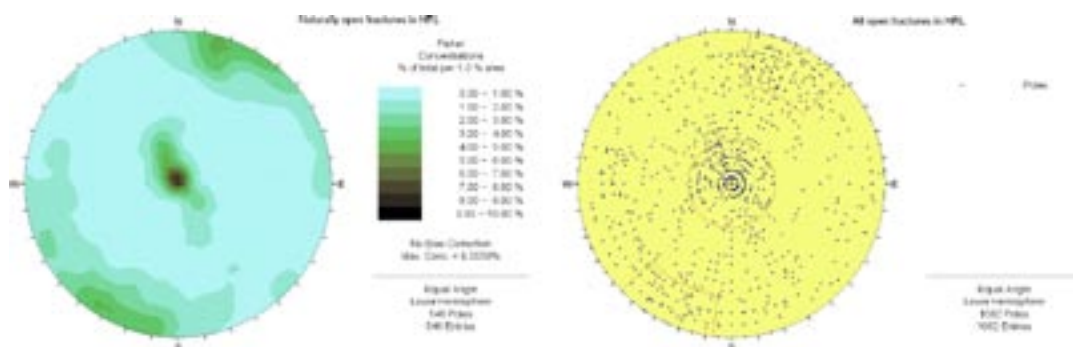
Figure A-7. All natural open fractures from Äspö HRL tunnel wall mapping (TMS database), compiled by SKB /Magnor 2005/.
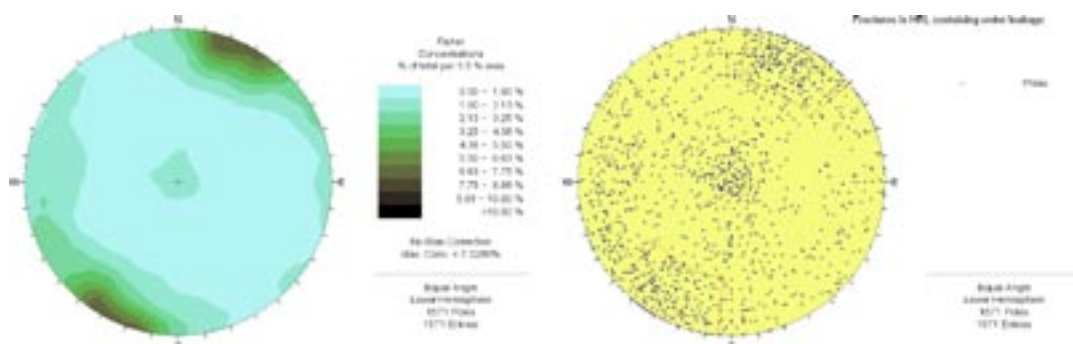

Figure A-8. All open fractures with leakage from Äspö HRL tunnel wall mapping (TMS database), compiled by SKB /Magnor 2005/.

Table A-3. Fracture set statistics (degrees relate to geographical north).

Set	Strike (°)	Dip (°)	Dispersion
1	280	80	4
2	30	87	11
3	18	5	9

Table A-4. Fracture set intensity.

Set	Intensity factor (α_{DT})[3]	Percentage
1	0.07	64%
2	0.03	27%
3	0.01	9%

The stochastic fractures are generated in accordance with a Power law relationship /Follin et al. 2006/ governing the fractures size. The largest fracture size is equal to the smallest structure scale used, in our simulation 500 metres. The smallest fracture size is specified in accordance with the grid cell size. In our 10,000 years simulations the used grid cell size results in a smallest fracture size of 50 metres; in the tunnel simulations the discretisation close to the tunnel is much smaller and fractures down to 20 metres are generated (cf to relevant appendix).

---

[3] Fracture intensity factor used in DarcyTools, see /Follin et al. 2006/.

4 Fracture properties
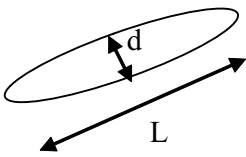
4.1 Conceptual issues

The used approach to assign individual fracture properties rests on the assumption that fracture size distributions follow a Power law and that all properties can be related to the fracture size. Below some concepts used in the assigning are briefly described.

It should be stated that the empirical relationships that are established are just local trends valid for the Äspö HRL and that statistical distributions are assumptions. It is out of the scope of this report to present and discuss the established empirical relationships in relation to theoretical approaches and hypothesis.

4.1.1 Linear elastic fracture mechanics

The theoretical approach to fracture mechanics rests on many weak assumptions. Rocks, deep down in the Earth's crust, are well confined and under a significant influence of a temperature field. Furthermore, the loads in nature are mainly from tectonic processes acting over a significant time frame. These are not conditions supporting the assumptions behind the theories of brittle failures; neither is the rock a homogeneous and isotropic material

However, if it is assumed that the rock mass behaves as a perfect elastic, homogeneous, and isotropic body then linear elastic fracture mechanics can be successful in many rock mechanical problems /Olson 2003/, including the analysis of joint spacing and clustering /e.g. Pollard and Segall 1987/. A standard assumption in the reported works is that all fractures within a population opened up in response to one driving stress event. This assumption yields a nice theoretical relationship between fracture length and maximum fracture opening (aperture):

$$d_{max} = (u - \sigma_n)\left(\frac{2(1-v^2)}{E}\right)L \quad \text{where}$$

and where v is Poisson's number and E stands for Young's modulus. As it is realistic to assume that the change both in pore pressure, u, and the normal load on the fracture, σ_n, due to a load can be expressed through a constant and the volumetric change of the fracture, it is plausible that the maximal opening of a fracture can be expressed on the form:

$$d = a \cdot L^b$$

4.1.2 Length

The length notation is subject to uncertainties; this since it frequently refers to a variation of entities such as: fracture trace length, adjusted fracture trace length, simulated fracture length; calculated fracture length, etc. All these entities reflect different properties that may have a significant impact on the established relationships. Additionally, the adjustment and simulation of a fracture require an assumption of fracture geometry and assumptions from triangular and quadratic to circular and elliptical shapes further constrain the estimated fracture length value.

4.1.3 Cubic law

Fluxes of a Newtonian liquid (e.g. water) within a medium can theoretically be expressed by the Navier–Stokes equation. For the case of flow between smooth and parallel plates the Navier–Stokes equations results in a solution known as the Cubic law:

$$Q_f = \frac{e^3 \rho g}{12\mu} \frac{\partial h}{\partial x}$$

The likeness with Darcy's law is evident and hence the transmissivity (fractures have a finite thickness/width) can elementary be stated as:

$$T_f = \frac{e^3 \rho g}{12\mu}$$

A natural fracture does not, however, fulfil the smoothness nor the parallelarity. These deviations cause fracture flow effects known as tortuousity and channelling. These effects result due to the spatial pattern of the aperture distribution. A series of flow experiments on rock cores performed by /Witherspoon et al. 1980/ concluded that the flow in a natural fracture is reduced as compared with the theoretical smooth-parallel plate flow. These and other results indicate that cubic law calculated transmissivity-estimates are too high.

4.1.4 Aperture

The concept of aperture is frequently used in both rock mechanics and hydrogeology of fractured rocks. Although the notation used is the same the intrinsic meaning is not. Within rock mechanics the aperture physically stands for the opening at a specific location in a fracture, and does as such varies spatially over the fracture. In fracture hydrogeology the aperture more frequently represents a smooth, constant value back-calculated from the fracture transmissivity by the cubic law, theoretically derived from the Navier–Stokes equation.

/Alm 1999/ performed a brief compilation of laboratory-derived data with an inter-comparison between mechanical apertures and hydraulically derived apertures. This referred compilation arrived at a median of the "mechanical aperture over hydraulic aperture" ration of 1.45. However, the mean value was 3.20 and the data scattered between 1 and 16. An interesting observation is that the smallest value of 1.08 corresponds with the largest observation on mechanical aperture while on the other hand the largest ratio of more than 16 corresponds with the smallest mechanical aperture measured.

It is nowadays well-established that there exist a relationship between applied normal stress and the fracture opening (aperture). /Alm 1999/ addressed the possibility that a change in normal stress may firstly effect the areas in the fracture with largest apertures; if so – since the fracture transmissivity mostly is controlled by the small apertures – the fracture transmissivity may be less effected by stress changes than the mechanical aperture reflect. This however is not true for the transportation pathways within the fracture that are more controlled by large correlated aperture corridors.

In order to simulate transport of chemical species in a fractured rock mass a series of different transport parameters are of importance. One of these parameters is the transport aperture. The transport aperture is defined through the kinematic porosity and the hydraulic width (mostly equal the geological width) of the conductive structure.

As the concept of porosity is dubious within a single fracture it is perhaps more conceptually realistic to view the transport aperture for a single fracture as more similar to the hydraulic aperture defined through the cubic law; however in transport issues accounting for transportation time that is incorporating a larger volume. However, if the hydraulic conductor is a fracture zone it is created by a network of fractures, which when the fracture intensity is large approach a porous medium. In this latter case the concept of kinematic porosity is valid. The transport aperture is in such cases viewed as a fracture approximation of a porous medium.

4.1.5 Storativity

In an aquifer one will find that the mass accumulation is dependant on, among other factors, the compressibility of both the fluid (water) and the aquifer skeleton. The combination of these factors within an aquifer is defined as the storativity (S). In the traditional hydrogeology the storativity is defined within a porous medium and therein expressed as:

$$S = b(\alpha \rho g + n\beta \rho g)$$

where b is the aquifer thickness, α is the compressibility of the water, n is the porosity, and b is the compressibility of the aquifer.

On a larger scale it is plausible that this concept of storativity is valid for a fracture aquifer, however at the scale of individual fractures the concept of porosity is as earlier stated dubious and the release or accumulation of mass from a fracture is maybe best described by the hydro-mechanical responses depending on, among other factors, the fracture stiffness /e.g. Rutqvist and Stephansson 2003/.

4.2   Aperture observations

/Vermilye and Scholz 1995/ presented out-crop data on the relation between vein length and aperture from a couple of hard rock sites. The data presented in Figure A-9 contain some of the single segment features from their data set.

/Vermilye and Scholz 1995/ concluded that their data were in agreement with several published data on mafic dikes and faults. The proposed relationship for single segment features are veri-fied by the results presented by /Gudmundsson 2000/, however this latter data set compiled data over a much smaller length interval and may therefore not be significant while analysing the length trend of the data.

The data presented by /Vermilye and Scholz 1995/ are measured along the trace of the vein and do therefore not reflect the true relation between fracture length and its corresponding maximum opening. How this deviation from the "true" length and maximum opening influences the results is impossible to quantify. However, one could argue that the length is more affected by this deviation than are the maximum opening.
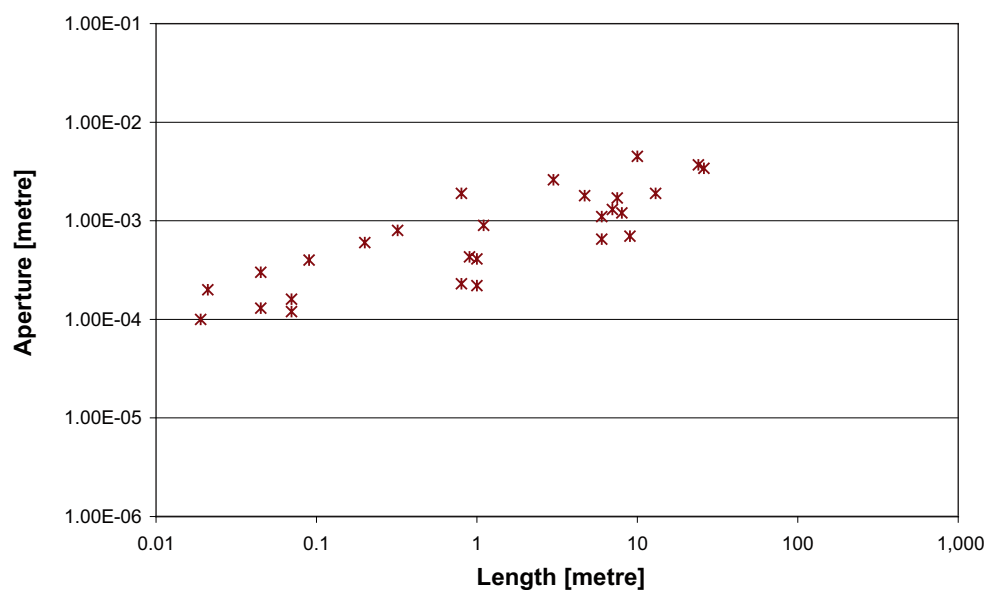

Figure A-9. *Aperture (maximum width on veins) in relation with measured length (trace length). Reproduction of some of the compiled data presented in /Vermilye and Scholz 1995/.*

Figure A-10 illustrates some approximate locations of apertures in relation to the length of the fracture. For most of these fracture data no length value is presented and therefore the exact location for these aperture observations is uncertain. However, extracting characterisation information yields some bounds for the possible fracture lengths. The aperture data from /Gudmundsson 2000/ are similar to the one by /Vermilye and Scholz 1995/ in so what that it is field measured "fracture openings" from out-crops, however from an Icelandic site. The data by /Hakami and Larsson 1996, Olsson 1998, Johansson and Stephansson 1998/ and /Birgersson et al. 2000/ are all from Äspö HRL extracted from fractures in cores at a depth of more than 100 metres. The data reported by /Alm 1999/ are taken from a hard rock site on the Swedish west coast from a depth of approximately 20 metres.

The data presented by /Straford et al. 1990/ and /Gale 1990/ give apertures two to three orders of magnitude smaller. These data are taken from an old Swedish mine (Stripa), which has worked as an experimental site for the Swedish Nuclear Fuel and Waste Management Company (SKB). These data are the result of a resin experiment on core samples under high normal stresses and sheared to almost failure, and are as such not relevant as an aperture measure for in situ fracture apertures.

4.3   Aperture based transmissivity-estimates

The aperture value has frequently been used within DFN models as a mean of expressing the fracture transmissivity or vice versa. This kind of transformation is normally done by the cubic law. However as previously discussed the aperture that relates to a fracture transmissivity is not the same as the aperture measured in a natural fracture. The compilation by /Alm 1999/ concludes that the hydraulic aperture is smaller than the averaged value of measured opening by up to an order of magnitude or more.
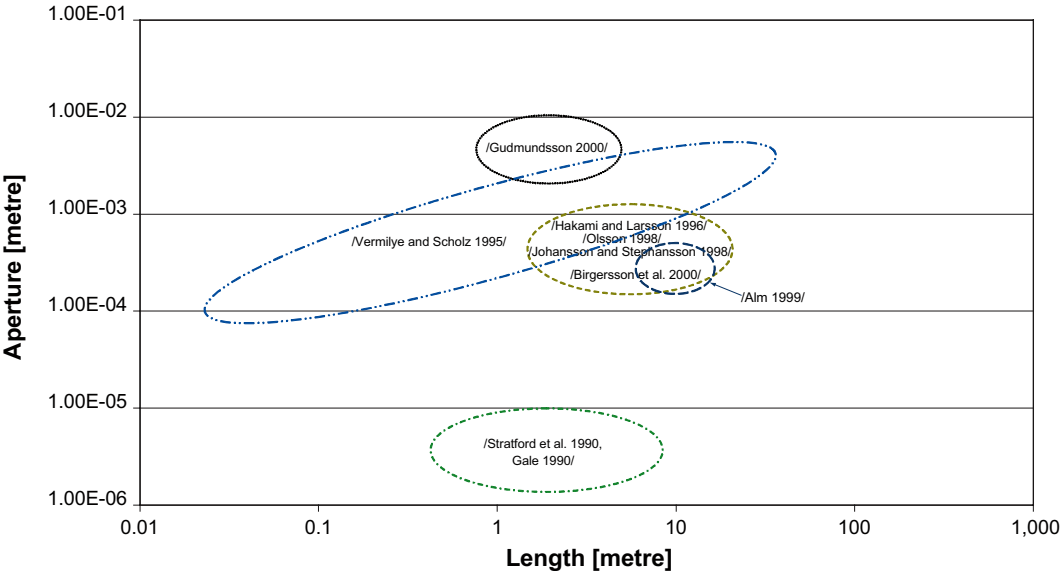

Figure A-10. *Compilation of aperture versus fracture length data found in literature. Illustration shows the circumference of the data scatter reported.*

At Äspö HRL an experiment with resin concluded on a series of different aperture distributions established for each of a number of extracted cores /Hakami 1995/. As a simplified description these distributions seem lognormal and results in a scatter between 100 and 600 micrometres, with a mean value around 300 micrometres. This interval for apertures agrees with the majority of all reported values of our findings.

Using cubic law to transform this mean value into a transmissivity value results in a transmissivity of $2 \cdot 10^{-5}$ m^2/s for one of the investigated fractures. It is, however, conclusive that this value is too high by several orders of magnitude. The resin filled fracture were hydraulically characterised before the injection of resin. This characterisation describes the fracture with values in the magnitude of $1 \cdot 10^{-8}$ m^2/s /Birgersson et al. 2000/, see Figure A-11 below. Similar discrepancy as here described is also found in the field data presented by /Alm 1999/.

4.4 Transmissivity observations

Adopting the philosophy and theory concerning the relationship between aperture and fracture length by /e.g. Vermilye and Scholz 1995/ it is justified to assume that a relationship between the fracture length and the fracture transmissivity likewise exists.

In Figure A-12 a compilation of estimated fracture transmissivity values from the Äspö HRL is presented. Within this data the length criterion is established in the same manner as for the earlier described aperture data. That is the data may be based on extracted characterisation data for the small structures as well as trace length of linked lineaments for the large features.
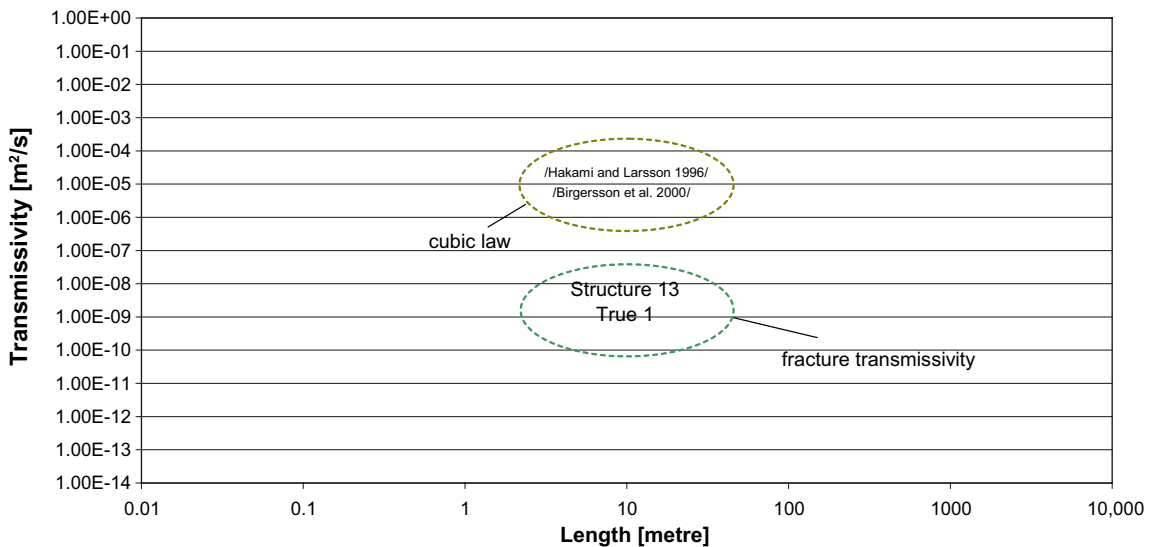

Figure A-11. *Comparison between the originally evaluated fracture transmissivity values and the forward-calculated transmissivity values based on established apertures from core analyses on the resin filled fracture. Illustration shows the circumference of the data scatter reported.*
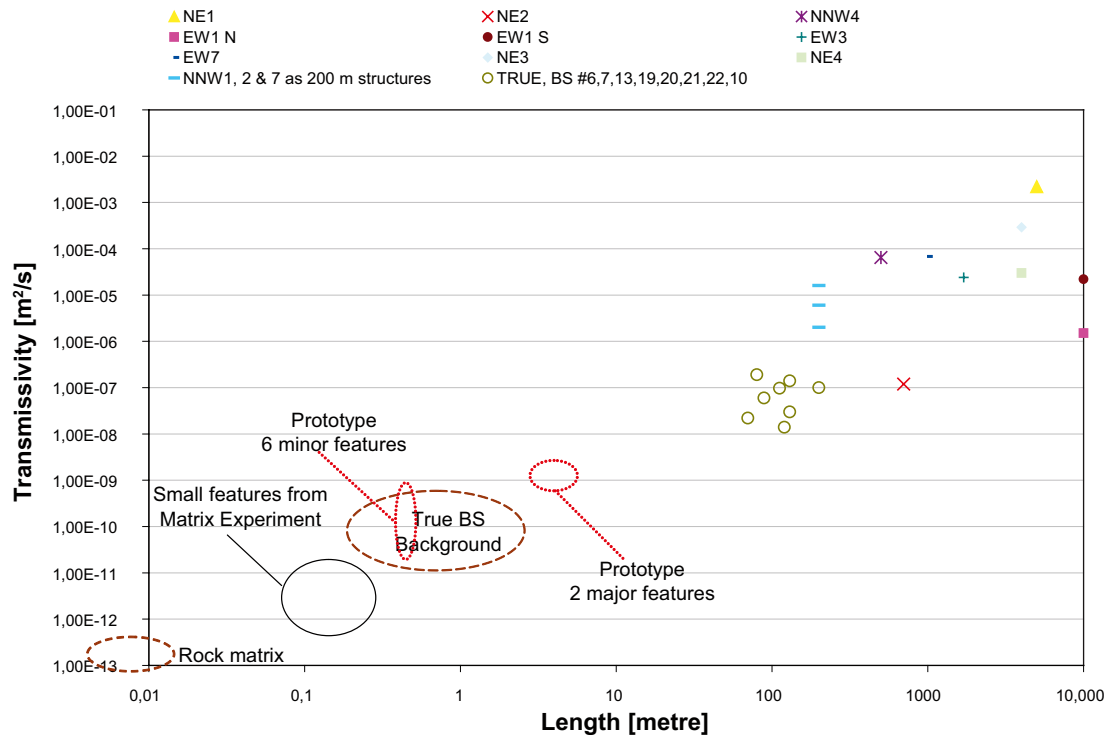
Figure A-12. *Compilation of transmissivity values for unique fractures/structures and their length. Circular illustrations indicate the possible location of the feature based on extracted constrains in characterisation information. TRUE BS deterministic data is evaluated feature transmissivity and modelled length (modelled length based on geoscientific investigations, e.g. borehole radar, extensive drilling, and hydraulic testing among others. The large scale structures are structure trace lengths along with transmissivity values based on few interference tests along the structure. Data are collected from /Smellie et al. 2003, Rhén and Forsmark 2001, Hermansson et al. 2002, Rhén et al. 1997/.*

4.5   Discussion on transmissivity and length of the hydraulic conductor

Based on the field data from Äspö HRL presented above one could propose a power law relation between hydraulic conductor length and transmissivity. In a hypothetic relationship in Figure A-13 a smaller scatter (or a better fit) is observed for features within the length interval of 1 to 100 metres which for Äspö HRL applications are most likely needed to be stochastically generated. In larger scales the structures are supposed to be more deterministically known and therefore the large scatter around the trend line is not so important.

Transmissivity [m²/s] versus length [m]:

$T = 1 \cdot 10^{-10} \cdot L^{1.37}$ [L < 100 metres]

$T = 1 \cdot 10^{-09} \cdot L^{1.35}$ [L > 100 metres]

Relationships as the ones presented above and in Figure A-13 must of course be viewed as site specific and as such it is interesting to investigate how the relationship stands in comparison with other field data and theoretical relationship. Figure A-14 plots our proposed relationship with a couple of others. As can be seen the relationships are found within two groups. One group referrers back to a theoretical single vein and the second group in which our compilation is found (among with many others) referrers back to a theoretical relationship for En Echelon fracture systems.
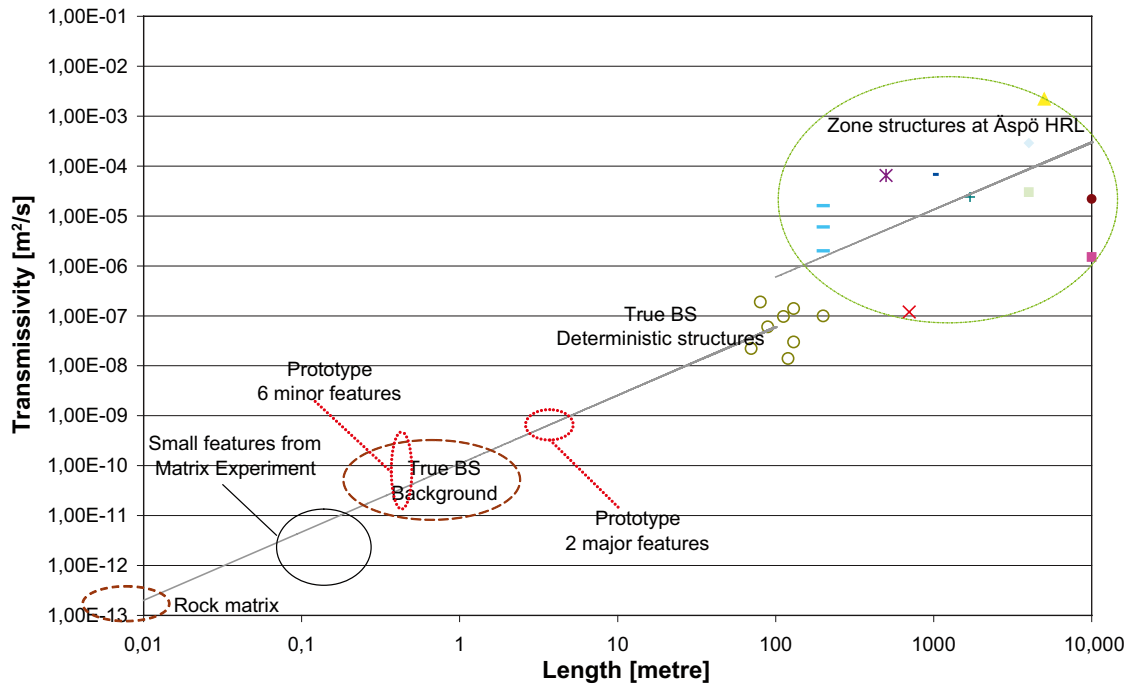
Figure A-13. *Proposed relationship between transmissivity and length for Äspö HRL features.*
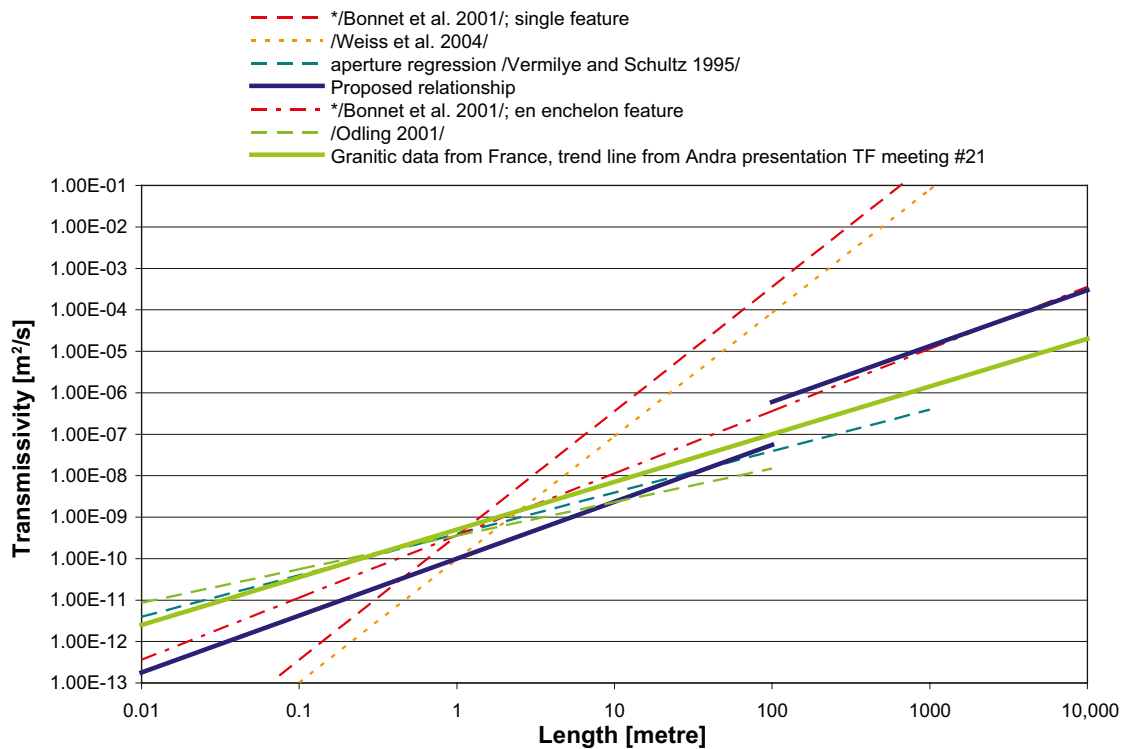

Figure A-14. *Comparison of chosen relationship and trends of other data (mostly aperture) and some theoretical relationships (marked with * in the figure). For detailed information see references. All relationships have been transformed to transmissivity values inter-agreeing around the length of 1 metre. The correct reference to the French data is /Dossier Granite 2005 Tome/: analyse de sûreté du stockage géologique, Figure 6.1–21 – page 165, Juin 2005 – ANDRA. The report is available on-line (in French). For references see Figure chart.*

If the observations are placed in a geological frame one could suggest that some of the indications in Figure A-13 points to a dependence on direction. Some of the large scale deterministic structures suggest that one could use two relationships as shown in Figure A-15. However, in more detailed surveys such as TRUE BS it is not verified that this is a certainty. The anisotropy in evaluated transmissivity values (hydraulic tests with a packer spacing scale of 15 metres) at Äspö HRL /e.g. Rhén et al. 1997/ are more likely the combined result of different effects occurring in different direction. The TRUE BS rock block is extensively investigated and suggests that the intensity of fractures orientated in NW is significantly larger than the intensity of the fractures orientated in NE. This difference in fracture intensity is plausibly a more important cause for the large anisotropy in evaluated transmissivity values (from packer tests) than are stress dependence and other effects working in certain directions.

4.6   Specific storage estimates at Äspö HRL

Some interference tests on southern Äspö were used to establish an estimate of the specific storage in the order of $2.0 \cdot 10^{-6}$ m^{-1} for hydraulic rock mass domains /Rhén et al. 1997/. Based on this data and an estimate based on evaluated rock mechanical properties /Rhén et al. 1997/ established a linear relationship between the logarithms of the hydraulic conductivity and the specific storage.

Figure A-16 and Figure A-17 present the established specific storage values in relation to hydraulic conductivity from the La Scala – and the Prototype Repository experiment, respectively. The relationship established by /Rhén et al. 1997/ is presented in Figure A-16 and Figure A-17, as compared to the compiled data.

The results from the La Scala experiment indicate higher values for the specific storage than presented by /Rhén et al. 1997/. Figure A-16 shows the specific storage in relation to hydraulic conductivity. Estimates for the specific storage from the hydraulic tests performed in the Prototype Repository experiment (Figure A-17) indicate a lower limit for the specific storage than the previously suggested by /Rhén et al. 1997/.
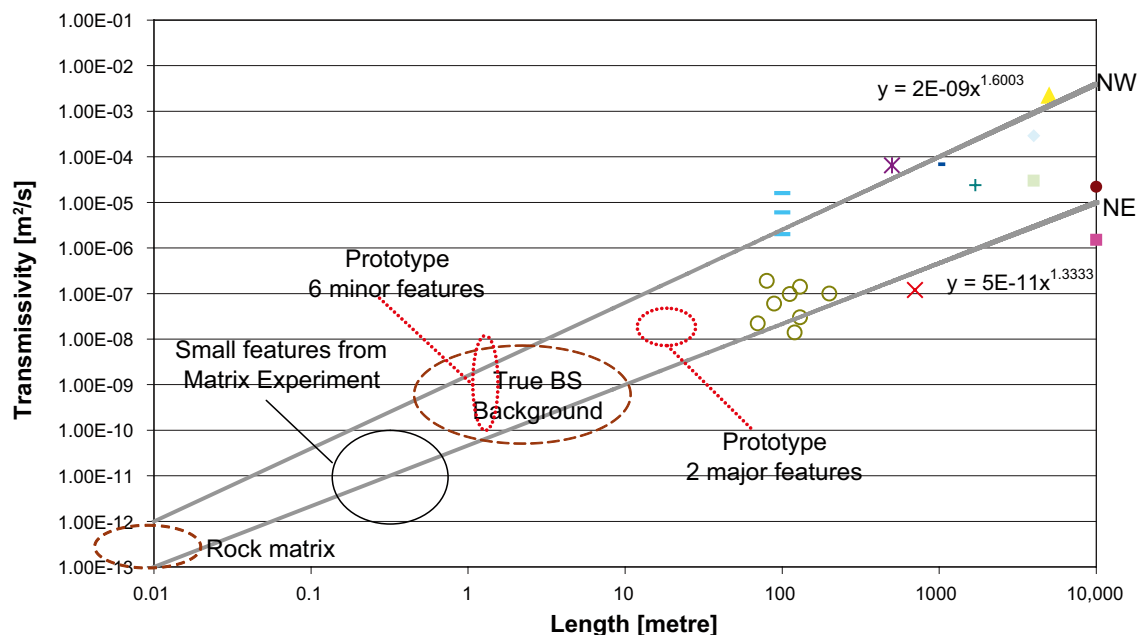

Figure A-15. *An alternative way of using the compiled transmissivity data. Two relationships are proposed depending on direction.*
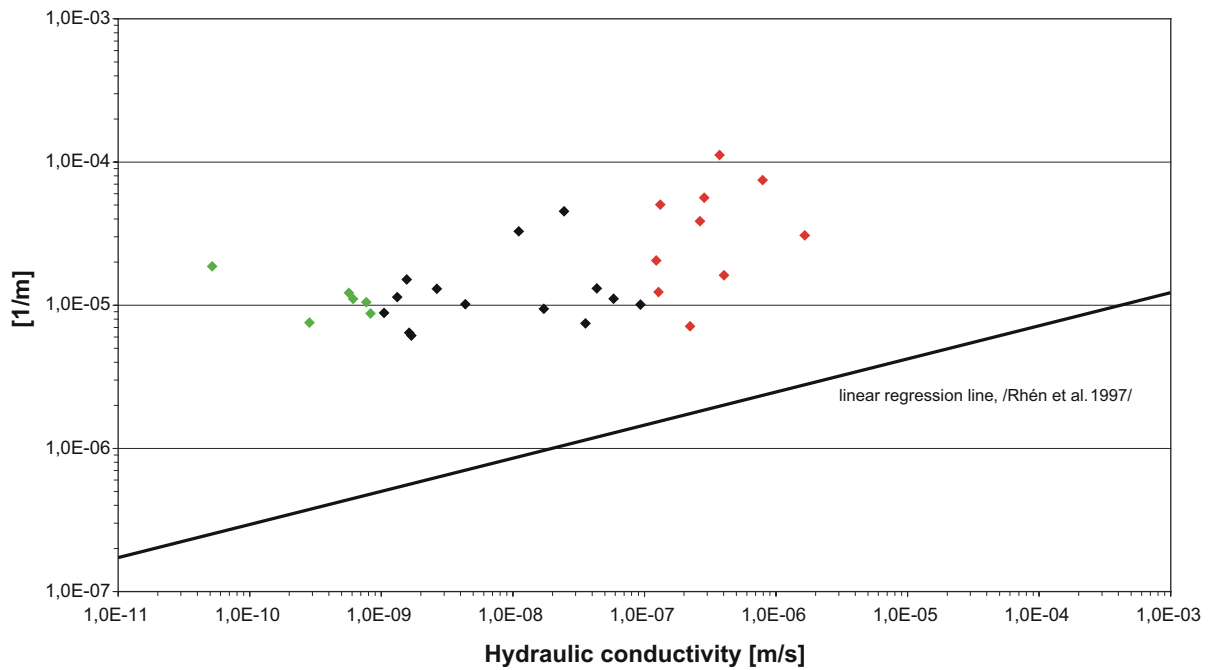
Figure A-16. *Estimated specific storage from the La Scala experiment /Vidstrand 2003/.*
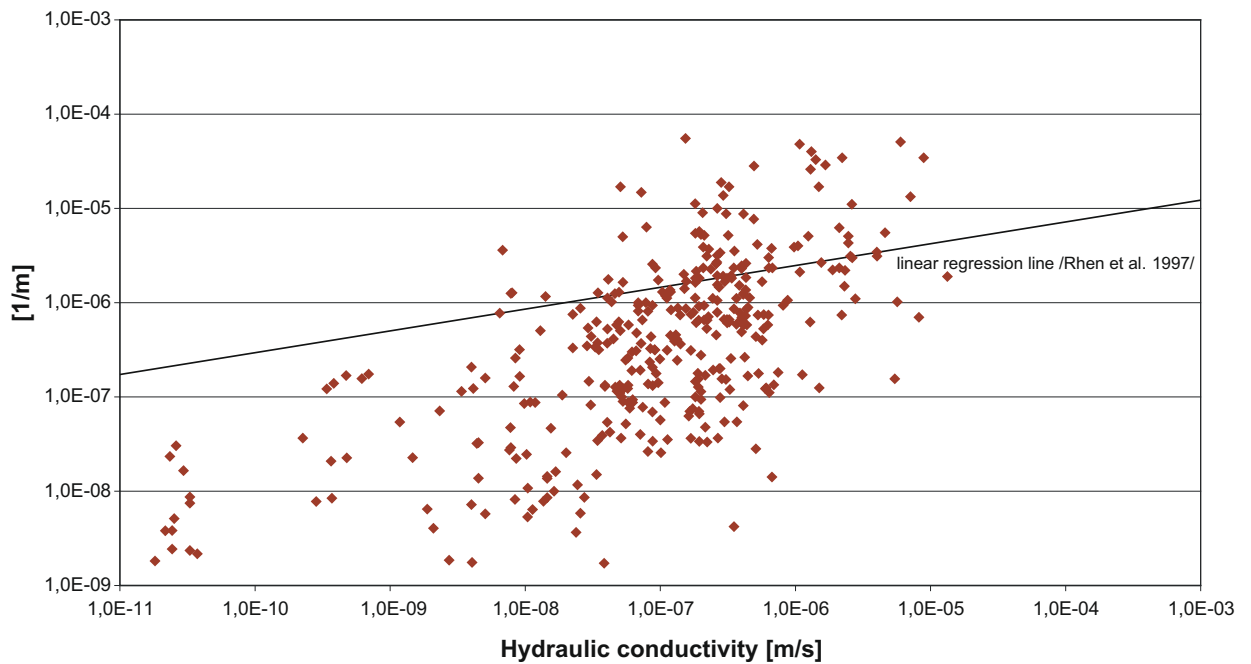

Figure A-17. *Estimated specific storage from the Prototype Repository experiment /Rhén and Forsmark 2001/.*

In the La Scala experiment /Vidstrand 1999/ (performed in borehole KA2598A) the specific storage was evaluated based on single-borehole tests evaluated with Hantush methodology. A common estimated flow dimension at Äspö HRL is somewhere in between 2.2 and 2.8. These kinds of flow dimensions indicate that a leaky-aquifer methodology may be valid for evaluation of the hydraulic conductivity and specific storage of the rock mass.

Established specific storage values from the La Scala experiment rely on the validity of the Hantush methodology; and the specific storage values from the Prototype Repository experiment rely on a valid transformation of the diffusivity value. However, both methodologies are frequently used and seem equally justified.

4.7 Discussion on transmissivity and storativity of the hydraulic conductor

Established values for the storage coefficient at Äspö HRL are not as frequent as are transmissivity values. There are other compilations containing values (as a majority) collected from the crystalline bedrocks of Sweden. A compilation presented in /Almén et al. 1986/ yielded specific storage values on bulk rock between 10^{-10} m^{-1} and 10^{-6} m^{-1} with the majority between 10^{-8} m^{-1} and 10^{-7} m^{-1}. For rock defined as belonging to fracture zones the values were found between 10^{-7} m^{-1} and 10^{-4} m^{-1}. /Niemi et al. 2000/ compiled data from the nineties with similar results.

Rock mechanics place a constraint on the lower limit of the specific storage. A specific storage values around $1.0 \cdot 10^{-8}$ correspond to theoretical specific storage values for a case with fresh water, compressibility of the rock $1.0 \cdot 10^{-11}$ m^2/N, and porosity 1%. These are not unrealistic values and therefore the empirical data from the Prototype experiment may be a realistic data set to use for Äspö HRL.

An analysis of Äspö HRL data performed by /Ushida et al. 1994/ resulted in a transmissivity versus storage relationship that fits the data from the Prototype repository site which were collected at a later time. The data from Prototype together with the analysis by /Ushida et al. 1994/ indicate that the La Scala data herein presented may represent an anomaly on the high value side.

If the two sets (La Scala and Prototype) herein presented are combined the early regression by /Rhén et al. 1997/ is found to fit reasonably well. However, based on the theoretical estimates for a tight rock mass the lower limit is proposed to be lowered.

The presented data further indicate (Figure A-18) that for high hydraulic conductivity values the related specific storage values approach the line that represents a one to one relation of transmissivity and storativity. However for low hydraulic conductivity values the relationship is more like a theoretical line based on the cubic law. This approach was tested by /Niemi et al. 2000/; in which they assumed a relationship between the fracture aperture usable for storage and the effective hydraulic aperture of 10 ($b_{storage}/b_{hydraulic} = 10$). Herein however in order to
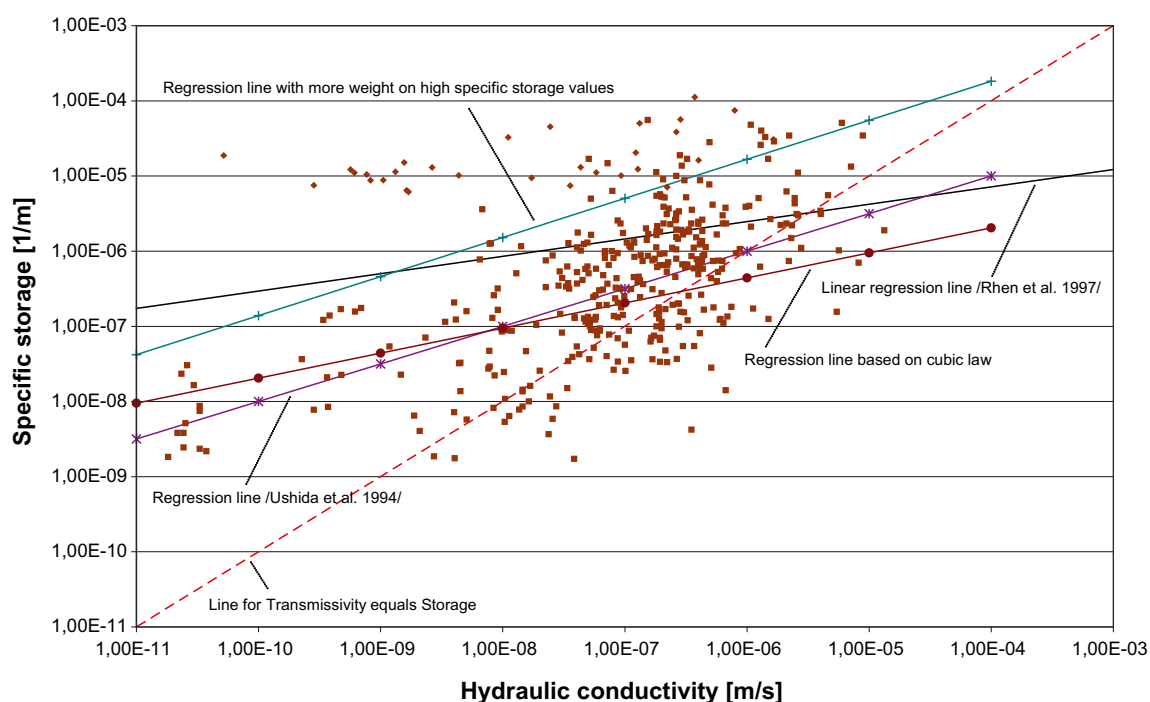

Figure A-18. *Estimated specific storage values from the Prototype Repository experiment and the La Scala data compared with proposed relationships between transmissivity and storage.*

reach a reasonable fit one need to assume a relationship on the order of 1,000. This order seems unrealistic when compared with estimated differences in transmissivity values based on hydraulic apertures and measured mechanical apertures at Äspö HRL, /e.g. Birgersson et al. 2000/. A relationship based on the cubic law is a good relationship for the fractures (unique structure) and it is plausible for the low transmissivity values.

4.8 Discussion on transport aperture and length of the hydraulic conductor

In DarcyTools fractures need to be assigned a hydrogeological width and a kinematic porosity. For fractures the concept of porosity is as stated dubious but could be based on a relationship with the transport aperture. The concept of transport aperture is frequently used and at Äspö HRL the empirically established Doe's law has been used:

$$e_T = 0.5 \cdot T^{0.5}$$

Following the logics discussed above the transport aperture in relation to the transmissivity of the hydraulic conductor will be bounded on the lower side by the aperture value derived through the cubic law. Assuming that the field measurements by /Vermylie and Schulz 1995/ are representative for actual aperture values, it may be realistic to assume that only about 0.1 to 1.0 per cent of the fracture aperture is hydraulic active. This since these field data needs to be decreased by approximate two to three orders of magnitude in order to produce relevant transmissivity values through the cubic law concept (cf Figure A-19 and the line of enhanced 100%). This assumption could be used to place an upper bound for the relationship between transport aperture and transmissivity.

The orange coloured line in Figure A-19 is a relationship proposed by /Rhén et al. 1997/; the green line uses the same relationship but has adopted the general relationship shown in Figure A-14 and based on the compilation shown in Figure A-12.
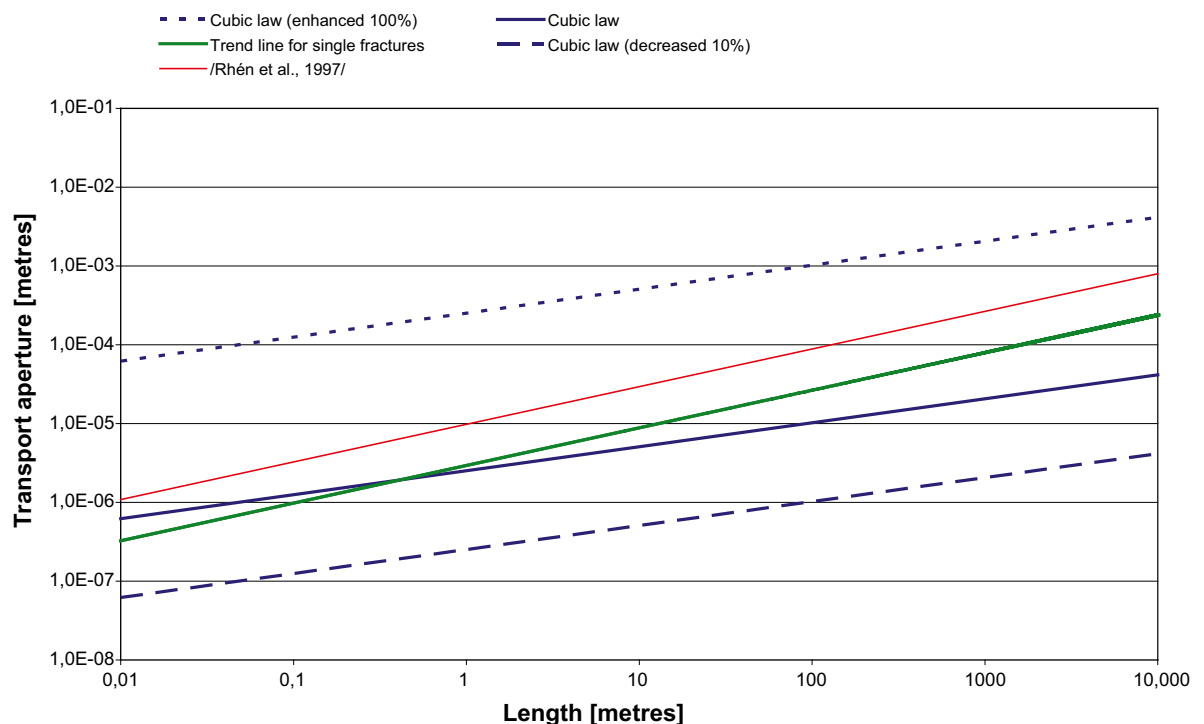

Figure A-19. *Relationship between fracture length and transport aperture. Suggested for features of a scale shorter than 100 metres.*

As a mean of moving between kinematic porosity and transport aperture one needs to assign the hydraulic conductor a geological width. As discussed above this is a bit dubious however for larger structures it may be of interest to assign a width to a fracture zone. Especially the continuum codes may need a volumetric value to assess to a structure in order to assign plausible properties to numerical cells. Figure A-20 presents the result of a scoping comparison between different assumptions that may be used. In earlier versions of DarcyTools the relationship has been assumed to be width equals one hundredth of the length. For small single fractures it is likely that the width coincide with the aperture values back-calculated from the transmissivity of the hydraulic conductor. As discussed previously the field observations of /Vermilye and Scholz 1995/ are of good quality and does, according to /Vermilye and Scholz 1995/, also fit large structures such as mafic dikes. As such it is a good first assumption that these data present some kind of geological width information. Fitting two of the theoretical relationships from /Bonnet et al. 2001/ yielded that the theoretical line for an En Echelon system gives a reasonable fit. However for the known zones at Äspö these relationships all yield too low geological width instead here a L/100 relationship yields a fine approximation of the zones.

Using the latter kind of relationship of the geological width it is possible to move between kinematic porosity and transport aperture, however constrained by the definition of transport aperture.
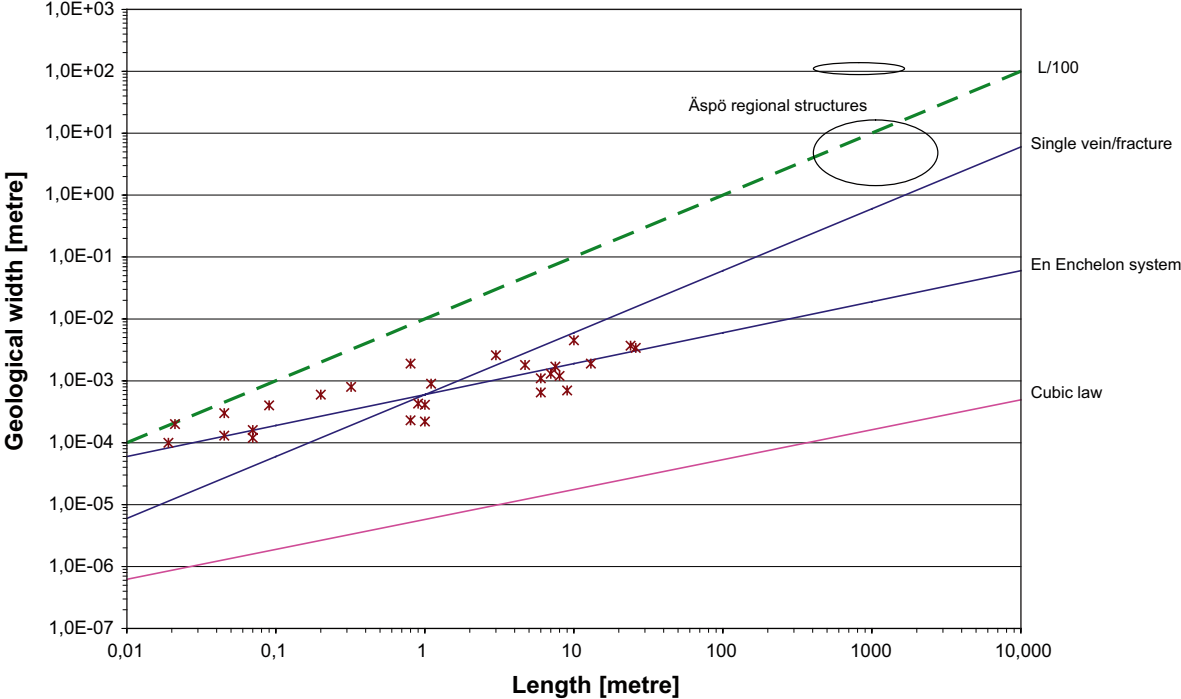

Figure A-20. *Relationship for estimates of the geological width of a hydraulic conductor. The point data represents the data set by /Vermilye and Scholz 1995/.*

5   Tunnel wall conductivity and Baltic Sea bottom conductivity

The tunnel floor, wall, and ceiling is assumed grouted so that no part have a permeability larger than $1 \cdot 10^{-15}$ m^2 /Eriksson and Stille 2005/.

The Baltic Sea bottom has been assigned the same hydraulic conductivity as the bedrock. For the simulations presented herein the Baltic Sea is assigned as a specified head boundary; and as DarcyTools does not contain the option of two groundwater tables a specified head situation makes the omission of a possible low-permeable layer less significant. The treatment of the seabed material and this associated boundary condition is however potentially crucial for getting the correct recharge of water, amount and type, into drained bedrock close to the shoreline.

6 Concluding remarks and recommendations

One unresolved issue in parameterisation of hydraulic features in relation to length is the transition between unique single fractures and fracture zones. Herein we assign structures smaller than 100 metres single fracture properties and for structures larger than 100 metres we assign zone properties.

The compiled data indicate a large scatter and it is recommended that the proposed relationships are used along with some statistic distribution so that one reproduces such a scatter in data. The compilation has not had any possibility to assign any statistical distribution on this scatter and a log-normal distribution may equally well be replaced by a more simple uniform distribution. Again it should be stated that the empirical relationships that are established are local trends valid for the investigated specific data set of Äspö HRL.

Further, there are known and unknown parameters on fracture distributions. It is however important, based on findings herein and also frequently previously observed, that the fractures are described belonging to different sets with different statistical properties for each unique set and especially that fracture intensity is set specific.

In building a model of Äspö HRL the relationships presented below have been used while assigning properties to all hydraulic conductors (fractures) generated within DarcyTools.

Transmissivity [m²/s] versus length [m]:

$T = 1 \cdot 10^{-10} \cdot L^{1.37}$ [L < 100 metres]

$T = 1 \cdot 10^{-09} \cdot L^{1.35}$ [L > 100 metres]

Scatter: two orders of magnitude. Hence data could be expected within four orders of magnitude spread above and below the mean trend line.

Transport aperture [m] versus transmissivity [m²/s]:

$e_T = 1.62 \cdot T^{0.53}$ [L < 100 metres]

$e_T = 960 \cdot T^{0.82}$ [L > 100 metres]

Hydrogeological width [m] versus length [m]:

$W = 6 \cdot 10^{-04} \cdot L^{0.5}$ [L < 100 metres]

$W = 1 \cdot 10^{-02} \cdot L$ [L > 100 metres]

Scatter: one order of magnitude. Hence data could be expected within four orders of magnitude spread above and below the mean trend line.

Specific Storage [1/m] versus Hydraulic conductivity [m/s]:

$S_s = 4 \cdot 10^{-5} \cdot \sqrt[3]{K}$ [L < 100 metres]

$S_s = 1 \cdot K$ [L > 100 metres]

Scatter: three orders of magnitude. Hence data could be expected within four orders of magnitude spread above and below the mean trend line.

The presented data is of course site specific and could only be used for Äspö HRL, however the trend for aperture values with length established at different sites in different parts of the world indicates that at least the slope may be universal but needed to say again the scatter and location of the trend may differ significantly from site to site. Field data indicate that the scatter could be in the order of two to three orders of magnitude within the most common fracture transmissivity values.

An important note is that the established trends not only describe a single fracture transmissivity relationship with that single fracture size. The established trends do also incorporate some kind of large scale connectivity information. That is a large structure is more likely to be connected with other structures and as connected in the long time frame to continuously yield water (overall rock mass hydraulic conductivity).

7 References

Alm P, 1999. Hydro-mechanical behaviour of a pressurised single fracture: an in situ experiment. PhD thesis 1999, Chalmers University of Technology, Göteborg, Sweden, ISBN 91-7197-822-4

Almén K-E, Andersson J-E, Carlsson L, Hansson K, Larsson N-Å, 1986. Hydraulic testing in crystalline rock. A comparative study of single-hole test methods. SKB TR 86-27, Svensk Kärnbränslehantering AB.

Berglund J, Curtis P, Eliasson T, Olsson T, Starzec P, Tullborg E-L, 2003. Äspö Hard Rock Laboratory, Update of the geological model 2002. SKB IPR-03-34, Svensk Kärnbränslehantering AB.

Birgersson L, Gale J, Hakami E, 2000. Äspö HRL First True stage Pilot resin experiment summary report. SKB IPR-00-04, Svensk Kärnbränslehantering AB.

Bonnet E, Bour O, Odling N, Main I, Berkowitz B, Davy P, Cowie P, 2001. Scaling of fracture systems in geological media. Review of Geophysics, Vol. 39, pp347–383.

Dossier Granite 2005 Tome. Analyse de sûreté du stockage géologique, Figure 6.1–21 – page 165, Juin 2005 – ANDRA The report is available on-line (in French).

Eriksson M, Stille H, 2005. Cementinjektering I hart berg Rapport K22 SveBeFo – Stiftelsen Svensk Bergteknisk Forskning, Stockholm (in Swedish).

Follin S, Stigsson M, Svensson U, 2004. Variable-density groundwater flow simulations and particle tracking – Numerical modelling using DarcyTools Preliminary site description of the Simpewarp area – version 1.1. SKB R-04-65, Svensk Kärnbränslehantering AB.

Follin S, Stigsson M, Svensson U, 2006. Hydrogeological DFN modelling using structural and hydraulic data from KLX04, Preliminary site description Laxemar subarea – version 1.2. SKB R-06-24, Svensk Kärnbränslehantering AB.

Gale J, 1990. Hydraulic behaviour of rock joints, In Rock joints, pp 351-362, Balkema, Rotterdam, Holland.

Gudmundsson A, 2000. Fracture dimensions, displacements and fluid transport, Journal of structural geology, Vol. 22, pp 1221–1231.

Hakami E, 1995. Aperture distribution of fractures, PhD thesis, Division of Geology, Department of Civil and Environmental Engineering, Royal Institute of Technology, Stockholm, Sweden,

Hakami E, Larsson E, 1996, Aperture measurement and Flow experiments on a single natural fracture, International journal of rock mechanicals and mining sciences, Vol. 33, No. 4, pp 395–404.

Hermansson J, Nilsson P, Nyberg G, Winberg A, 2002. True Block Scale Updating of structural-hydraulic model and compilation of scoping data set. SKB IPR-02-13, Svensk Kärnbränslehantering AB.

Johansson M, Stephansson O, 1998. Determination of in-situ fracture apertures from digital borehole images, Proceedings of the 3rd Äspö International Seminar. SKB TR-98-10, 367–373, Svensk Kärnbränslehantering AB.

Magnor B, 2005. Site geologist Äspö HRL, personal communication and distributed illustrations.

Niemi A, Kontio K, Kuusela-Lahtinen A, Poteri A, 2000. Hydraulic characterization and upscaling of fracture networks based on multiple-scale well test data. Water Resources Research, Vol. 36, No. 12, Pages 3481–3497.

Odling N E, 2001. The scaling of hydraulic conductivity in rock fracture zones, Geophysical research letters, Vol. 28, No. 15, pp 3019–3022.

Olson J E, 2003. Sublinear scaling of fracture aperture versus length: An exception of the rule?, Journal of Geophysical research, Vol. 108, No. B9, 2413.

Olsson R, 1998. Mechanical and hydromechanical behaviour of hard rock joints, a laboratory study, PhD thesis, Chalmers University of Technology, Göteborg, Sweden, ISBN 91-7197-748-1.

Pollard D D, Segall P, 1987. Theoretical displacement and stresses near fractures in rock: With applications to fault, joints, veins, dikes and solution surfaces, In Fracture mechanics of rock, pp 277–350. Academic, San Diego, California, USA.

Rhén I, Gustafsson G, Stanfors R, Wikberg P, 1997. Äspö HRL – Geoscientific evaluation 1997/5 Models based on site characterization 1986–1995. SKB TR 97-06, Svensk Kärnbränslehantering AB.

Rhén I, Forsmark T, 2001. Äspö Hard Rock Laboratory, Prototype Repository, Hydrogeology, Summary report of investigations before the operation phase. SKB IPR-01-65, Svensk Kärnbränslehantering AB.

Rhén I, Follin S, Hermansson J, 2003. Hydrogeological Site Descriptive Model – a strategy for its development during Site Investigations. SKB R-03-08, Svensk Kärnbränslehantering AB.

Rutqvist J, Stephansson O, 2003. The role of hydromechanical coupling in fractured rock engineering, Hydrogeological Journal (2003), 11:7-40.

SKB 2006. Preliminary site description. Laxemar subarea version 1.2. SKB R-06-10, Svensk Kärnbränslehantering AB.

Smellie J, Waber H N, Frape S K, 2003. Matrix fluid chemistry experiment Final report June 1998 – March 2003. SKB TR-03-18, Svensk Kärnbränslehantering AB.

Stigsson M, Outters N, Hermansson J, 2001. Äspö Hard Rock Laboratory Prototype Repository Hydraulic DFN model no:2. SKB IPR-01-39, Svensk Kärnbränslehantering AB.

Stratford R G, Herbert A W, Jackson C P, 1990. A parameter study of the influence of aperture variation on fracture flow and the consequences in a fracture network. In Rock Joints, pp 413–422, ISBN 9061911095, A.A Balkema, Rotterdam, Netherlands.

Svensson U, 1999. A laboratory scale analysis of groundwater flow and salinity distribution in the Äspö area. SKB TR-99-24, Svensk Kärnbränslehantering AB.

Ushida M, Doe T, Derschowtz W, Thomas A, Wallmann P, Sawada A, 1994. Discrete-fracture modelling of the Äspö LPT-2, large-scale pumping and tracer test. SKB International cooperation report 94-09, Svensk Kärnbränslehantering AB.

Vermilye J M, Scholz C H, 1995. Relation between vein length and aperture, Journal of structural geology, Vol. 17, No. 3, 423–434.

Vidstrand, P, 1999. Hydrogeological scale effects in Crystalline rocks, Comparison of field data from Äspö HRL with data from predictive upscaling methods, Licentiate thesis 1999, Chalmers University of Technology, Göteborg, Sweden, ISSN 1104-9839.

Vidstrand, P, 2003, Äspö Hard Rock Laboratory, Update of the hydrogeological model 2002, SKB IPR-03-35, Svensk Kärnbränslehantering AB.

Weiss et al. 2004. In: Proceedings of the second international symposium on: Dynamics of fluids in fractured rock. February 10-12 2004. Edited by Boris Faybishenko and Paul A. Witherspoon. Earth Science Division, Berkeley, California, USA.

Description of the different end-members identified from interpretations of groundwater chemistry and mixing models; results from Äspö and Laxemar area

Bill Wallin, Geokema

Marcus Laaksoharju, Geoprint AB

Eva-Lena Tullborg, Terralogica AB

October 2007

Contents

1 Background

The hydrogeochemical evaluation approach being used in this study is based on some 25 years of collective experience within the SKB waste management programme /Smellie and Laaksoharju 1992, Laaksoharju et al. 1995, Laaksoharju and Wallin 1997, Laaksoharju et al. 2004/. During this time sampling procedures, analytical methods, hydrochemical concepts and model development have evolved through a continuous process of modification and refinement, a process which is ongoing at present. Several key issues addressed over the years which have helped steer the direction of the on-going hydrogeochemical evaluation include:

- Understanding the post-glacial evolution of the Swedish east coastal margin and the Baltic Sea /Wallin 1995/. For example, to bear in mind the possibility of finding residual groundwater components in the bedrock introduced during the Quaternary period, in particular during Holocene times. Groundwater components may include glacial melt water introduced during ice degradation and retreat, and the introduction of marine/non-marine waters during periodic transgressions driven by the isostatic recovery of the land mass.

- The use of fracture mineral phases as potential palaeomarkers was recognised, in particular the value of calcite, Fe-oxyhydroxides and to a lesser extent pyrite in establishing redox front evolution during and since the last glaciation /e.g. Tullborg 1989/.

- Because of the successive introduction of different water types into the bedrock during the Holocene and their subsequent complete or partial removal by flushing out by later introduced water types, groundwater mixing tends to dominate over water-rock reactions in the upper 250–500 m. The mixing depths are dependent on local hydrological conditions.

- Because mixing was a major mechanism in explaining present groundwater chemistry and distribution, this led to the development of the M3 modelling approach /Laaksoharju et al. 1995/ and /Laaksoharju et al. 1999/.

Since hydrogeology and hydrogeochemistry deal with the same geological and hydrodynamic properties, these two disciplines will complement each other when describing/modelling the groundwater system. The simulation of groundwater flow over a period in the past introduces a challenge that tests our understanding of the site-scale hydrogeological flow concept. Hydrogeochemical information may provide a means of improving the credibility of the site-scale groundwater flow model. This approach may be useful over well-known period of time, because conservative hydrogeochemical parameters in particular contain a record of cumulative changes. The degree of progressive mixing between water masses is a characteristic of groundwater movement, which is exposed more clearly in hydrochemistry than is possible from physical measurements alone. The advantages with such an approach were identified as follows:

- Hydrogeological models will be constrained by a new data set. If, as an example, the hydrogeological model, which treats advection and diffusion processes in highly heterogeneous media, cannot produce any meteoric water at a certain depth and the hydrogeochemical data indicate that there is a certain fraction of this water type at this depth, then the model parameters and/or processes have to be revised.

- Hydrogeological models are fully three dimensional and transient processes such as shoreline displacement and variable-density flow can be treated, which means that the spatial variability of flow-related hydrogeochemical processes can be modelled, visualised and communicated. In particular, the role of the nearby borehole hydraulic conditions for the chemical sampling can be described.

- Hydrogeochemical models generally focus on the effects from reactions on the obtained groundwater rather than on the effects from transport. An integrated modelling approach can describe flow directions and hence help to understand the origin of the groundwater. The turnover time of the groundwater system can indicate the age of the groundwater and, knowing the flow rate, can be used to indicate the reaction rate. The obtained groundwater chemistry is a result of reactions and transport, and therefore only an integrated description can be used to correctly describe the measurements.

- By comparing two independent modelling approaches, a consistency check can be made. As a result greater confidence in active processes, geometrical description and material properties can be gained.

The following data sources are available for groundwater chemistry and fracture minerals of importance for palaeohydrogeological interpretations:

- Stable isotope analyses (water, calcite, minerals)

- Radioactive isotopes (water and calcite)

- Radiogenic isotope analyses (water, calcite and other minerals)

- Chemical analyses (water and minerals)

- Laser probe analyses (calcite and other minerals)

- INAA analyses

- ICP analyses

- Fluid inclusion measurements

- M3 modelling

Mineralogical data can only used to support the interpretations but can usually not be used to identify end-members.

2 Summary of groundwater characteristics

2.1 Meteoric water

Meteoric water is defined as rainwater or snow recharging the basement rock with and $\delta^{18}O$ and δ^2H isotope characteristic that projects along the global meteoric water line (MWL). The water is of a Na-HCO$_3$ rich water type. The chemical and isotopic characteristics are given in the table below.

Cl (mg/L)	Na (mg/L)	K (mg/L)	Ca (mg/L)	Mg (mg/L)	HCO$_3$ (mg/L)	SO$_4$ (mg/L)	3H (TU)	δ^2H‰	$\delta^{18}O$‰
0.23	0.4	0.29	0.24	0.1	12.2	1.4	2,000*	−80	−10.5

*Within the M3 modelling the sampled modern meteoric water was given a high tritium (2,000 TU) for modelling purposes.

2.1.1 Basic facts (average values representative for the end-member)

- Chloride: 0.23 mg/L
- Bromide: below detection limit
- Br/Cl ratio: 0
- TDS (sum of ions): 20.89 mg/L
- Density: 0.998 g/ml
- $\delta^{18}O$ signature: –10.5‰

2.1.2 Maximum penetration depth

The maximum penetration depth documented for meteoric water at Laxemar is 800–1,000 m (ongoing site investigation indicate a penetration depth of 400–500 m), and at Äspö 100–150 m. These values are deduced from the following observations:

- Observed dilute groundwater (Cl <10 mg/L) of a Na-HCO$_3$ type.
- Observed $\delta^{18}O$ signature of –10 to −11‰ in groundwater at Äspö and Laxemar.

2.1.3 Maximum and minimum age

The freshwater lens at Laxemar started to form after the glaciation but at Äspö the formation is governed by land up-lift process and started to form about 3,000 years ago when Äspö was elevated above the sea level.

2.1.4 Origin of water and salt

Meteoric water originates from evaporation of ocean water and condensation at site or from contribution of local run-off surface waters.

2.1.5 Conceptual models

Conceptual models for the present day infiltration of Meteoric water (B-1) and the major water types and major reactions at Laxemar (Figure B-2) and at Äspö after the HRL construction phase (Figure B-3) /Laaksoharju 2004/.
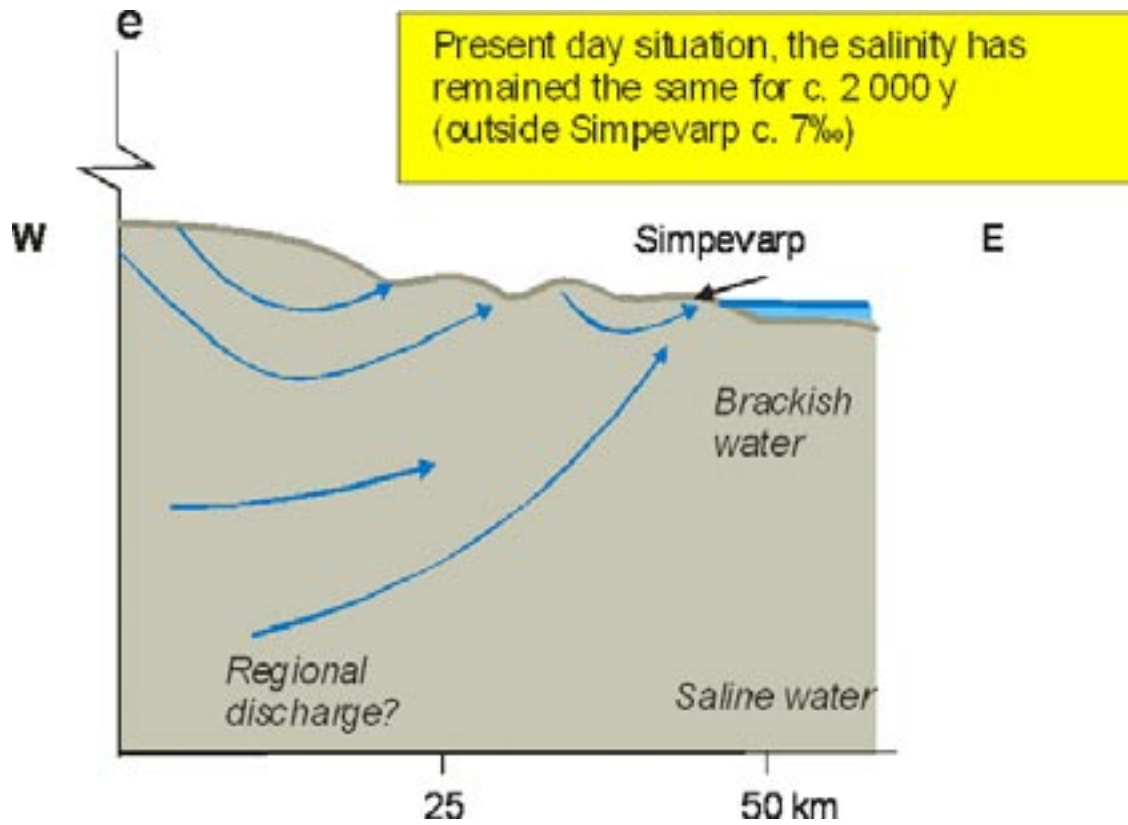
Figure B-1. *Conceptual model for Laxemar and Simpevarp showing the present day influence of meteoric water.*
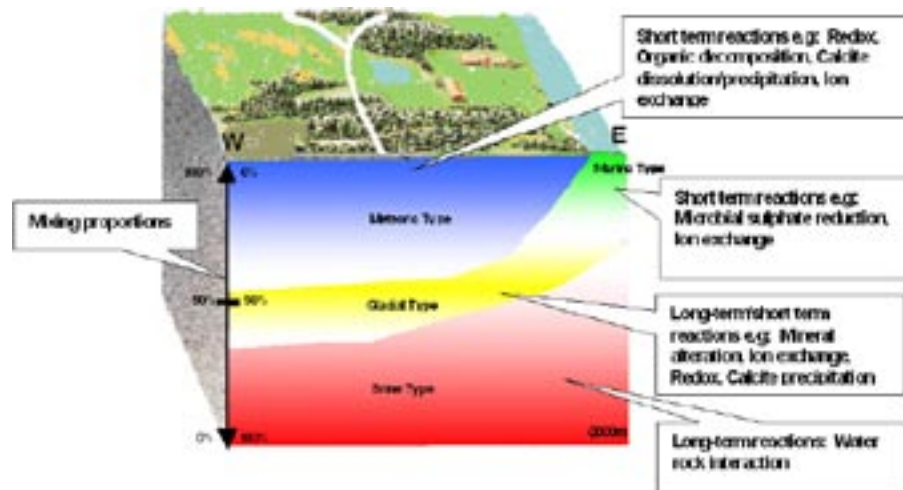

Figure B-2. *Conceptual model showing the development of different water types and major reactions at Laxemar /Laaksoharju et al. 2004/.*
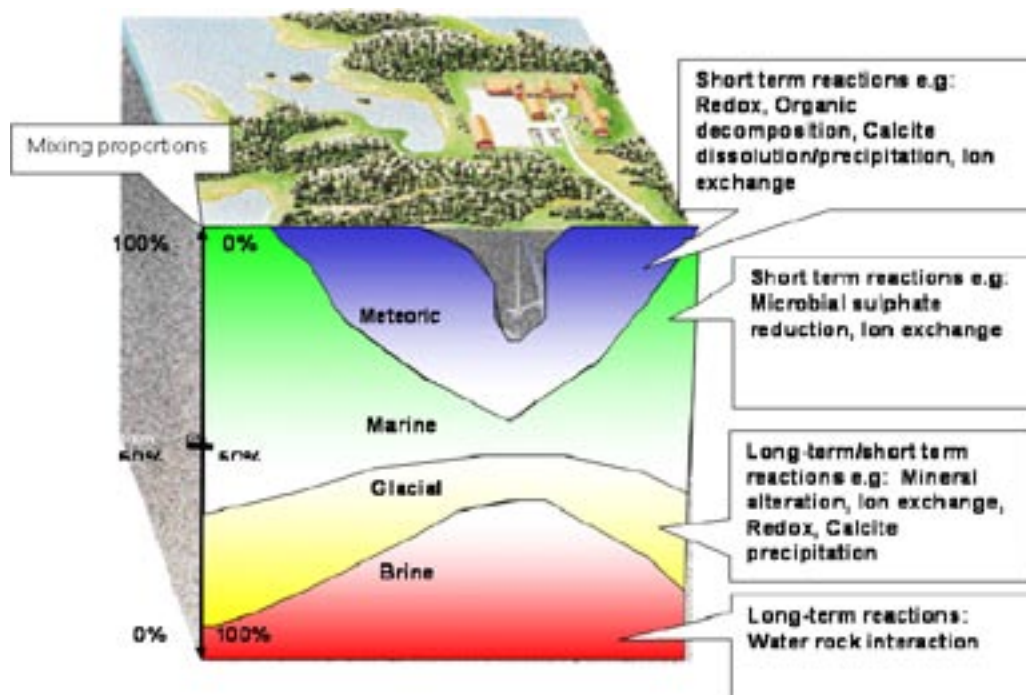
Figure B-3. *Conceptual model showing the development of different water types and major reactions at Äspö after the HRL tunnel construction. /Laaksoharju et al. 2004/.*

2.1.6   Parameter recommendations

The strongest parameter for meteoric water is $\delta^{18}O$ and a low TDS value.

2.2   Baltic Sea water

The Baltic Sea water is characterized by a Cl concentration of 3,750 mg/l and a Br/Cl ratio of typical marine signature, 3.40×10^{-3}. The Baltic Sea water characteristics observed at Äspö/ Laxemar is similar to those found outside Äspö in the sea, although variations may occur. The water is characterized as a Na-Cl rich water type. The water is isotopically defined /Wallin and Peterman 1999/. The general chemical and isotopic characteristics are given in the table below.

Cl (mg/L)	Na (mg/L)	K (mg/L)	Ca (mg/L)	Mg (mg/L)	HCO₃ (mg/L)	SO₄ (mg/L)	3H (TU)	δ²H‰	δ¹⁸O‰
3,750	1,960	95	93.7	234	90	325	20	−53.3	−5.9

2.2.1   Basic facts (average values representative for the end-member)

- Chloride: 3,760 mg/L
- Bromide: 12.8 mg/L
- Br/Cl ratio: 3.40×10^{-3}
- TDS=f (sum of ions): 6,615 mg/L
- Density: 1.0015 g/ml
- $\delta^{18}O$ signature: −5.9‰
- $^{87}Sr/^{86}Sr$: 0.7092

2.2.2 Maximum penetration depth

Baltic Sea water interacts with meteoric water at the coast of Laxemar and Simpevarp driven by changes in seawater level due changes in pressure and wind. At Äspö penetration can occur along the fracture zones (100–150 m) driven by the hydraulic sink from Äspö HRL.

2.2.3 Maximum and minimum age

Taking into account the past evolution of the site, the interpreted age is post-Littorina to present day.

2.2.4 Origin of water and salt

Most of the salinity is from Ocean water which was mixed with meteoric run off water in the Baltic Sea.

2.2.5 Conceptual models

The marine water (Baltic Sea), other water types and major reactions at Laxemar is shown in Figure B-2 and for Äspö after the HRL construction phase in Figure B-3 /Laaksoharju 2004/.

2.2.6 Parameter recommendations

The strongest parameter for Baltic Sea water is $\delta^{18}O$ and Cl and Cl/Br.

2.3 Littorina water

The Littorina water was characterized by a Cl concentration of 6,500 mg/l and a Br/Cl ratio of typical marine signature, 2×10^{-3}. The water is of a Na-Cl rich water type. The general chemical and isotopic characteristics are given in the table below.

Cl (mg/L)	Na (mg/L)	K (mg/L)	Ca (mg/L)	Mg (mg/L)	HCO$_3$ (mg/L)	SO$_4$ (mg/L)	3H (TU)	δ^2H‰	δ^{18}O‰
6,500	3,674	134	151	448	93	890	0	−38	−4.7

2.3.1 Basic facts (average values representative for the end-member):

- Chloride: 6,500 mg/L
- Bromide: 22.2 mg/L
- Br/Cl ratio: 3.41×10^{-3}
- TDS (sum of ions): 12,061 mg/L
- Density: 1.005 g/ml
- $\delta^{18}O$ signature: −4.7‰
- $^{87}Sr/^{86}Sr$: 0.7092

2.3.2 Maximum penetration depth

Littorina signatures are found at depth down to 500 m.

2.3.3 Maximum and minimum age

The Littorina stage lasted between 7,500 BC and 1,000 years BC with maximum salinity estimated at about 4,500–2,000 BC.

2.3.4 Origin of water and salt

Marine water observed today is most likely Littorina water. Most of the salinity was from Ocean water which was mixed with meteoric run off water in the Baltic Sea.

2.3.5 Conceptual models

Conceptual models for the Littorina Sea water penetration at Laxemar and Simpevarp (Figure B-4). The Littorina sea water, other water types and major reactions at Laxemar is shown in Figure B-2 and for Äspö after the HRL construction phase in Figure B-3 /Laaksoharju 2004/.

2.3.6 Parameter recommendations

The strongest parameter for Littorina Sea water is $\delta^{18}O$ and Cl and Cl/Br and Mg.
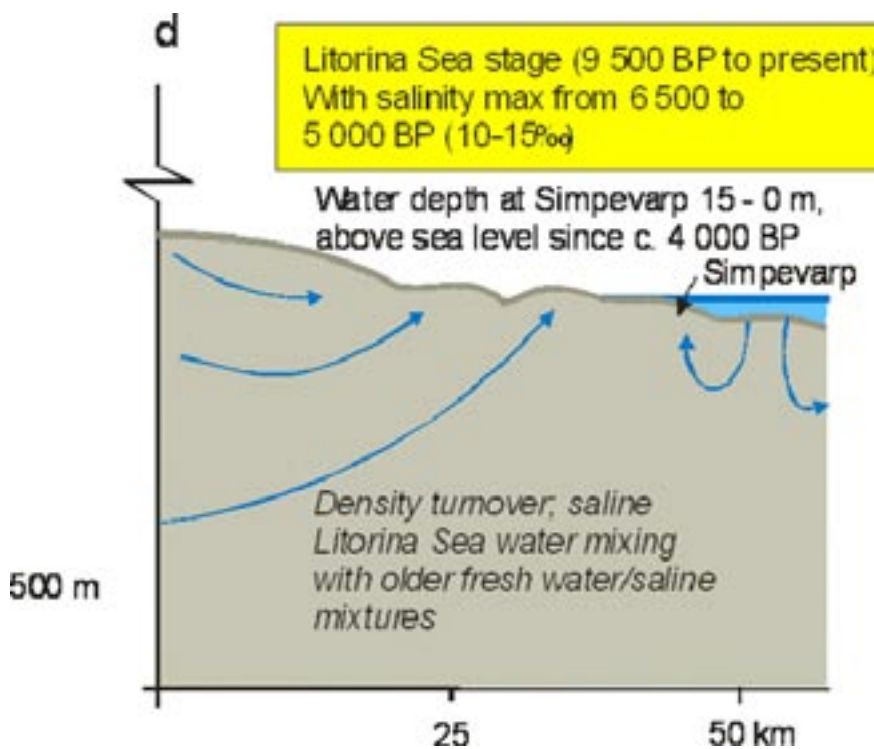
Figure B-4. *Conceptual model for Laxemar and Simpevarp showing the penetration due to density turnover of Littorina sea water.*

2.4 Glacial water

Glacial water is defined as meltwater from glacial ice sheets formed during the Pleistocene and Holocene. This water represents a possible melt-water composition from the last glaciation > 11,000 BC. The δ^2H value (−158‰ SMOW) is a calculated value based on the equation ($\delta H = 8 \times \delta^{18}O + 10$) for the meteoric water line. The water is a diluted K-Ca-SO$_4$ water type. The brine is isotopically defined (Wallin and Peterman, 199). The chemical and isotopic characteristics are given in the table below.

Cl (mg/L)	Na (mg/L)	K (mg/L)	Ca (mg/L)	Mg (mg/L)	HCO$_3$ (mg/L)	SO$_4$ (mg/L)	3H(TU)	δ²H‰	δ¹⁸O‰
0.5	0.17	0.4	0.18	0.1	0.12	0.5	0	−158*	−21*

* Modern sampled glacial melt water from Norway was used for the major elements and the δ¹⁸O isotope value (−21‰ SMOW) was based on measured values of δ¹⁸O in calcite surface deposits /Tullborg and Larsson 1984/.

2.4.1 Basic facts (average values representative for the end-member):

- Chloride: = 0.5 mg/L
- Bromide: below detection limit
- Br/Cl ratio: –
- TDS (sum of ions): 2.95 mg/L
- Density: 0.995 g/ml
- $\delta^{18}O$ signature: −21‰

2.4.2 Maximum penetration depth

Signs of glacial water proportions at 200–1,000 m depth at Laxemar and between 100–840 m at Äspö.

2.4.3 Maximum and minimum age

Taking into account the past evolution of the region, glacial water and run-off water from postglacial period have a maximum age at Äspö of about 12,000 BC and a minimum age of 7,500 BC (prior to Littorina water) which implies:

- Low ^{14}C content ("ages" older than 12,000 BC)
- Tritium free waters

2.4.4 Origin of water and salt

The processes involved in formation of glacial water are, evaporation of preferentially seawater, condensation and precipitation according to the sequence – water vapor – rain – snow – firn – ice – and finally melting and penetration into the basement rocks. The penetration into the basement rocks is mainly governed by the hydrostatic pressure of the ice overburden /Svensson 1996/ according to the conceptual model at Äspö (see, Figure B-5).

2.4.5 Conceptual models

Conceptual models for the glacial water penetration at Laxemar and Simpevarp (Figure B-5). The glacial water, other water types and major reactions at Laxemar is shown in Figure B-2 and for Äspö after the HRL construction phase in Figure B-3 /Laaksoharju 2004/.

2.4.6 Parameter recommendations

The strongest parameter for glacial water is $\delta^{18}O$ and the low TDS value. Carefully consider the density-temperature relation for the recharging glacial water.

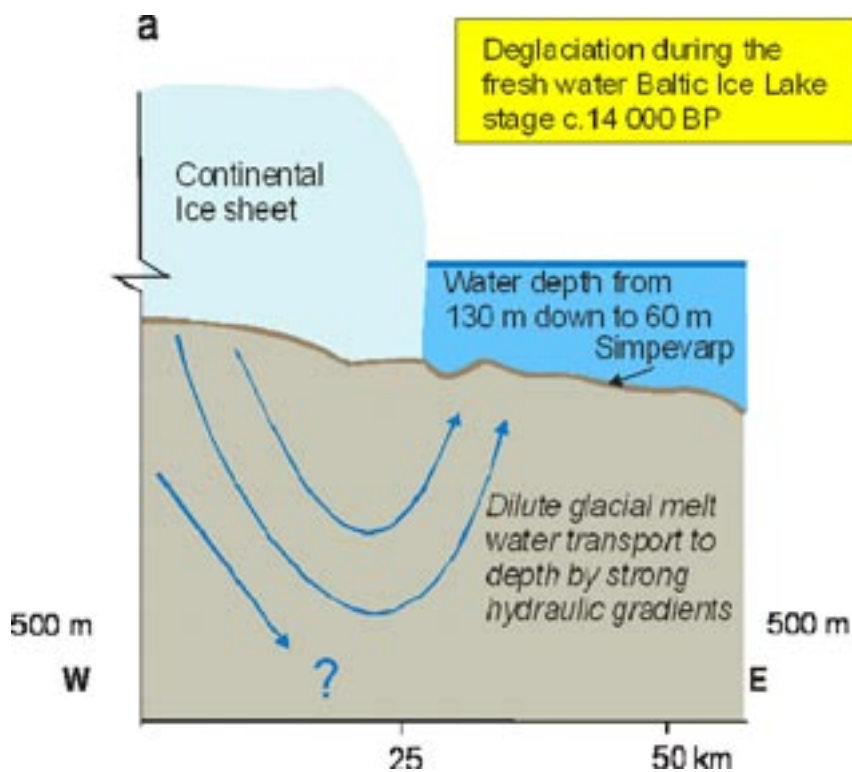**Figure B-5.** *Conceptual model for Laxemar and Simpevarp showing the penetration of glacial water.*

2.5　Brine

Brine water is defined as a water with a "considerably higher salinity" /Alley 1993, Frape et al. 1984, Frape and Fritz 1987/ than seawater which contains ~ 20,000 mg/l Cl. The brine sample from Laxemar close to Äspö (47,200 mg/l, Cl) meets that requirement. In many international publications a brine is defined by a 100,000 TDS. The "Äspö brine" is therefore more dilute compared with some definitions. In the following text the term 'Brine' refers always to the Äspö brine salinity of 47,200 mg/l Cl. The water is characterized as a Ca-Na-Cl rich water type and represents the sampled water found in KLX02: 1,631–1,681 m /Laaksoharju et al. 1995/. The general chemical and isotopic characteristics are given in the table below.

Cl (mg/L)	Na (mg/L)	K (mg/L)	Ca (mg/L)	Mg (mg/L)	HCO$_3$ (mg/L)	SO$_4$ (mg/L)	3H (TU)	δ^{2}H‰	δ^{18}O‰
47,200	8,500	45.5	19,300	2.12	14.1	906	0	−44.9	−8.9

2.5.1　Basic hard facts (average values representative for the end-member)

- Chloride: 47,200 mg/L
- Bromide: 323.6 mg/L
- Br/Cl ratio: 6.85×10^{-3}
- TDS = f(sum of ions): 78,652 mg/L
- Density: 1.058 g/ml
- δ^{18}O signature: −8,9‰
- ^{87}Sr/^{86}Sr: 0.71850

2.5.2 Maximum/minimum observation depth

At depths below 1,000–1,200 m the Brine groundwater mixing portion starts to play an important role at Laxemar, although possibly already at 800 m depth at Äspö.

2.5.3 Maximum and minimum age

Age determination by ^{36}Cl suggests ages more than 1.5 million years.

2.5.4 Origin of water and salt

The salt is interpreted to be dissolved salts from e.g. rock formation fluids, water rock interaction processes and sedimentary rocks. The significant deviation from MWL (δ^{18}O = −10.4 to −8.9‰; δ^{2}H −60.2 to −44.9‰) is ascribed to water/rock interaction during long periods of time. This is supported by ^{87}Sr/^{86}Sr data in the groundwater which are typical for crystalline basement brines. Additional support by δ^{34}S isotope signatures of dissolved sulphate in groundwater (+ 10‰) typical of rock sulphur source and/or possible dissolved evaporates (gypsum).

2.5.5 Conceptual models

The Brine water, other water types and major reactions at Laxemar is shown in Figure B-2 and for Äspö after the HRL construction phase in Figure B-3 /Laaksoharju 2004/.

2.5.6 Parameter recommendations

The strongest parameter for brine water is the high TDS, Cl value and Br/Cl ratio.

3 Supporting evidences from fracture mineralogy

Palaeohydrogeological studies using fracture coatings have been carried out on Äspö /Wallin and Peterman 1999, Bath et al. 2000, Milodowski et al. 2005/ and at Laxemar/Simpevarp /Tullborg and Wallin 1991, Tullborg 2004, Drake and Tullborg 2007/ (Drake et al. in manuscript). These studies have concentrated on calcite fracture coatings since these are present in many fractures and also can be precipitated during very different physiochemical conditions. Stable isotopes ($\delta^{18}O$ and $\delta^{13}C$) in combination with crystal morphology, fluid inclusion, and chemical composition and Sr isotope ratios have been used in order to reveal the formation conditions and the origin of the fluids from which the calcites precipitated.

Large amounts of the calcites found in the fractures of the region are of hydrothermal origin (co-precipitated with hydrothermal minerals like epidote, prehnite and laumontite), which means that these calcites are old and can not be related to any groundwaters found in the bedrock today.

Calcite precipitated from brine solutions at elevated temperatures (100 to 150°C) are common in fractures of the area and are related to Palaeozoic conditions. Because many of these fractures are still water conducting it is indicated that they have had a long history including at least intermittent groundwater circulation. Many calcites of these type show therefore later overgrowth of low temperature calcites.

Calcites with a supposed low temperature origin are found as thin coatings or small crystals on the outermost layer of the fracture coatings. The amount of this type of calcite is very small which put a strict limit to analytical possibilities. Stable isotopes (O, C) and morphology (when euhedral crystals) and in some cases Sr isotope ratios are the methods that have been possible to use. Nevertheless, several different formation conditions have been possible to determine. These are:

1) Precipitation from a Meteoric water with similar isotopic composition as present precipitation. (The fresh water origin of the precipitates determined from morphology).

2) Precipitates from brackish to saline water similar to present Baltic Sea water.

It is however, very few calcite samples that show both $\delta^{18}O$ and Sr isotope values in equilibria with present waters, which indicates that similar conditions have occurred in the past (probably repeatedly) but the amounts of calcites produced in postglacial.

4   Summary and conclusions

This study provides a summary of essential hydrogeochemical information important for the integration with hydrogeological modelling. Knowlage from water chemistry, and hydrogeo-chemical mixing modeling has been used to provide the appropriate end-member composition affecting the groundwater system.

The water types found at Äspö are:

Meteoric water type – is defined as rainwater or snow recharging the basement rock with and $\delta^{18}O$ and δ^2H isotope characteristic that projects along the global meteoric water line (MWL). The water is of a $Na-HCO_3$ rich water type.

Baltic Sea water – is characterized by a Cl concentration of 3,750 mg/l and a Br/Cl ratio of typical marine signature. The Baltic Sea water characteristics observed at Äspö/Laxemar is similar to those found outside Äspö in the sea, although variations may occur. The water is characterized as a Na-Cl rich water type.

Littorina Sea water was characterized by a Cl concentration of 10,000 mg/l and a Br/Cl ratio of typical marine signature, 2×10^{-3}. The water is of a Na-Cl rich water type.

Glacial water component – Glacial water is defined as meltwater from glacials formed during the Pleistocene and Holocene. Represents a possible melt-water composition from the last glaciation > 13,000 BP. The δ^2H value ($-158‰$ SMOW) is a calculated value based on the equation ($\delta H = 8 \times \delta^{18}O + 10$) for the meteoric water line. The water is a diluted $K-Ca-SO_4$ water type.

Brine water is defined as a water with a "considerably higher salinity" than seawater which contains ~ 20,000 mg/l Cl. The brine sample from Laxemar (47,200 mg/l, Cl) meets that requirement. The water is characterized as a Ca-Na-Cl rich water type and represents the sampled water found in KLX02: 1,631–1,681 m.

The groundwater ages are still uncertain, however, there is possible to delineate relative ages between the different waters residing now at Äspö, where Brine water is the oldest (> 1.5 MA). Glacial water is introduced ≥ 12,000 BC in the basement rocks, followed by Marine water such as Littorina about 4,500–2,000 BC and postglacial precipitation as Meteoric water starting about 1,000 BC.

5 References

Alley W M (ed.), 1993. Regional groundwater quality. Van Nostrand Reinhold, New York, USA, pp 634. ISBN 0-442-00937-2.

Bath A, Milodowski A, Ruotsalainen P, Tullborg E-L, Cortés Ruiz A, J-F A, 2000. Evidences from mineralogy and geochemistry for the evolution of groundwater systems during the quaternary for use in radioactive waste repository safety assessment (EQUIP project). pp. EUR report 19613.

Drake H, Tullborg E-L, 2007. Paleohydrogeology of the Simpevarp area, southeastern Sweden, as evidenced by stable isotopes in fracture minerals. In: Bullen, T.D. and Wang, Y. (Eds), Water-Rock Interaction: Proceedings of the 12th International Symposium on Water-Rock Interaction WRI-12. Taylor & Francis, London, pp. 723–726.

Frape S K, Fritz P, McNutt R H, 1984. The role of water-rock interaction in the chemical evolution of groundwaters from the Canadian shield. Geochim. et Cosmochim. Acta, 48:1617-1627.

Frape S K, Fritz P, 1987. Geochemical trends for groundwaters from the Canadian shield. In: Fritz, P. and Frape, S. K, Saline water and gases in crystalline rocks. Geol. Assoc. of Canada Spec. Pap, 33:19-38.

Laaksoharju M, Smellie J, Nilsson A-C, Skårman C, 1995. Groundwater sampling and chemical characterisation of the Laxemar deep borehole KLX02. SKB TR 95-05, Svensk Kärnbränslehantering AB.

Laaksoharju M, Wallin B, 1997. Evolution of the groundwater chemistry at the Äspö Hard Rock Laboratory. Proceedings of the second Äspö International Geochemistry Workshop, June 6-7. SKB Progress Report PR HRL-97-25, Svensk Kärnbränslehantering AB.

Laaksoharju M, Skårman C, Skårman E, 1999. Multivariate Mixing and Mass-balance (M3) calculations, a new tool for decoding hydrogeochemical information. Applied Geochemistry Vol. 14, #7, 1999, Elsevier Science Ltd, pp 861–871.

Laaksoharju M (Ed), 2004. Project Äspö model 2005: Evolutionary aspects and M3 modelling of the groundwater data from the Äspö area. Arbetsrapport.

Laaksoharju M, Smellie J, Gimeno M, Auqué L, Gómez J, Tullborg E-L, Gurban I, 2004. Hydrogeochemical evaluation of the Simpevarp area, model version 1.1. SKB R-04-16. Svensk Kärnbränslehantering AB.

Laaksoharju M, Gurban I, 2007. Sampling of surface water and shallow groundwater at Laxemar. Possible indicators for interaction between deep groundwater and water in contact with the biosphere. SKB R-07-03. Svensk Kärnbränslehantering AB.

Milodowski A E, Tullborg E-L, Buil B, Gomez P, Turrero M-J, Haszeldine S, England G, Gillespie M R, Torres T, Ortiz J E, Zacharias J, Silar J, Chvatal M, Strnad L, Sebek O, Bouch J E, Chenery S R, Chenery C, Shepherd T J, McKervey J A, 2005. Application of Mineralogical, Petrological and Geochemical tools for Evaluating the Palaeohydrogeological Evolution of the PADAMOT Study Sites. PADAMOT Project Technical Report WP2.

Smellie J A T, Laaksoharju M, 1992. The Äspö Hard Rock Laboratory: Final evaluation of the hydrogeochemical pre-investigations in relation to existing geologic and hydraulic conditions: SKB TR 92-31. Svensk Kärnbränslehantering AB.

Svensson U, 1996. SKB Palaeohydrogeological programme. Regional groundwater flow due to advancing and retreating glacier-scoping calculations. In: SKB Project Report U 96-35. Svensk Kärnbränslehantering AB.

Tullborg E-L, Larson S Å, 1984. d18O and d13C for limestones,calcite fissure infillings and calcite precipitates from Sweden. Geologiska Föreningens i Stockholm Förhandlingar, 106, 127–130.

Tullborg E-L, 1989. The influence of recharge water on fissure-filling minerals – A study from Klipperås, southern Sweden. Chemical Geology, 76, 309–320.

Tullborg E -L, Wallin B, 1991. Stable isotope studies of calcite fracture fillings (^{18}O, ^{13}C and groundwaters (^{18}O, D). In: Tullborg, E-L, Wallin, B, and Landström, O, Hydrogeochemical studies of fracture minerals from water conducting fractures and deep groundwaters at Äspö. SKB Progress Report, 25-90-01, 1-24. Svensk Kärnbränslehantering AB.

Tullborg E-L, 2004. Palaeohydrogeological evidences from fracture filling minerals – Results from the Äspö/Laxemar area, Mat.Res.Soc.Symp.Proc. Vol 807, 2004. Pages 873–878.

Wallin B, 1995. Palaeohydrological implications in the Baltic area and its relation to the groundwater at Äspö, south-eastern Sweden – A literature study, SKB Technical Report, 95-06, 1-68. Svensk Kärnbränslehantering AB.

Wallin B, Peterman Z E, 1999. Synopsis of strontium isotope variations in groundwater at Äspö, southern Sweden, App. Geochem. 14, pp 939–951.

Dispersion and mixing in fractured rocks

Influence on saltwater profiles in deep fractured rocks

Ivars Neretnieks, Department of Chemical Engineering and Technology
Royal Institute of Technology, KTH

Drafted July 2003
Revised April 2006

Abstract

Salt water that has been present in the fractured rocks in Sweden since the last ice age is gradually washed out by intruding fresh meteoric water. The infiltrating water dispels the saltwater in the fractures at different rates in different flowpaths. Fast paths will be washed out earlier than slow paths. The three dimensional flowpaths are very complex in the fractured rock as are the mixing processes. It is a wish to use observations of salt water profiles to validate hydrological models used in performance assessment. However, it is recognised that there are a number of processes that give rise to complex displacement and mixing processes, which must be understood in order to correctly interpret the observed salt water profiles. This report addresses those processes that are deemed to have some influence on the mixing and displacement processes and attempts to assess their relative importance.

Sammanfattning

Saltvatten som har funnits i bergssprickor sedan senaste istiden tvättas långsamt ut av regnvatten. Färskvattnet undantränger saltvattnet från sprickorna olika fort i olika flödesvägar. Snabba flödesvägar tvättas ut fortare än långsamma. Flödesvägarna och blandningsmekanismerna är komplexa i det tredimensionella nätverket av kanaler i sprickorna i berget. Det har föreslagits att observerade saltvattengradienter skulle kunna användas för att validera hydrologiska modeller i säkerhetsanalysen. För att detta skall kunna göras måste man känna till och förstå de olika processerna som påverkar blandning mellan och förträngning av salt och sötvatten. Denna rapport går igenom de viktigaste processerna och söker belysa deras relativa betydelse.

Executive summary

Old salt water in deep lying fractured rock systems will be displaced by fresh intruding rainwater. The old water is present in the fractures and fracture zones of the rock and, more importantly, also in the micropores of the rock matrix itself. The latter water volume is 20 to 100 times larger than the water volume in the flowing fractures. It is deemed that the freshwater circulation started mainly at the end of the last ice age some 5,000 to 10,000 years ago. Old salt water has been found at depth and fresh water in the shallower parts of the rock. However, very complex salt profiles are present because there are large variations of hydraulic transmissivity in the fractures and fractures zones that make up a very complex 3 dimensional network of flowpaths with varying lengths and hydraulic properties. It is thought that the observed salt profiles could be used to validate the hydrologic and transport models that are used in performance assessment.

This report describes the different displacement and mixing processes that take place in flowing fractured systems and attempts to quantify their importance in PA time and distance scales.

The higher density of saltwater will tend to stabilize the saltwater at depth. The less dense freshwater will choose paths closer to the surface unless the hydraulic gradient is large enough to overcome the density difference. Mixing will occur between salt and freshwater over the joint interface. The mixing is caused by molecular diffusion, which is a slow process. Stagnant water in the micropores of the rock matrix will also contribute to the change of the salt content and density of the flowing water. The complex network structure can also have a very large impact on where fresh and salt water boundaries could be located at present.

There is much more water in the matrix pores than there is flowing water in the fractures. Mixing due to molecular diffusion in the matrix of the rock blocks is the by far dominating mixing process between salt and fresh water. This will considerably delay the washing out of the saltwater. In inflow areas scoping calculations suggest that matrix pores in bocks smaller than a few metres will have been depleted of their original salt whereas blocks larger than 10 metres still can have considerable salt concentrations in their interior.

Sample calculations on the effects of different mixing processes are presented. Taylor dispersion, diffusional mixing between streams with different velocities and mixing due to subsurface tidal waves, although probably present, are overshadowed by matrix diffusion effects.

Contents

1   Introduction

Man made tracer tests are in practice difficult to make under natural gradient conditions over distances and times of interest for Performance Assessment (PA) purposes for radioactive waste repositories. There travel distances of 100 to 1,000 m and water travel times of at least ten to many hundreds of years must be considered.

Not only is the travel time of the flowing water of interest but even more so of solutes. Non-sorbing solutes that are carried by the flowing water will enter the rock matrix by molecular diffusion and move up to 20 to 100 times slower than the flowing water. This is because for long residence times of the flowing water it will have time to mix with the stagnant water in the micropores in the rock. If full equilibration with the matrix pore water were to be established the tracer would have time to reside in both the mobile and the immobile water that has 20–100 times larger volume. This effect would be very noticeable in PA time scales but would scarcely be noticeable in man made experiments because only a very small part of the matrix water would have time to mix with the flowing water.

As the matrix diffusion is the by far most important retardation mechanism for the (especially sorbing) radionuclides it is of interest to find long time and distance evidence that supports this.

It has been suggested that the washing out of saltwater from the rock by freshwater after the last ice age could be used to study the extent of the displacement and the various mechanisms involved in displacing and mixing fresh and salt water.

In many deep boreholes it has been found that at shallow depths the water is "fresh" whereas at larger depths the water is saline. The flow patterns are complex because the topography is not simple and because there are large variations in the hydraulic properties of the rock. Fracture zones often have much higher flowrates than the small fractures in the rock mass. A further complication is that in the regions where samples have been obtained there have been considerable changes in hydraulic gradients due to land rise after the last ice age some 5,000 to 10,000 years ago. This has caused changes in flow pattern over time.

The time of interest to consider in this report thus is several thousand years and travel distances of interest are from a few 100 to a several thousand meters. It is expected that the displacement process is not a simple plug flow displacement. There will be mixing between the displacing and the displaced water by several mechanisms and it is expected that there will be a diffuse boundary between the waters.

The aim of this note is to explore some common mixing mechanisms to get information on their impact and which mechanisms may be more important than other. This may aid interpretation of available observations and suggest how new observations could be made.

It will be seen that matrix diffusion effects are expected to be very important as well as the complex network nature of the rock itself for interpretation of the observations.

This report starts with a short section on mixing processes in general, followed by sections on mixing in the flowing water in conduits by molecular diffusion perpendicular to the flow direction. Then follows a section on mixing between streams, across fracture apertures, along fractures and at fracture intersections with the emphasis on how much mixing to expect over different times and distances. Two sections on the consequences of non-mixing between flowpaths and the effects of mixing in complex 3D networks of flowpaths follow. A little section on the possible effects of subsurface tidal waves on mixing is also included. The last but probably most important section is on mixing between mobile and immobile water by diffusion.

In some sections simple examples are used to illustrate the magnitude of the mixing effects in the PA time scale. In some sections conclusions for that section are made.

The main thrust of this note has been to use exploratory scoping calculations to identify the processes that may have a large influence on the mixing processes for PA time scales.

2   Mixing processes and mechanisms

Mixing on a microscopic scale in fluids is caused by molecular diffusion. The packets of fluids must be in contact long enough for the random movement of the molecules to pervade the space of the neighbouring fluid packet. The larger the distance is that the molecules must travel the longer it takes for mixing to have occurred. In fact, an increase in spatial scale by a certain factor will require the time to be the square of that factor. E.g. an increase in size by factor of two will require a four times longer time for the mixing. Deformation of the packets by agitation of the fluids may stretch and bend the packets and intertwine them so that the diffusion distances become shorter. Vigorous agitation that gives rise to turbulent vortices speeds up mixing.

In the present note we are concerned with so low velocities that no turbulence will occur. The fluid flow is either stationary meaning that the fluid packets can be followed along streamlines or the flowpaths change so slowly that the packets could be followed by "particle tracking".

The scales of mixing of interest can vary over many orders of magnitude. There is an important mixing process across the aperture of a channel that counteracts the spreading of a tracer package that would otherwise be caused by the different fluid velocities at different distances from the walls of the channel. The distances of interest here are from less than 0.1 to 1 mm.

Fluid velocities also vary over the width of a channel. Mixing of two packets that flow side by side in a channel in a fracture can occur over scales of 0.1 to 1 metre. The mixing of the flowing water in the fractures with the stagnant water in the porous rock blocks, that are many meters in size will take a very long time. The mixing of different packages will be strongly influenced by both the space and the time scales.

For later use and for visualisation purposes a term "Mixing width" is introduced. It is illustrated in Figure 1 where two bodies of fluid, one with a solute with concentration 1 and one without any solute are brought together. The sharp concentration front becomes more diffuse over time.

For molecular diffusion the standard deviation of the mixing profile $\sigma = (2D\,t)^{0.5}$. For hydrodynamic dispersion around a travelling interface the dispersion coefficient D_L is used for D and t for the travel time. A commonly used entity is the Peclet number. $Pe = vz/D$ where z is some characteristic length and v the velocity. For a travelling pulse usually the travel length L is used as the characteristic length. L/v then is the travel time and $\sigma = L(2/Pe)^{0.5}$.
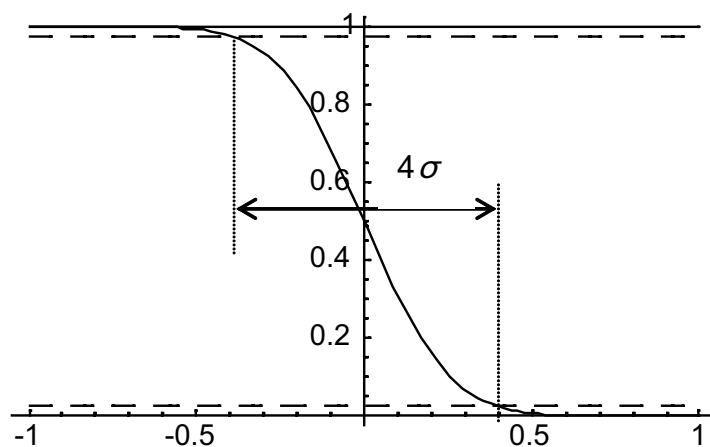
Figure 1. *Illustration of "Mixing width" arbitrarily taken to be 4 times the standard deviation σ. Outside of this region less than 2.5% concentration change has occurred in the fluids.*

A $Pe = 2$ suggests that σ is as large as the travel distance, which means a very strong mixing. A Pe of 3–10 is often considered to mean considerable mixing, the solute being dispersed at a rate comparable to that of advection. For a 1,000 year contact time and typical diffusion coefficient for salt in water of 10^{-9} m²/s σ is about 8 meters.

2.1   Taylor dispersion

A fluid that flows in a tube or narrow slit will develop a parabolic velocity profile after some distance from the inlet if the flow is laminar. The fluid at the wall is stagnant and the highest velocity is found in the centre. A thin slug of a tracer will be spread out as the fast fluid in the centre carries the tracer faster than the streamlines nearer to the wall. See Figure 2. However, molecular diffusion will even out the concentration profile across the flowpath /Bird et al. 2002, Logan 1999/. This effect considerably decreases the spread of the tracer pulse in the flow direction.

We are interested in the spread of the concentration pulse in relation to its mean travel time. The spreading of a travelling pulse downstream of an injection point can be described by the diffusion equation to which a the solution for this case is

$$c = \frac{M}{2\sqrt{\pi D_L t}} e^{-\frac{(x-vt)^2}{4D_L t}} \tag{1}$$

This is illustrated in Figure 3 for $D_L = 0.02$ m²/year, $t = 5$ and 10 years and $M = 1$ (arbitrary unit)

The dispersion coefficient for Taylor dispersion has been determined by solving the flow and diffusion equations. It has been confirmed by experiments to be /Bird et al. 2002/

$$\frac{D_L}{D_w} = (1 + \frac{1}{48}\frac{R^2 v^2}{D_w^2}) \tag{2}$$
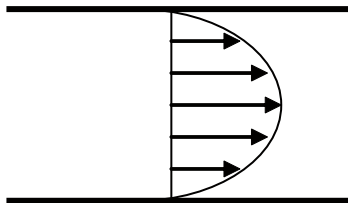
Figure 2. *Velocity profile for laminar flow in a slit or tube.*
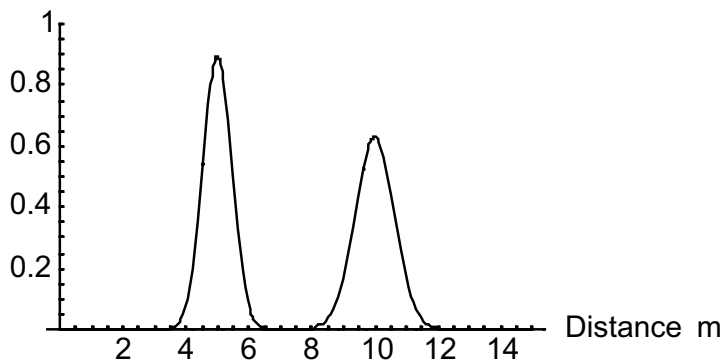
Figure 3. *Examples of concentration profiles for a travelling pulse when travel time is doubled.*

It is seen that for very low velocities or radius R the first term will dominate and the longitudinal dispersion coefficient is equal to the diffusion coefficient. This means that the longitudinal spreading of the pulse will be caused by molecular diffusion.

The dispersion in a slit will be very similar, the difference being that the constant 48 is 52.5 instead and R is exchanged for the half aperture b of the slit. In fact for laminar flow in ducts with a constant velocity profile the same expression can be used by just using a different constant. This will be shown in the next section.

Illustrative example for a thin fracture

Using the data for the central case in Table 1 in the appendix the velocity in the fracture $v = Ki/\varepsilon_f = 10^{-7}$ m/s or 3.15 m/a. The ratio of the longitudinal dispersion coefficient to the molecular diffusion coefficient, D_L/D_w, then becomes

$$\frac{D_L}{D_w} = 1 + \frac{1}{52.5}\frac{b^2 v^2}{D_w^2} = 1 + \frac{Pe_b^2}{52.5} = 1 + \frac{1}{52.5}\frac{0.0001^2(10^{-7})^2}{4\cdot(10^{-9})^2} = 1 + 0.5\cdot10^{-6}$$

Dispersion and mixing in this case is totally dominated by molecular diffusion in the flow direction.

The Peclet number based on the half slit aperture is defined as

$$Pe_b = \frac{bv}{D_w} \tag{3}$$

For $Pe_b \ll 1$ diffusion dominates the transport over distance b and for $Pe_b \gg 1$ advection dominate.

It is seen from Equation 2 that for about $Pe_b = 7$ there will be the same contribution to dispersion from molecular diffusion as from the Taylor dispersion component.

In the example molecular diffusion totally dominates over Taylor dispersion in the fracture. The aperture or the velocity would have to be some three orders of magnitude larger for the Taylor dispersion to begin to influence the dispersion.

For the above data a pulse moving slowly downstream in a fracture will after one year have spread by molecular diffusion as shown in Figure 4.

It is seen from the examples in Figures 4 and 5 that molecular diffusion is noticeable but does not play a significant role in spreading the solute pulse over large distances when the residence time is long. However, real fractures are not parallel smooth walled slits. The aperture varies and the fluid moves in undulating channels that contract and widen. This will influence the dispersion.
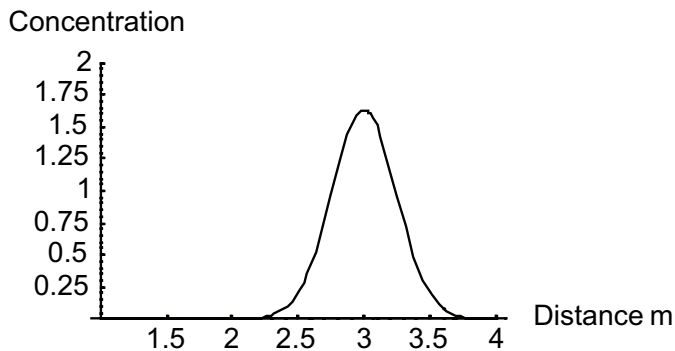
Figure 4. Concentration profile downstream after one year in a fracture. The spreading is totally dominated by molecular diffusion.
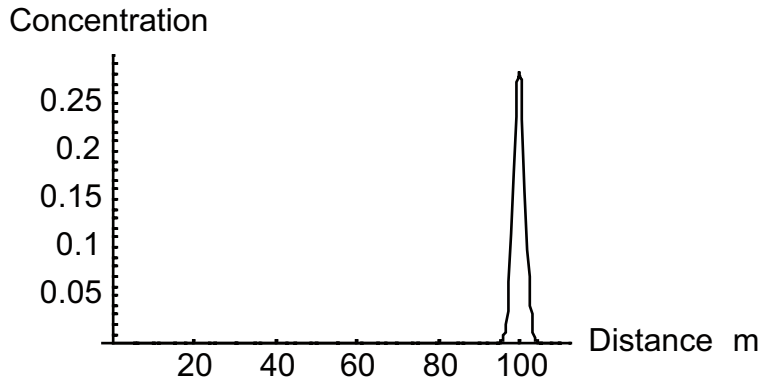
Concentration

Figure 5. *Concentration profile down stream after 33 years in a fracture. The spreading is totally dominated by molecular diffusion.*

/Hoagland and Prudhomme 1985/ studied the longitudinal dispersion in tubes with sinusoidally varying cross sections. They found that with increasing amplitude and decreasing wavelength dispersion increased. In their examples the increase is negligible for $Pe_b < 1$. In our case $Pe_b = 5 \ 10^{-3}$ and the variable nature of aperture can be deemed to have negligible influence.

Conclusion

Taylor dispersion due to velocity variations across the fracture apertures will have a small influence compared to other dispersion mechanisms For PA time scales.

2.2 "Taylor dispersion" across a channel

The water flows in only parts of the fractures, seeking those paths where the resistance to flow is smallest. This is called channelling. Observations /Neretnieks et al. 1985, 1987/ suggest that channel widths are in the range 0.1–1 m although also tube like channels have been observed, especially at fracture intersections.

The water velocity varies across the channels and solutes will diffuse between the "streamlines" in the fracture plane in the same way as in the Taylor diffusion. The impact of the velocity profile can be assessed in the same way as for the previous case and the results can be summarised in the same form of formula. For a given velocity profile

$$\frac{D_L}{D_w} = 1 + \frac{Pe_w^2}{Const_w} \tag{4}$$

where the Peclet number is defined with the characteristic length W/2, where W is the width of the fracture.

$$Pe_w = \frac{W v_{mean}}{2 D_w} \tag{5}$$

It is seen from the above expression that the dispersion coefficient increases proportionally to the channel width squared when the longitudinal diffusion (1 + term) can not be neglected.

For a parabolic velocity distribution the $Const_w$ is the same as in the slit case i.e. 52.5.

For other profiles the constants would differ.

If the velocity distribution $v(y)$ is known the constant can be evaluated by integrating the evening out of the concentration by diffusion over all the streamlines, /Logan 1999/.

$$\frac{D_L}{D_w} = 1 + \frac{1}{WD_w^2} \int_0^W v'(y) \int_0^y \int_0^y v'(y) \, dy \, dy \, dy \tag{6}$$

An example is where there is a linear velocity profile over the channel width with zero velocity at one side and 2 v_{mean} at the other side. For this case the $Const_W = 15/8$.

Illustrative example

Using the data from Table 1, $W = 0.3$ m, $D_w = 10^{-9}$ m²/s and $v = 10^{-7}$ m/s, $Pe_W = 15$.

For the linear velocity profile the $Const_W = 15/8$ and $D_L/D_w = 121$. Figure 6 shows the pulse (flat curve) after 100 m for the above two cases. The length Peclet number $Pe_L = v_{mean}L/D_w$ for this case is 83. The peaked curve is for molecular diffusion only. The results show that velocity gradients over a channel can cause noticeable spread of a pulse.

Conclusions

The above results suggest that the velocity profile and the channel width can have very strong influence on the dispersion and that this could contribute at least partly to the observed field dispersion.
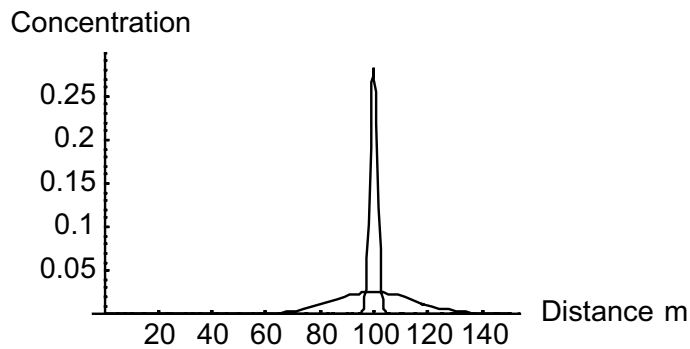
Figure 6. Concentration profile downstream after 33 years in a fracture for $D_L/D_w = 121$ flat curve and when only molecular diffusion is active.

3 Mixing between streams, across fracture apertures, along fractures and at fracture intersections

3.1 Diffusional mixing

In laminar flow or in stagnant liquids, mixing takes place by molecular diffusion. Consider a stream of water b thick, originally pure, that is suddenly exposed to a constant concentration c_o of a species at one side of the stream. The stream is invaded by the diffusing species and will eventually attain the concentration that is maintained at the surface. The concentration profile in the stream will evolve over time as shown in Figure 7. b could be the half aperture or half the stream width of a stream exposed at both sides to concentration. c_o. The figure shows how the diffusing species penetrates further and further into the stream with time. For dimensionless time, Dt/b^2, less than 0.01 the diffusing species have penetrated a very short distance. For a dimensionless time larger that 1 the stream has practically equilibrated with the surface concentration /Carslaw and Jaeger 1959/.

With these simple criteria one can readily determine weather there is good or poor mixing in a stream or between streams.

First consider the diffusional mixing across the fracture aperture. The diffusivity in water of small molecules is on the order of $D_w = 10^{-9}$ m²/s. Typical fracture apertures range from 1 mm and downwards. The time needed for full mixing, $Dt/b^2 = 1$, across a 0.5 mm fracture, $b = 0.25$ mm is 60 seconds. This is a very short time compared to the residence times expected in fractures under PA conditions. Thus if two different streams meet and travel in a fracture flat side touching flat side they will be fully mixed after a very short time.

Two different streams that enter a fracture side by side, touching as shown in Figure 8, will need a longer contact time and will travel a longer distance before they loose their identity as we conceive them to be much wider that the aperture.

As an example consider a case where the rock has a hydraulic conductivity of $K = 10^{-8}$ m/s, a flow porosity of $\varepsilon_f = 3 \times 10^{-4}$ and there is hydraulic gradient $i = 0.003$. See Table 1. These are not unusual values encountered in fractured rocks at depth and for PA conditions.
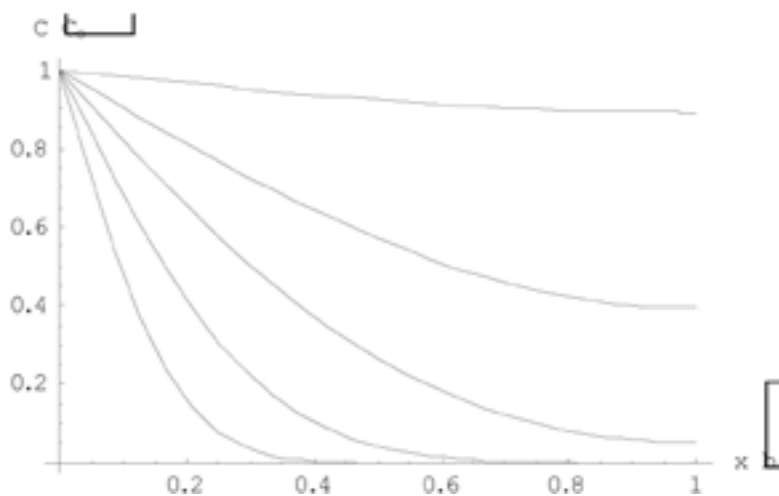
Figure 7. *Concentration profile in a stream that has been exposed to a surface concentration for different dimensionless times Dt/b^2-curves from below; 0.01, 0.03, 0.1, 0.3, 1.*
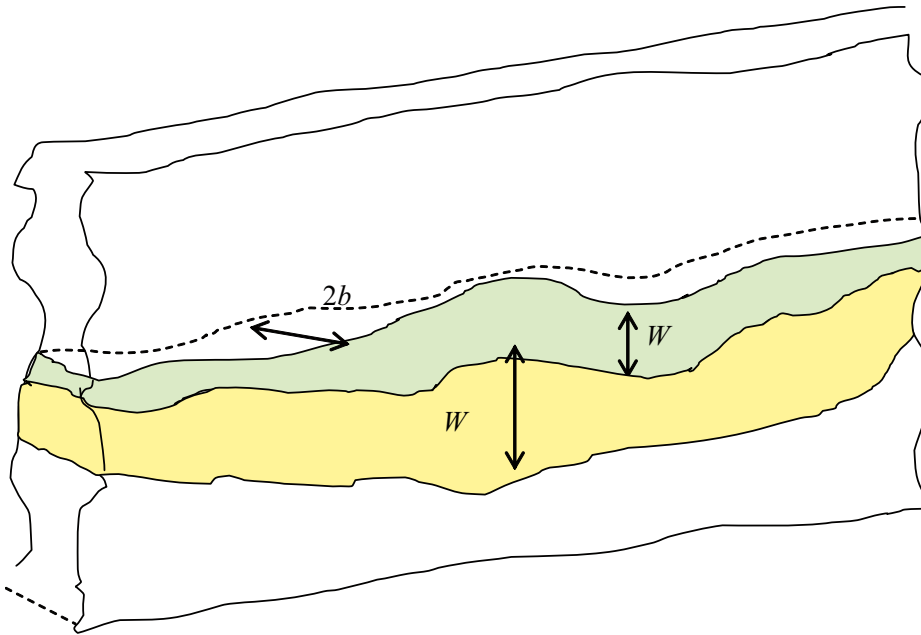
Figure 8. *Two streams travel side by side in a fracture and exchange dissolved species with one another by molecular diffusion.*

The average water velocity is $v = 10^{-7}$ m/s or 3 m/a in the fractures. The residence time in a 3 m long fracture is 1 year. A stream would then loose its identity if it is less than 0.2 m wide. In a fracture with ten times lower transmissivity, streams more than half a meter wide would loose their identity.

Conclusions

It is assured that there is a negligible concentration difference across a fracture aperture Streams that travel side by side in a fracture may or may not mix well depending on their widths and residence times. Mixing is expected to take place over distances ranging from tens of cm to meters in PA conditions for a channel in a 10 m long path. However, full mixing over the width of wide channels in fractures is not assured.

3.2   Effect of non-mixing between channels

In many field tracer tests it is found that the dispersion coefficient D_L increases with the observation distance /Gelhar 1993/. This is inconsistent with the basic idea of the advection-dispersion equation. Then it is expected that the dispersion coefficient would attain a constant value for sufficiently long distances.

Several reasons have been suggested for this discrepancy. Two are mentioned here. One cause could be that the networks are self-similar at different scales. It has been suggested that the fractures have a fractal distribution /Turcotte 1997/. This would directly lead to the observed increase of dispersion coefficient. In practice this could mean that the larger region one studies the larger is the chance of having a larger fracture in the region. In even larger regions the chances increase to include an even larger fracture zone, etc.

Another cause can be that there is a large number of channels that are independent and do not mix their waters underway. Such channels would traverse fracture after fracture in the network. Mixing only takes place when the sampling is made by pumping in a collection point. Only then the different channels with different velocities and flowrates mix their waters. If one could sample the waters in the individual channels the picture could be very different /Neretnieks 2002/.

4   Mixing in fracture networks

Observations suggest that water flow is very unevenly distributed in fractures. Often only a small part of the fracture carries most of the water /Neretnieks et al. 1985, 1987, Abelin et al.1994, Tsang and Neretnieks 1998/. This has been visualised as channelling. The channels are not necessarily deemed to be fixed paths in a fracture; the water may trace out a different channel under different directions of the hydraulic gradient. However, for a given gradient the channels will form a network in the network of fractures. The channel(s) in one fracture may fully or partly continue in the same fracture after a fracture intersection. Part of the water in a channel may continue its flowpath in the intersecting fracture.

It has been shown above in the section on Taylor dispersion that under PA conditions there will be a considerable mixing across the fracture aperture but not necessarily across the width W of a channel. On the other hand if two channels come to travel side by side, narrow channels will mix their waters whereas wide channels or channels that are not in direct contact with each other will not be mixed, /Neretnieks 2002/.

It is conceivable and even expected that "non-mixed" freshwater channels can trace out paths in what is a region of mostly saltwater distances. Over long distances and times even such intruding channels would mix their waters with the other channels, at least by matrix diffusion.

It is not simple to take water samples from individual fractures without disturbing the original flow field and risking sampling a mixture of waters from different flowpaths induced by the sampling procedure.

Simulations using fracture or channel network models might give some indications on how serious this effect might be.

5   Impact of tidal waves

Tidal waves induce the groundwater to move up and down. It has been suggested that such a movement could cause mixing by Taylor dispersion. When the water moves upward in a fracture the velocity profile would carry some part of a body of water faster than another. Molecular diffusion across the different parts will even out the concentration. A freshwater/saltwater interface would be dispersed in the direction of water movement. When the water moves in the other direction about half a day later the smeared pulse would be further smeared. Some of the solute will be left behind in the non-moving water when the moving water in the fracture withdraws. The down coming fresh water that replaces part of the saltwater will receive some solute from the saltwater by diffusion. The swinging up and down will carry some solute further and further upward.

A simple model has been devised to study the magnitude of this mixing in the direction of the tidal movement. Half of the water in a fracture is stagnant and does not move with the tide. The other half moves with an amplitude A_T. When the mobile water has reached the top it encounters stagnant water that has a different salt concentration. The two bodies of water strive to equilibrate. The water then swings back and the procedure is repeated. This is illustrated in Figure 9.

If the pillars fully equilibrate, 100% of the concentration difference disappears. $\varepsilon_{mix} = 1$. For $\varepsilon_{mix} = 0.1$ only 10% of concentration difference disappears.

Figure 10 shows the concentration profile for $\varepsilon_{mix} = 1$ after 400 cycles. The salt/freshwater interface was at point "50" originally. The standard deviation σ_{mix} of the front width is about 14 amplitudes A_T or 1.4 m for $A_T = 0.1$ m.

The standard deviation of the width of the mixing front is shown in Figure 11 as a function of time for $A_T = 0.1$ m and $\varepsilon_{mix} = 1, 0.4, 0.1$ and 0.025.

What mixing ratio ε is expected and how is it influenced by the channel width is explored below. This is obtained from the solution of the diffusion equation.
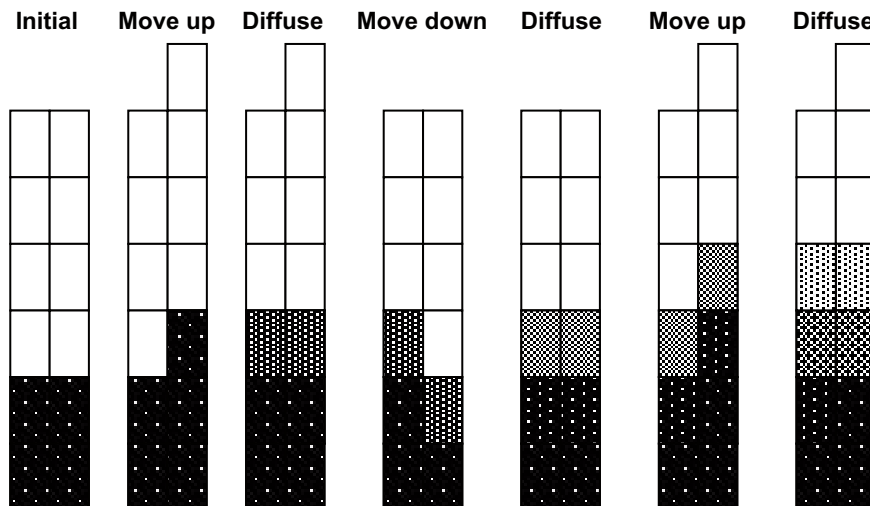
Figure 9. *The left water pillar is immobile. The right pillar moves up with the tide. The concentration between the pillars tends to equilibrate due to transverse diffusion. Next the right pillar moves down with the reversal of the tide. Thereafter, equilibration takes place and the cycle is repeated.*
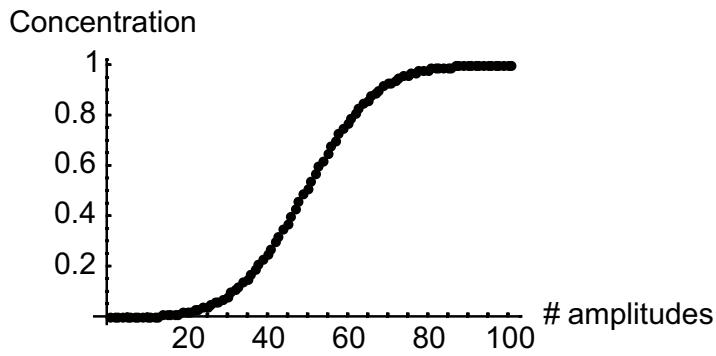
Concentration

Figure 10. *Concentration profile at the freshwater-saltwater interface after 400 cycles.*
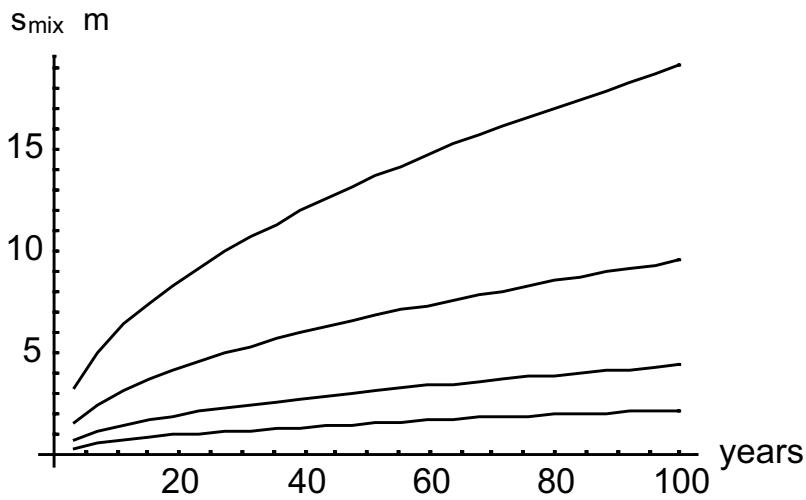
Figure 11. *Standard deviation of width of mixing front as a function of time for ε_{mix} = 1, 0.4, 0.1 and 0.025 for the curves from top down.*

Figure 12 shows how the mixing ratio ε_{mix} decreases with the width of the channel.

For a mixing ratio ε_{mix} = 0.4 the channel width W is 1.9 cm and for ε_{mix} = 0.1 the channel width W is 7.4 cm. For a 0.3 m channel width the mixing ratio ε_{mix} = 0.025.
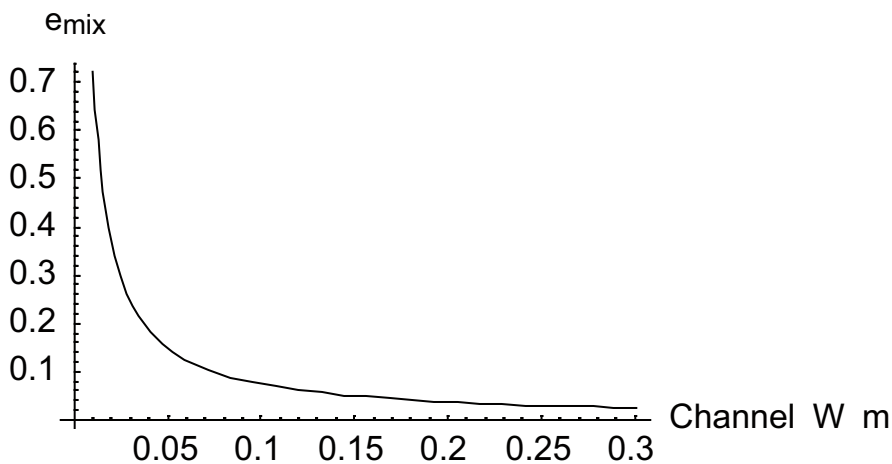
Figure 12. *Mixing ratio ε_{mix} as a function of channel width W. 12 hour contact time and diffusivity in water as in Table 1.*

Conclusions

The mixing due to tidal effects could have some impact if different narrow bodies of water move different distances during a tidal cycle. For the water in a 0.3 m wide channel the mixing width (4 σ_{mix}) due to tidal effects over 100 years is on the order of 10 m.

The mixing width due to molecular diffusion in the same direction will also be on the order of 10 m as the standard deviation for diffusion $\sigma_{diff}=(2D_w t)^{0.5} = 2.5$ m. For narrower channels the impact of tidal waves will be greater.

There are a number of considerable uncertainties in this simplified analysis. For the central case data in Table 1 the water will travel a distance of about 300 m in the gradient direction in a complex network of channels with varying widths. The same "pillars" of water will thus not be in contact as the model assumes. The model is thus severely oversimplified but suggests that tidal mixing may not be important compared to the other effects.

6   Matrix diffusion

6.1   Penetration depth

Matrix diffusion has a strong impact on mixing. The water volume in the micropores of the rock matrix is much larger than the mobile water in the flowing fractures. Solutes are exchanged by molecular diffusion between the mobile water and the stagnant water in the matrix. In the same way as discussed earlier for solute exchange between streams the time to considerably penetrate (mix) the pore water with water at the surface of the rock can be approximately estimated by

$$t \approx \frac{r_p^2}{D_p}$$

Figure 13 illustrates the time needed to "fully" mix the pore water with water at the block surfaces.

6.2   Dispersion caused by matrix diffusion

Another way to illustrate the influence of the matrix pore water is by the van Deemter equation /Perry et al. 1997/.

The van Deemter equation describes the sum effects of different dispersion mechanisms in a dual or even triple porosity system. It can be used to calculate the spreading (variance σ_t^2) of a pulse as it travels through a column filled with particles (spheres) that are porous and in which the solute can diffuse. It is readily conceived that if the particles are small and the diffusion in and out of them is fast the pore water in the particles is practically in equilibrium with the water that flows between them. The inner porosity will not cause additional spreading of the pulse by delaying part of it. On the other hand with large particles the pore water in the particles will be only partly penetrated by the solute. As the pulse in the mobile water passes a particle some solute will reside in the particle and only slowly diffuse out after the front of the pulse has passed. This will lead to a considerable spreading of the original pulse.
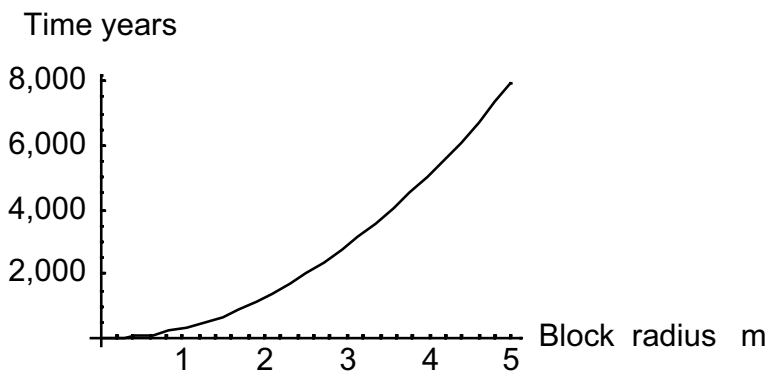
Figure 13. *Time to mix the matrix pore water by molecular diffusion for a non sorbing species for different block sizes. Data from Table 1.*

The van Deemter equation (simplified to consider our problem only) is

$$\left(\frac{\sigma_t}{t_{mean}}\right)^2 = \frac{2}{Pec_{total}} = \frac{2}{Pec_{hydrodynamic}} + \frac{2}{t_w(1+k)^2} \frac{\varepsilon k^2}{(1-\varepsilon)} \frac{r_p^2}{15\varepsilon_p D_p} \tag{7}$$

where

$$k = \frac{1-\varepsilon}{\varepsilon}(\varepsilon_p + K_d \rho) \tag{8}$$

and

$$t_{meam} = t_w(1+k) \tag{9}$$

The expression is used to illustrate the contribution due to matrix diffusion to the total dispersion. Data are taken from Table 1. $k = 30$ in this example which means that there is 30 times more water volume in the matrix pores than in the flowing fracture. For short times or large blocks a pulse will seem to arrive after the water residence time t_w whereas for long times or small blocks the pulse will seem to arrive at $t_w(1+k)$. In the first case there will be a very long but low tail. In intermediate cases a pulse will be very drawn out.

Figure 14 shows the contribution to the Peclet number for a system with blocks with 5 m radius for different residence times of water. It may be noted that Peclet numbers below 3–10 can be considered to be dominated by diffusion effects over advection effects.

Figure 15 shows the contribution to the Peclet number, Pe_L, as a function of the block size for a water residence time of 33 years. Small blocks will equilibrate considerably and not contribute to widen a pulse. Larger blocks will not equilibrate in the interior and a pulse will have a very drawn out tail.
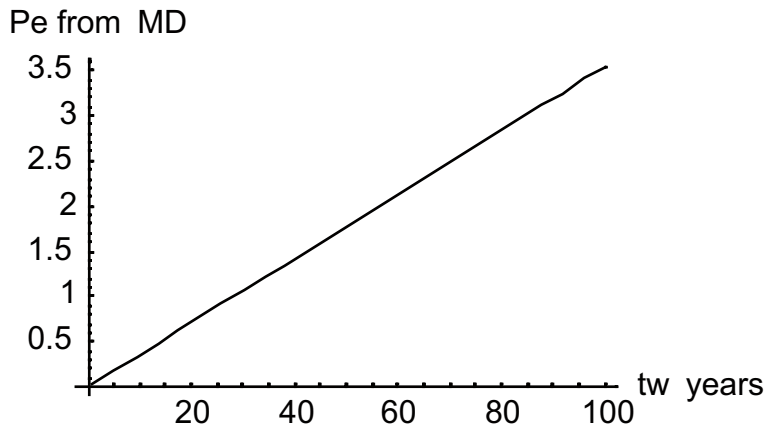
Figure 14. *Contribution to the Peclet number, Pe_L, from matrix diffusion effects for different water residence times. Block size 5 m radius.*

106
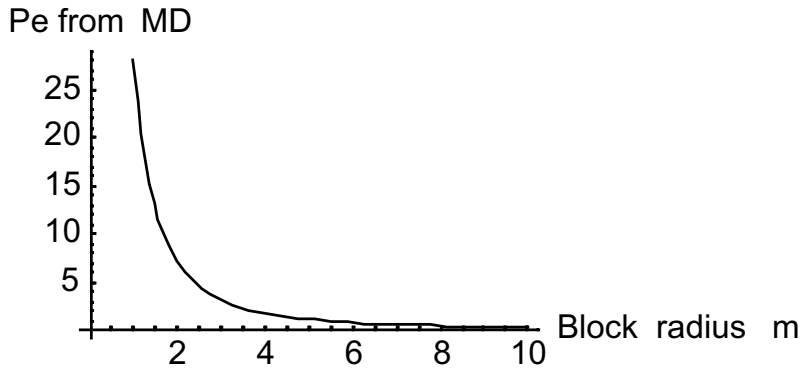
Figure 15. *Contribution to the Peclet number, Pe_L, from matrix diffusion effects for different block sizes. Water residence time 33 years.*

6.3 Mixing and displacement of saltwater by freshwater: Influence of matrix diffusion

Assume that there has been saltwater in the fractures and all the matrix pores of a large volume of rock. At some time freshwater starts to infiltrate a persistent fracture or fracture zone in the rock and displace the saltwater there. The water in the fracture would be displaced by the incoming water with some mixing at the interface. That mixing would be caused mainly by Taylor dispersion effects as described previously. However, salt from the pores in the rock matrix diffuses out and mixes with the flowing water and the mixing length would become much larger as was illustrated by the van Deemter relation previously.

The salt concentration at a point downstream in the fracture in the flowing water as well as at a distance into the matrix is described by /Neretnieks 1980/.

$$\frac{c_{salt}}{c_{saltinitial}} = Erfc(\frac{t_w}{2b}\varepsilon_p\sqrt{\frac{D_p}{t-t_w}} + \frac{x}{2\sqrt{D_p(t-t_w)}}) = Erfc(\frac{L}{Ti}\varepsilon_p\sqrt{\frac{D_p}{t-t_w}} + \frac{x}{2\sqrt{D_p(t-t_w)}}) \quad (10)$$

The water velocity and fracture aperture is not possible to determine in practice. The first Erfc expression is then difficult to use. Therefore the following relation is used to obtain entities that are more readily observable.

$$\frac{t_w}{2b} = \frac{L}{v2b} = \frac{L}{Ti} \quad (11)$$

This is much more convenient because the transmissivity T is typically measured in boreholes for individual fractures and the gradient i is assessed from hydraulic calculations based on Darcy's law, topography and "known" boundary conditions. The other residence time t_w under the square root in the expressions in practice has no influence on the residence time distribution when matrix diffusion is active, as is the case here.

Figure 16 illustrates how the salt concentration changes over time 500 m from the inlet of a fracture zone (lower curve). The zone has a transmissivity of $2\cdot10^{-7}$ m²/s and a gradient i of 0.003 m/m. The distance to the next major zone is assumed to be so large (>> 10 m) that the diffusion front in practice never reaches half way to the other zone. After 3,000 years the water 500 m from the inlet still contains nearly 20% of the original salt concentration.

1 m into the rock the concentration is still 40% after 3,000 years and more than 80% at 5 m distance into the rock.

Figure 17 shows that at all distances along the fracture the pore water some 5 m into the rock still contains most of the original salt after 3,000 years.
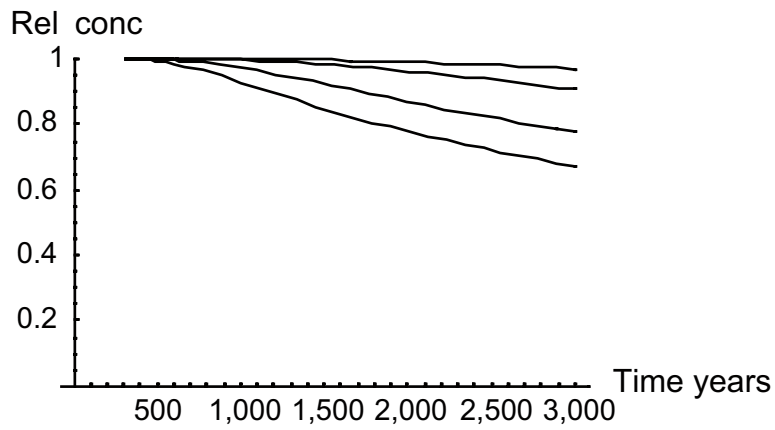
Rel conc
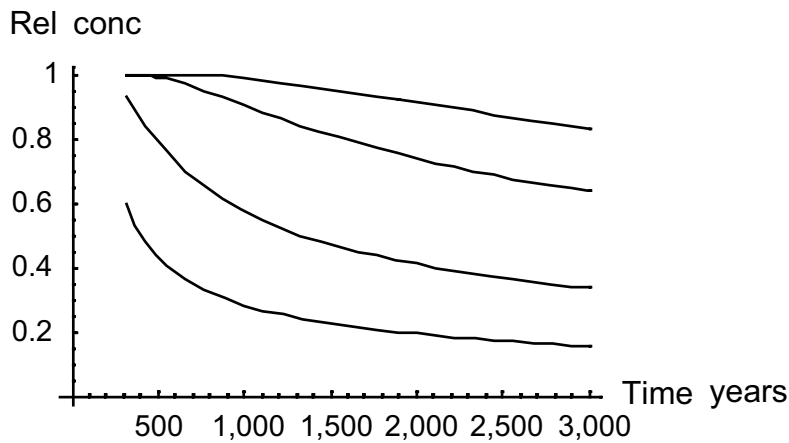
Figure 16. Salt concentration in the water 500 m downstream in a fracture with $T = 2 \cdot 10^{-7}$, m²/s lower curve, and in pore water 1, 3 and 5 m into the rock matrix, next lowest curve and upward.

Rel conc
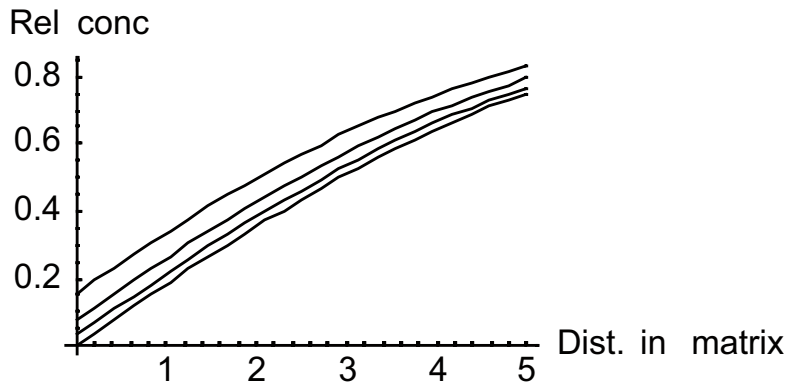
Figure 17. Salt concentration in the pore water in the rock matrix after 300 years. At the inlet, lower curve and at 100, 250 and 500 m downstream.

In less transmissive fractures the freshwater reaches shorter distances downstream. Figure 18 illustrates conditions after 3,000 years in a 5 times less conductive fracture.

The lower transmissivity fracture will have been very little influenced. On the other hand a fracture zone with a transmissivity of 10^{-6} m²/s will have about 3% of the original salt concentration at 500 m distance after 3,000 years. Deep in the rock matrix there will still be a high salt concentration even for a high flow fracture similar to what is shown in Figure 17.

Figures 19 and 20 show 3D plots of the salt concentration as a function of time and distance along the flowpath.

Conclusions

Matrix diffusion is deemed to be a major cause of dispersion in fractured rocks for low flow-rates. Mixing between flowing water and stagnant matrix pore water will take thousands of years for typical block sizes of 1–5 m radius. The water in transmissive fracture zones can be considerably displaced by fresh water in a few thousand years. Matrix water at distances more than 5 m from the zones will be only marginally depleted.

Figure 18. *Salt concentration in the water 500 m downstream in a fracture with T = 4·10⁻⁸, m²/s, lowest curve, and in pore water 1, 3 and 5 m into the rock matrix, next lowest curve and upward.*
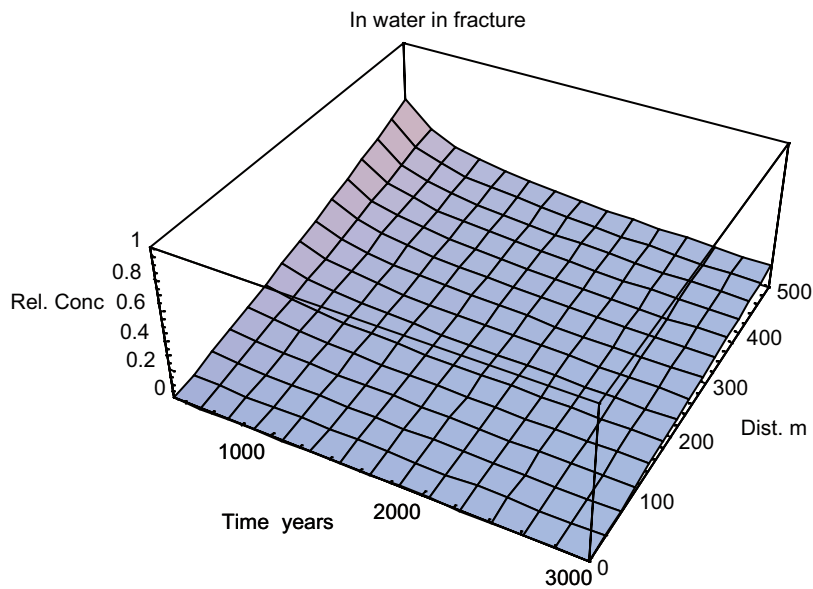
Figure 19. *Salt concentration in the water in a fracture with T = 2·10⁻⁷, m²/s as a function of time and distance.*
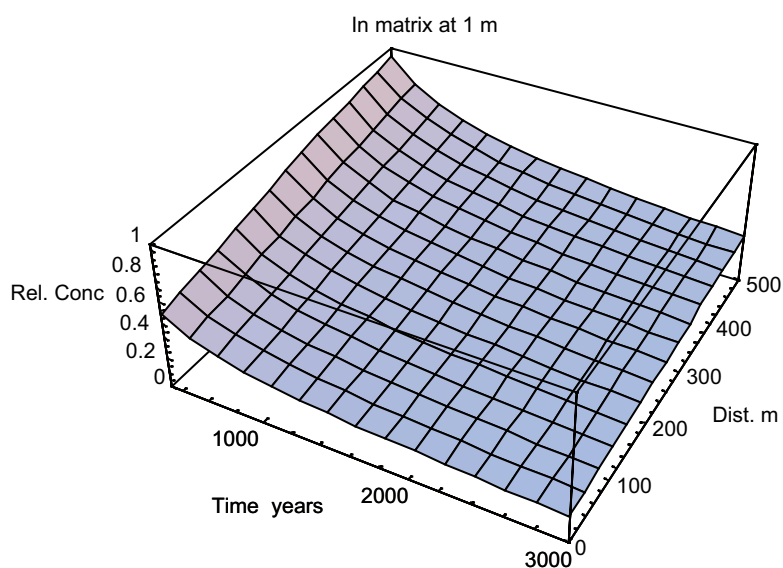
Figure 20. *Salt concentration in the water for a fracture with T = 4·10⁻⁸, m²/s as a function of time and distance.*

7 Discussion and conclusions

The cartoons below illustrate some of the effects described previously.

Figure 21 shows flowpaths of freshwater from the left displacing saltwater to the right. At shallow depths all salt is gone but the deeper the flow penetrates the less is the flowrate and the longer the flowpaths. The three semi-vertical lines indicate how boreholes could intersect salt at very different depths depending on if they are in an inflow or outflow region.

Figure 22 illustrates that water in the flowing fractures can be practically depleted of salt but the interior of the large blocks can still contain much salt.

Figure 23 shows that water in highly conductive fracture zones may contain freshwater while large rock masses at shallower depths may contain saltwater.
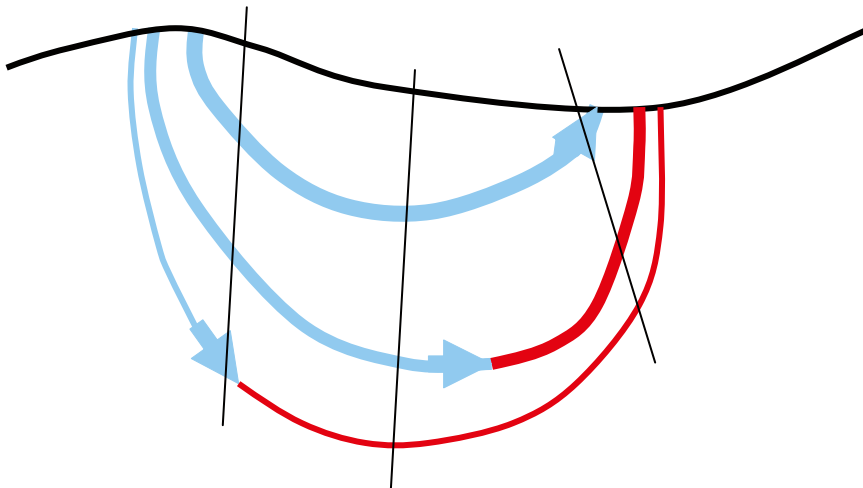
Figure 21. Boreholes in in and out flow regions will encounter salt at different depths.
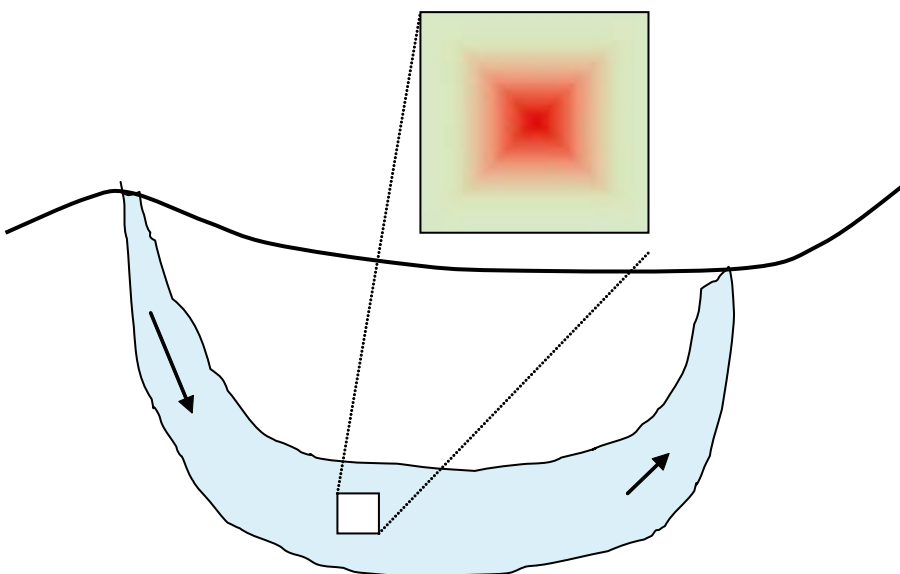
Figure 22. Water in the flowing fractures can be practically depleted of salt but the interior of the large blocks can still contain much salt.
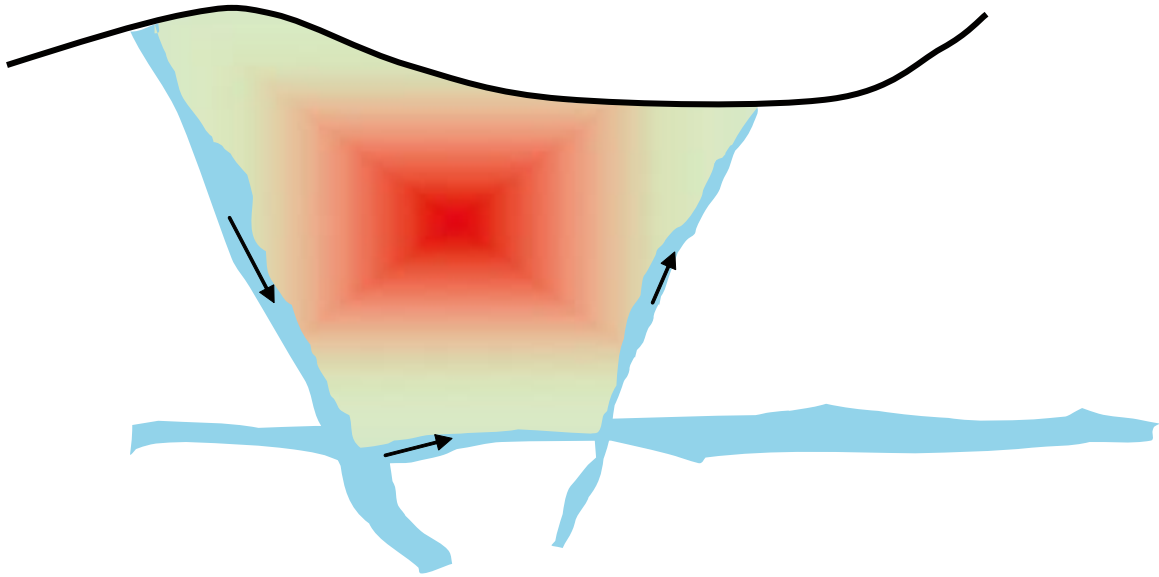
Figure 23. *Water in highly conductive fracture zones may contain freshwater while large rock masses at shallower depths may contain saltwater.*

Figure 24 shows that some fractures in the same volume of the network may contain salt whereas other fractures contain freshwater. If sampling is made by pumping, many fracture volumes of water from different fractures will mix.

These simple cartoons attempt to illustrate that the pattern of saltwater displacement can be quite complex. It may be worthwhile to develop sampling techniques that can resolve the details in the saltwater/freshwater "interface"

There are several processes that have displaced and mixed salt water by intruding freshwater. Advective flow brings in the fresh water into the fractures of the rock. The advective flow will have flushed the fractures at shallow depths many times since the ice age. No salt water can be expected to be found there. Also the water in the micropores of the rock matrix will have been
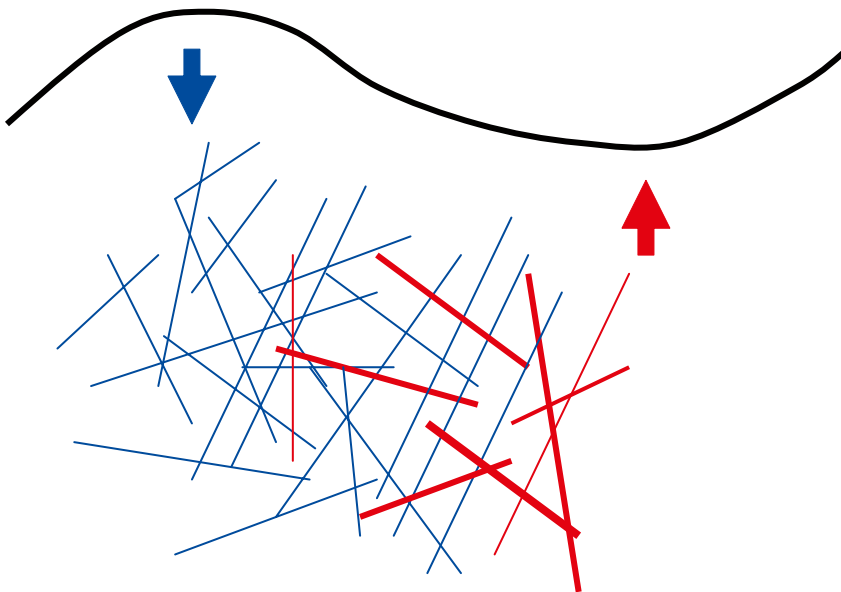
Figure 24. *Some fractures in the same volume of the network may contain salt whereas other fractures contain freshwater.*

"washed out" by molecular diffusion except in the largest blocks. At intermediate depth most of the salt will have been washed out of the fractures but the large rock blocks can be expected to have salt water in their interior.

Highly conductive fracture zones can be expected to be flushed but the rock matrix at 5–10 m distance can be expected to contain salt water.

The complex 3D networks nature of the stochastic channels makes it very complicated (impossible) to exactly pinpoint the location of the displacement front. It may even be an erroneous concept to speak about a displacement front in the normal sense of the word. The "front" is expected to consist of a network of channels where sometimes even close lying channels can have quite different salt concentrations. Also the salt concentration in different parts of the rock blocks is expected to be very different over distances of 5–10 m.

This suggests that sampling procedures should be developed that allow for taking many samples of water in different fractures with a minimum of disturbance and mixing due to sampling. It further suggests that samples of the rock matrix at known and different distances from prominent fractures or fracture zones can give valuable information on the diffusion processes.

Acknowledgements

8   Notation

A_T	Amplitude of tidal wave
b	Half aperture of fracture
D_L	Dispersion coefficient
D_p	Diffusion coefficient in pore water
D_w	Diffusion coefficient in unconfined water
i	Hydraulic gradient
K_d	Sorption coefficient
K_{hyd}	Hydraulic conductivity
L	Travel distance
M	Mass of solute pulse per cross section area
Pe_L	Peclet number based on the travel length $= vL/D_L$
r_p	Particle radius
R	Tube radius
t	Time
t_{mean}	Mean residence time of solute
t_w	Water residence time
v	Velocity
v_{mean}	Mean velocity
W	Channel width
x	Distance into matrix
z	Distance in flow direction
α	Dispersion length- mixing length D_L/v
ε_p	Matrix porosity
ε	Flow porosity
ε_{mix}	Mixing ratio
ρ	Rock density
σ	Standard deviation
σ_{mix}	Standard deviation of mixing front

9 References

Abelin H, Birgersson L, Widén H, Ågren T, Moreno L, Neretnieks I, 1994. Channeling experiments in crystalline fractured rocks. J. Contaminant Hydrology, 15, p 129–158.

Bird R B, Stewart W,E, Lightfoot E,N, 2002. Transport Phenomena, John Wiley and Sons Inc, N.Y. 2nd Ed.

Carslaw H S, Jaeger J C, 1959. Conduction of heat in solids, Oxford university press, Oxford.

Gelhar L W, 1993. Stochastic subsurface hydrology Prentice Hall.

Hoagland D A, Prudhomme R K, 1985. Taylor-Aris dispersion arising from flow in a sinusoidal tube, AIChE Journal 31 (2): 236-244.

Logan B E, 1999. Environmental transport processes, Wiley-Interscience.

Neretnieks I, 1980. Diffusion in the rock matrix: An important factor in radionuclide retardation? J. Geophys. Res. 85, p 4379–4397.

Neretnieks I, Abelin H, Birgersson L, Moreno L, Rasmuson A, Skagius K, 1985. Chemical Transport in Fractured Media. Proceedings of the "Fundamentals of Transport Phenomena in Porous Media", NATO/ASI Symposium, Delaware, July 14-23, p 475–550.

Neretnieks I, Abelin H, Birgersson L, 1987. Some recent observations of channeling in fractured rocks – Its potential impact on radionuclide migration. Paper presented at DOE/AECL conference, Sept. 15-17, 1987, San Francisco, USA. Proceedings, 1987.

Neretnieks I, 2002. A stochastic multi-channel model for solute transport – Analysis of tracer transport in fractured rock, J. Contaminant Hydrology, 55, p 175–211.

Neretnieks I, Moreno L, 2003. Prediction of some in situ tracer tests with sorbing tracers using independent data, 61, p 351–360.

Perry R H, Green W D, Maloney J O, 1997. Perry's Chemical Engineer's Handbook, MacGraw Hill 7th Ed, p 16–43.

Tsang C-F, Neretnieks I, 1998. Flow channeling in heterogeneous fractured rocks, Reviews of geophysics, 36, No 2, 275–298.

Turcotte D L, 1997. Fractals and Chaos in Geology and Geophysics, Cambridge University Press, 2nd Ed.

Table 1. Data for sample calculations

Entity	Notation and measure	Central value
Travel distance	L, m	500
Hydraulic transmissivity	T, m²/s	10^{-8}
Fracture aperture	$2b$, mm	0.1
Hydraulic gradient	i m/m	0.005
Flow porosity	ε	0.0001
Matrix porosity	ε_p	0.003
Solute diffusivity in water	D_w, m²/s	10^{-9}
Solute diffusivity in pore water	D_p, m²/s	$3\ 10^{-11}$
Channel width	W, m	0.3
Amplitude of tidal waves	A_T m	0.1

121

DarcyTools V3.0, basic concepts

Urban Svensson, CFE

Contents

1 Introduction

The project was initiated about two years ago. The development of DarcyTools V3.0 was started at about the same time. Hence, the work undertaken in the project has to some extent influenced the present version of DarcyTools. Considering this background, it seems motivated to give an overview of the concepts embodied in DarcyTools. This appendix is therefore devoted to an account of the geometrical, flow and transport models in DarcyTools. Also a brief account of the grid system is given.

2 Geometrical description

The situation considered is outlined in Figure 1; essentially it is a fracture network contained in some domain with a length scale, L.

A key assumption of DarcyTools is that "*the number of fractures in a certain length interval follows a power law*". This seems to be an undisputable assumption as it basically only states that there are more small fractures than big ones.

Numerical models normally discretize space in some way. DarcyTools is a finite-volume code and the domain in Figure 1 is meshed to consist of a large number of cells. Typically a grid of $100 \times 100 \times 100$ cells is used. The next assumption introduced is related to this grid and can be stated as follows: "*in a sparsely fractured granite, flow is assumed to be distributed on relatively few flow channels, that are due to large scale fractures and zones. It is assumed that all essential flow channels are due to fractures and zones that are larger than the grid size*". If the grid size, Δ, is 0.01 L this is thus the lower limit for water-carrying fractures.

Fractures smaller than the grid size, Δ, are, as discussed above, assumed to contribute negligible to the flow rate, but are assumed to be essential for dispersion and retention, when dealing with transport. A subgrid model, FRAME (FRActal scaling laws and Multirate Equations), has been developed to handle these processes.

The concepts introduced form the basis of DarcyTools. In fact, the concept that fractures larger than Δ carry the water and fractures smaller than Δ are responsible for dispersion and retention is called the SOS-concept (Separation Of Scales). Figure 2 summarises the SOS-concept.
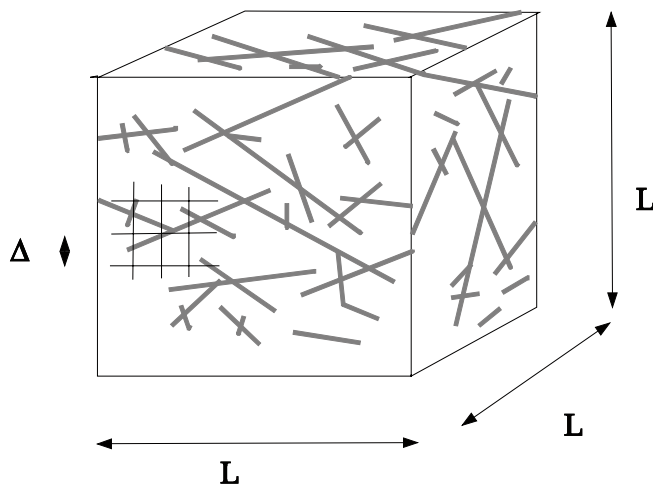
Figure 1. *Situation considered. A fractured network in a domain of length scale L. A grid with a cell size equal to Δ is also indicated.*

SIGNIFICANCE

Important for
transport

Important for
flow

LENGTH

0.1 mm

L/100

L

Δ

L

L

L
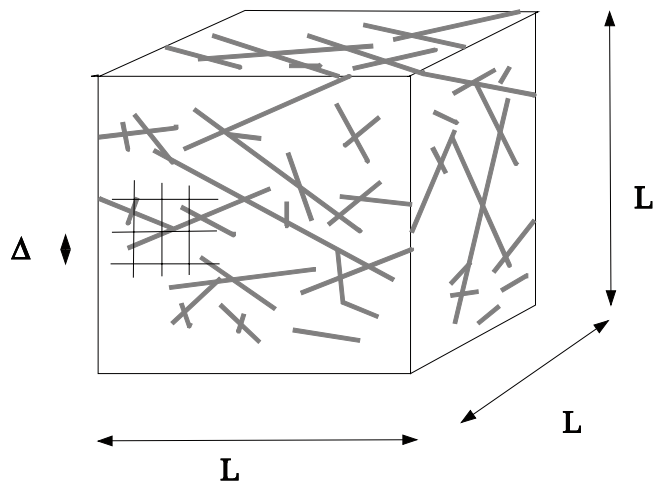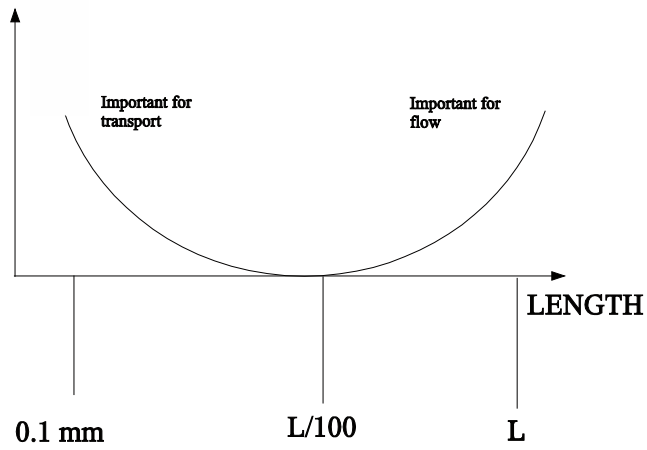
• Fractures larger than L/100 important for flow
• Fractures smaller than L/100 important for transport (dispersion, retention)
• ⇒ choose Δ ≈ L/100 and treat small fractures in a subgrid model

Figure 2. The SOS-concept (Separation Of Scales).

3 Flow model

Most numerical models of groundwater flow subdivide the studied domain into smaller volumes. If a computational grid is defined, we call these smaller volumes grid cells, and we apply the conservation laws and other constitutive relations to these. Also material properties, like hydraulic conductivity and porosity, need to be specified for the grid cells. These properties are often measured on a smaller scale (support scale) and a technique to express these on the scale of the grid cells is thus needed (upscaling). When material properties for all grid cells have been obtained, the flow simulation can be performed. In DarcyTools, we do however not follow this traditional route and the main argument for this can be stated as follows:

- In a sparsely fractured rock it is believed that most of the flow is due to a limited number of major fractures and fracture zones. The main task is thus to identify these and to represent them in the numerical model. If refined modelling is required, the next size class of fractures or fracture zones should be considered. From this point of view it seems more logical to first consider large fractures, and then progressively smaller ones, than to upscale properties from a small scale.

It is not possible to represent all fractures in the grid, simply because there are too many. In DarcyTools the smallest fracture considered will often be of the same size as the grid size. Smaller fractures, $l < l_{min}$, are however also of importance (for dispersion) and in DarcyTools represented as storage volumes (immobile zones), see Figure 3. In fact, storage volumes are defined as *all* immobile zones, with $l < l_{min}$, that exchange matter with the flowing water by molecular diffusion only.

SINGLE OPENING FRACTURE   CONDUCTIVE ELEMENT

FRACTURE ZONE   GRID REPRESENTATION
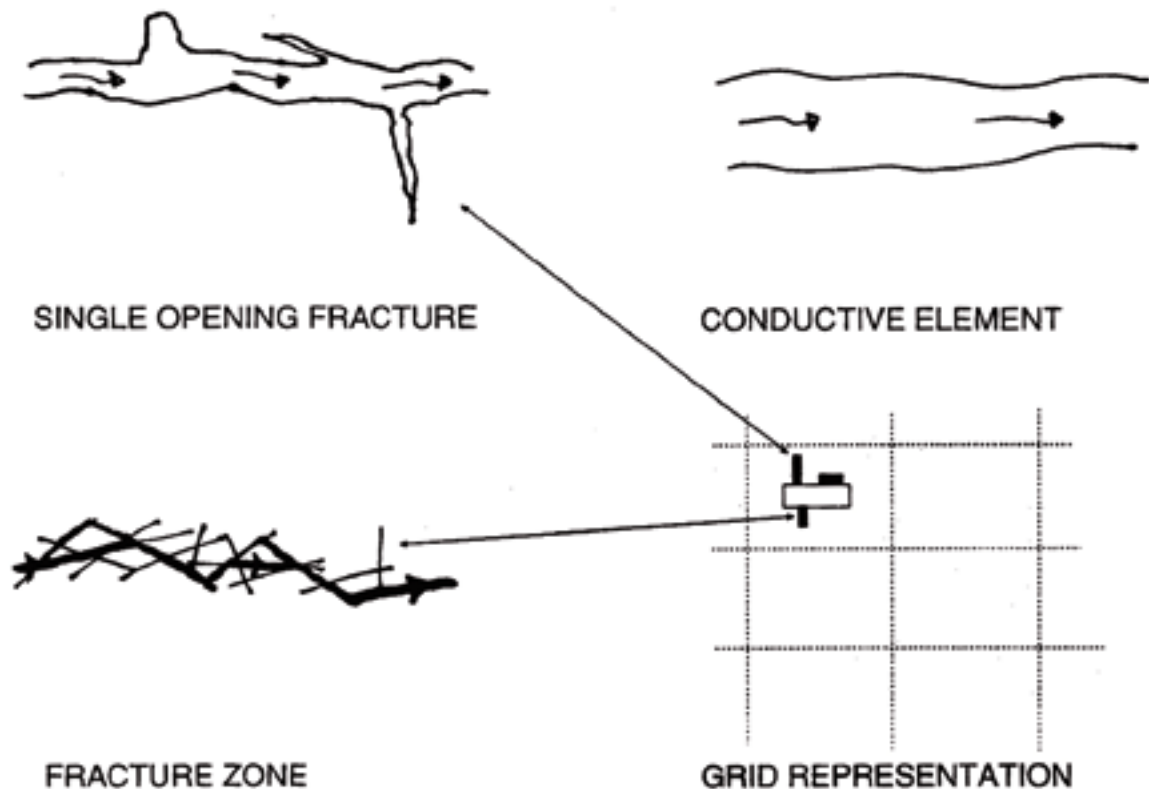
Figure 3. *Representation of kinematic (or mobile) and storage (or immobile) volumes in the grid. The open rectangle in the grid represents a kinematic volume (generated by the conductive element), while filled rectangles represent storage volumes.*

We have thus subdivided all fractures in contact (isolated fractures are not considered) into what will be called conductive elements and storage volumes. Storage volumes will be treated as subgrid effects and are represented in the subgrid model FRAME, to be described below. Conductive elements generate all grid properties by the GEHYCO-method which can now be formulated as:

- A conductive element contributes to the grid value of a variable by an amount which is equal to the intersecting volume times the value of the variable in question. Contributions from all elements that intersect the control volume are added and the sum is divided by the volume of the cell.

This basic principle will now be explained and illustrated, using Figure 4. A conductive element of thickness b is crossing a computational grid, which has a cell size of Δ . A staggered grid is to be used, which means that scalar quantities, like pressure and salinity, are stored at cell centres while velocity vectors are stored at cell wall centres, see Figure 4. This grid arrangement was first introduced by /Harlow and Welch 1965/ and is described in textbooks, see for example /Patankar 1980/. Each variable is assumed to be representative for a certain control volume, which is the volume the discretized equations are formulated for. For a velocity cell it is clear that the driving pressure force can be easily formulated. As we are going to apply the Darcy law to the velocity cell we also need a relevant cell conductivity to obtain the cell wall velocity. How to calculate this conductivity, and other properties, is the main subject of the GEHYCO-method.

To obtain the porosity, as an example, of the scalar cell marked in Figure 4 the following steps are performed.

- Calculate the intersecting volume between the conductive element and the cell; this volume is marked in the figure.

- If the porosity of the conducting element is θ_e, the contribution to the free volume is $\theta_e V_i$, where V_i is the intersecting volume.

- Calculate the contributions from all conductive elements that cross the cell.

- Obtain the cell porosity as the sum of all contributions divided by the cell volume.

In Figure 4 a control volume for a velocity cell is also marked. The procedure to obtain the conductivity for this control volume is analogue to the steps above.
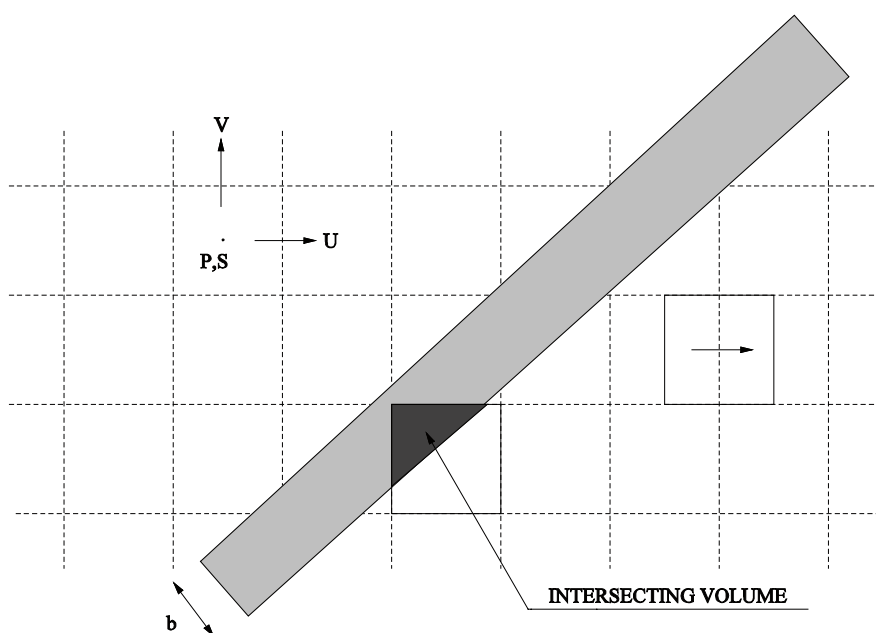
Figure 4. *Illustration of concepts and methods for calculating grid properties.*

By this procedure the porosity, flow wetted surface and storativity are determined for all scalar cells and the conductivities and diffusivities for all cell walls.

An assumption in the statement above is that "contributions from all elements that intersect a cell are added". If two, or more, fractures intersect a velocity cell, the cell conductivity should represent a fracture intersection (neglecting the case of parallel fractures of various orientation). /Neretnieks 1993/ discusses various concepts about channelling at intersections, but concludes that no firm information is available. He cites however a number of observations that support the idea that "fracture intersections form easy pathways". In lack of any firm information, it will therefore be assumed that contributions can be added. Fracture intersections will hence form "easy pathways".

The basic principle of the method is obviously very simple but, as has been demonstrated (see the DarcyTools documentation, /Svensson et al. 2006/ still general enough to handle even complex fracture networks. A few properties of the method can already at this stage be identified:

- All cell wall conductivities will be different, as we generate three conductivity values (in a 3D case) for each scalar cell. A conductivity field that is anisotropic on the cell scale is hence always generated.

- A fracture smaller than the cell size can not generally contribute to the anisotropy or correlation of the conductivity field.

Some simple calculations that illustrate the GEHYCO method, and also demonstrates the accuracy that can be expected, can be found in /Svensson et al. 2006/.

4   Transport model

When discussing transport and dispersion of solutes it is useful to distinguish between two different problems with respect to the time scale. The first kind of problem is the field experiment with a time scale from weeks to perhaps a year. A longer time scale, which may be thousands of years, needs to be considered when, for example, the water types present in the fracture network is to be analysed. At Äspö HRL, water from the last glaciation (about 11,000 years ago) has been found already at a depth of a few hundred metres. The relevant processes for the two problems will now be described, in turn.

Let us think of a typical field tracer experiment where a tracer is injected in one borehole and the arrival in another, pumped, borehole is studied. The curve describing the time distribution of the concentration in the pumped borehole is called the break through curve (BTC). Obviously the tracer is transported by advection between the two boreholes, and the flow field is hence an important element in the analysis. A number of dispersion processes will however affect the tracer as it travels through the fracture network. The most important of these are:

- **Intersections.** At a fracture intersection a tracer cloud may split up and enter pathways with different lengths and fluid velocities. This type of dispersion is often called macro-dispersion.

- **Channelling.** Spreading occurs within each fracture plane as the different streamlines have different path lengths and velocities. The flow channels may also merge or split up.

- **Taylor dispersion.** A velocity profile exists between the two bounding walls of the fracture. The resulting dispersion effect is called shear- or Taylor dispersion.

- **Matrix diffusion and sorption.** Interaction with the rock, stagnant pools and microfissures causes a number of processes that in effect lead to a delay and dispersion of a tracer pulse. These include: sorption on the fracture walls, diffusion into the rock matrix with sorption on inner surfaces and interaction with gouge.

As mentioned earlier, the diffusion into dead-end fractures of various sizes is by molecular diffusion. In order to illustrate the typical penetration depth for this process one may think of a substance with a certain molecular diffusion constant ($D_{mol} = 10^{-10}$ m^2/s) and an experimental time scale of, say, one month (t $\approx 2.6 \times 10^6$ s). The penetration length can then be estimated as $\sqrt{D_{mol} \times t} = 0.016$ metres. As the immobile zone is mainly made up of small fractures one can conclude that small scale dispersion is mainly governed by processes on the mm to cm scale.

For the transport problem on long time scales we may use the salinity field to illustrate some key features. First we can note the time scale for exchange in larger (> metres) dead-end fracture systems. If we put $D_{mol} = 10^{-10}$ m^2/s m^2/s and $L = 10$ metres, we find that the time scale is 10^{12} seconds, or 30,000 years ($t = L^2/D_{mol}$). It is thus not surprising to find water from the last glaciation, or the Litorina Sea ($\approx$ 7,000 years BP), in the fracture system at Äspö HRL. Gravitational forces may further enhance the entrapment of water in dead-end zones. If, for example, Litorina water (which has higher salinity than the present Baltic water) is located in a dead-end fracture extending downwards from the mobile zone gravitational forces will enhance the entrapment. The same principle applies to glaciation water (which has a lower density than present Baltic water) in a dead-end fracture extending upwards from the mobile zone. If we further note that the volume of all immobile zones is larger than the volume of the mobile zone, one can draw the conclusion that the salinity field is "stiff" and requires very long time scales to reach a steady state. On a shorter time scale all processes listed above is of course also active for the dispersion of salt.

DarcyTools has two built-in options for transport simulation; a particle tracking algorithm, PARTRACK, and advection/dispersion equations. The reasons why two methods are needed are based on the following assumptions:

- Salinity. The salinity field strongly influences the flow field through the density field. It is difficult to describe the salinity field by a set of particles and an advection/dispersion equation is therefore the best choice.

- Temperature. The main heat flux component is conduction and an advection/dispersion equation is hence the obvious choice for this variable. It will further be assumed that the water and rock is always in thermal equilibrium and only one temperature is thus solved for.

- Tracers. Simulation of tracer transport is best performed with a particle approach as this method is free from numerical dispersion effects. It is also possible to treat sorbing tracers (like radionuclides) with this technique.

These are the main scalars that need to be considered in applications. If additional scalar simulations are requested a decision about the most appropriate method has to be taken.

Transport of salt and tracers are assumed to be restricted to the water phase. Dispersion is hence due to mixing at fracture intersections (macro dispersion) and exchange with immobile zones (micro dispersion, as embodied in FRAME). FRAME is hence developed for both the advection/dispersion equation (as used for salt) and PARTRACK (as used for tracers).

FRAME rests on a number of concepts and assumptions of which the most essential are:

- *Fractures smaller than Δ are assumed to be filled with stagnant water (immobile volumes) and exchange matter with the flowing water (mobile volumes) by diffusion only.*

- *Subgrid fractures are assumed to follow a power-law (same as for resolved fractures).*

- *All immobile volumes can be represented by a set of boxes(or storage volumes), each with its own length scale, volume and effective diffusion coefficient.*

In Figure 5 some subgrid processes and concepts are illustrated. Let us consider a computational cell with a through flow, i.e. a cell with a flow channel. The flow "sees" a certain surface area, the flow wetted surface (FWS), as it passes the cell. The FWS may bring the flowing water in contact with other fractures, gouge material, stagnant pools, etc. Most of these volumes can be expected to have stagnant water and mass exchange is hence due to molecular diffusion. For a stagnant pool the relevant diffusion coefficient may be that for pure water, while diffusion into crossing fractures and the rock matrix may proceed with a diffusion rate that is several orders of magnitude smaller. As above, we will call the volume with flowing water the mobile zone and the volumes with no advection the immobile zone. Fractures and volumes which are not in contact with the mobile zone are of course of no relevance and can be excluded from the discussion. The situation outlined in Figure 5 is quite complicated and does not lend itself to direct descriptions of individual processes. The idealised problem is illustrated in Figure 6. The box with the smallest length-scale (dimension perpendicular to the mobile zone) will have the largest diffusion coefficient and normally also the largest contact area with the mobile zone. This volume will hence have a fast response. The multi rate diffusion technique /Haggerty and Gorelick 1995/ provides an efficient way to handle this problem computationally.
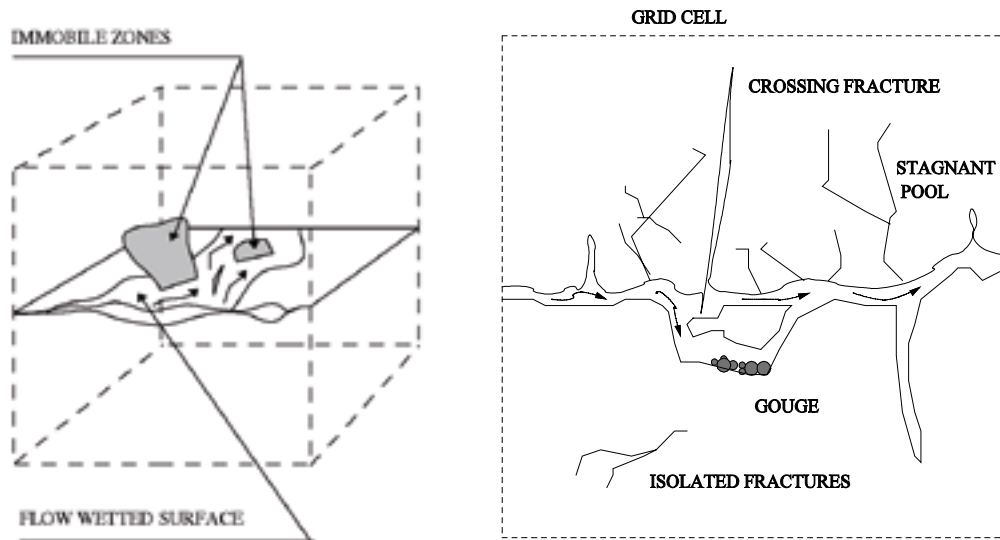
Figure 5. *Illustration of subgrid processes and concepts.*
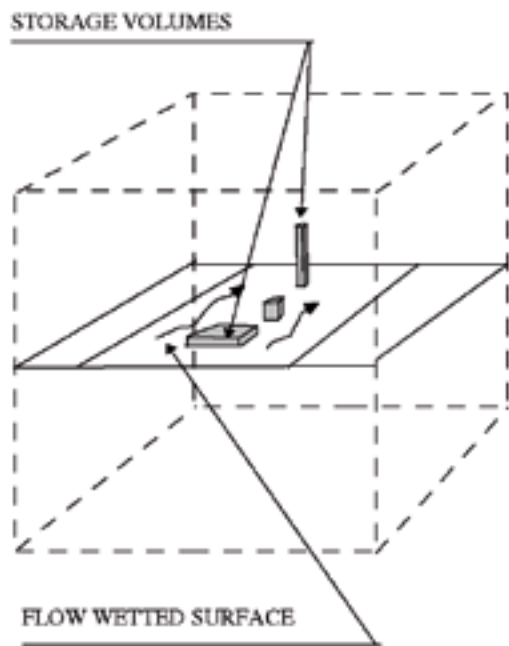
Figure 6. *The assumed structure of subgrid volumes and areas.*

135

5 Grid system

The arrangement of the computational grid is strictly not a conceptual issue. However, as it affects how well the fracture network is represented and what should be defined as "the sub grid scale", it is linked to the sub grid model FRAME.

In DarcyTools V3.0 the computational grid can be characterized as an "object based adaptive unstructured cartesian grid". The objects may be tunnels, boreholes, fracture zones, etc and the grid can be generated with conditions related to these objects. One may, for example, state that tunnel walls should be resolved with a cell size of 1 metre.

A 2D example of such a grid is shown in Figure 7. Major fracture zones, a tunnel and the surface layer have a refined resolution. It is further easy to understand how the cell size increases up to a maximum size. It is also possible to remove cells that are not part of the problem solution, for example cells with zero porosity.

The great advantage of this grid system is that the resolution can be distributed in a very efficient way. The fact that the grid is Cartesian simplifies the formulation of the finite volume equations and large grids (of the order of 10 million cells) can be used.
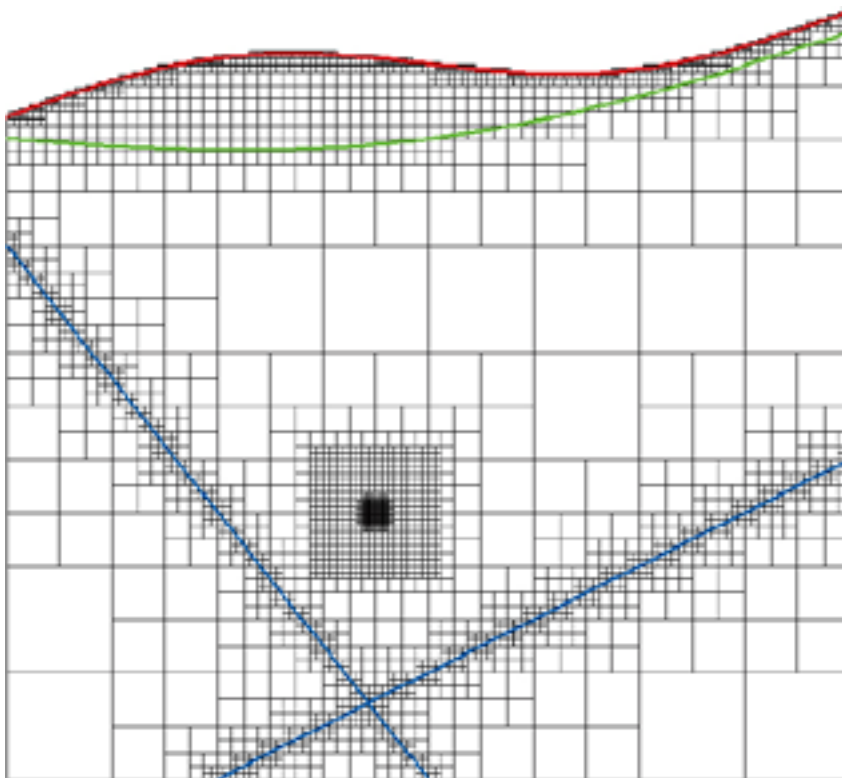
Figure 7. *The unstructured grid.*

References

Haggerty R, Gorelick S M, 1995. Multiple-rate mass transfer for modelling diffusion and surface reactions in media with pore-scale heterogeneity. Water Resour. Res, 31 (10), pp 2383–2400.

Harlow F H, Welch J E, 1965. Numerical Calculation of Time-Dependent Viscous Incompressible Flow of Fluid with Free Surface. Phys. Fluids, vol. 8, p. 2182.

Neretnieks I, 1993. Solute transport in fractured rock – applications to radionuclide waste repositories. In Flow and Contaminant Transport in Fractured Rock, 39–127. Academic Press, Inc.

Patankar S V, 1980. Numerical heat transfer an fluid flow. Hemisphere Publishing Corporation, McGraw-Hill Book Company.

Svensson U, Kuylenstierna H-O, Ferry M, 2006. DarcyTools v 3.0 – Concepts methods equations and demo simulations. SKB report in prep, Svensk Kärnbränslehantering AB.

Groundwater flow simulations of the last 10,000 years

Evolution of water types since the last de-glaciation

Patrik Vidstrand, Bergab

August 2007

Contents

1 Introduction

The regional Äspö model is used for simulation of the evolution of the groundwater chemistry (mixing) since the last deglaciation. The chemistry is characterised through some major end-members namely Glacial, Litorina, Baltic, and Meteoric waters entering from the top boundary. Additionally Brine water is apparent at depth at the initiation of the simulations along with a specified salinity. In order to discriminate between glacial fresh water and glacial saline waters, that is a mixture between brines and glacial waters that were already mixed at the initiation of the simulations, an artificial water type with the notation Mixed waters is also introduced.

The model properties are defined through a structural model and the DFN model (cf Appendix A).

The scope and objectives of this numerical model study was to set up a working model of Äspö HRL as described in the GeoMod project /Berglund et al. 2003, Laaksoharju and Gurban 2003, Vidstrand 2003/. It was further an objective to test the newly developed numerical code DarcyTools v3.0.

It has not been within the scope of this study to provide a fully calibrated model of Äspö HRL.

2 Initial and non-transient boundary conditions

The model domain have the approximate volume of 21·13·2 km³, and is geometrically bounded by the topography at the top surface. On this boundary the head is fixed at the ground surface as set by the numerical grid or at the sea bottom the head is fixed to the elevation of the sea at the time.

The topography for present day conditions is illustrated in Figure E-1. The maximum elevations within the model domain are between 40 and 50 metres above sea level.

The lateral boundaries are specified as no flow boundaries and are for present day conditions located along surface water divides that are topographical divides, or at sea.

Initially glacial waters occupy the top 500 metres within the entire model domain, between the –500 metre elevation and the –1,500 metre elevation the water type is specified as mixed water and below that, the water type is brine (see Figure E-2). The salinity of the top 500 metres is specified as being zero, that is fresh water conditions. From the –500 metre depth down to the domain bottom (–2,100 metres) the salinity is linearly increasing from zero to ten per cent.
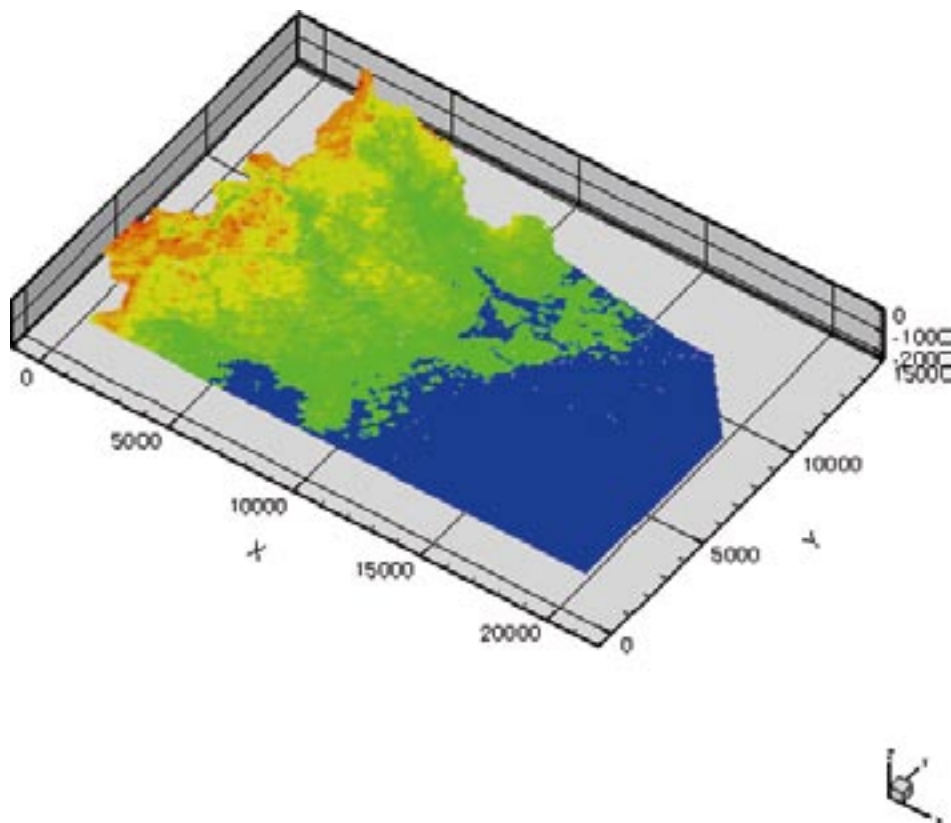
Figure E-1. *Schematic illustration of the elevation within the model domain in reference to present day sea level.*
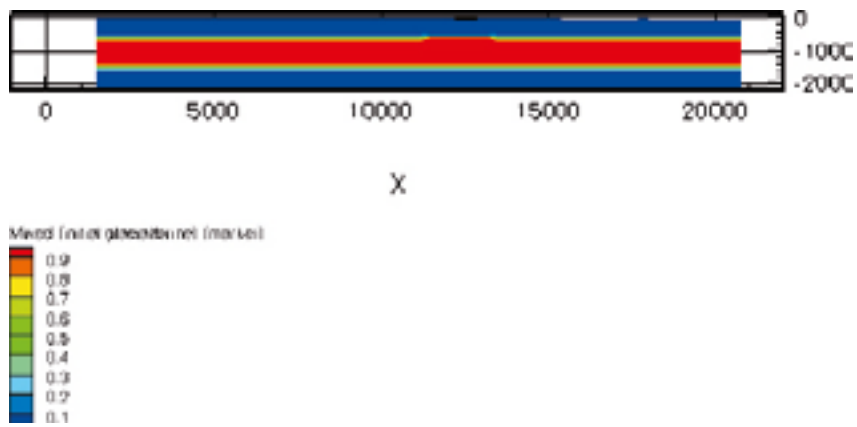
Figure E-2. *Schematic illustration of initial water type distribution. The sharper colour interface in the centre of the illustration is a contouring artefact due to the finer grid within this part of the model domain. Sitting on top of the mixed water is glacial water and below the mixed water zone the water type is brine.*

3 Transient boundary conditions

In regard to the top boundary the 10,000 years simulations are in a transient state. During this time span both the sea level and the sea water chemistry have changed significantly. The development of the Baltic Sea in the region of Oskarshamn has been simplified into three main transients functioning as a transient boundary condition.

The sea level immediately after the deglaciation stood high and the entire model domain was covered with sea water. Approximately 11,700 BP at the region of Oskarshamn the sea level dropped some 30 metres in only a few years. This kind of fast pressure drops on a top boundary is complicated to control in numerical models, especially with the time steps, by necessary, long in order to have reasonable simulation times for the entire model simulation. Sensitivity studies were performed and it was concluded that the necessary time step was too small and hence the starting time of the model simulation was moved forward 350 years and the sea level at the start of the simulation stood at 41 metres above present day level. The sea level variations in time during the first 4,000 years are still large and cause a small up-lifting movement of the deeper saline waters. However, it is believed that we now understand the main cause of this up-lift and also that in omitting the first 350 years the up-lift becomes small in comparison with the other processes that affect the model domain. However, we may introduce other errors presently not understood.

In lowering the initial sea level some of the high summits close to the lateral boundary in the west stand above sea. Therefore some glacial water parts of the model domain should have been replaced by meteoric waters. However, since both these waters are fresh waters the effect on the present day situation due to this initial error seems likely to be small, and the results also indicate that the entire land region is flushed of all other waters than the meteoric.
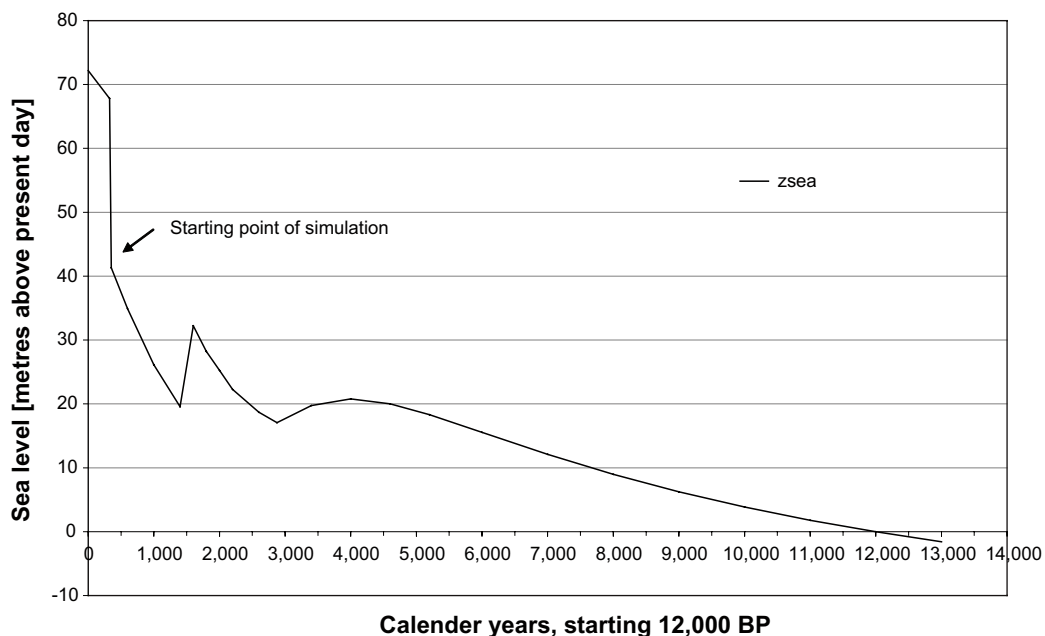
Figure E-3. Sea level development at the location of Oskarshamn since deglaciation used as a transient top boundary condition, based on information in /Påsse 1996/.

The chemistry of the sea water, described only as salinity, change throughout the Baltic Sea development due to opening and closure of discharge areas for the Baltic along with the possibility of marine waters to enter the Baltic Sea basin. In Figure E-4 the development of salinity at the location of Oskarshamn is illustrated. For the first years of the model simulation the sea water have characteristics of fresh water. There has been a debate on the characteristics of the Yoldia Sea phase (see Figure E-5), however in the Site Investigation programme the approach is that the Yoldia Sea in the region of Oskarshamn was a fresh water sea during the entire phase. Some sensitivity studies were performed and even if Yoldia Sea had a small salinity, this salinity was much smaller than the salinity of the Litorina Sea; under such conditions a salinity in the Yoldia Sea have little effect on the final results. This result however, is significantly affected by the up-lift effect discussed above and large time steps (tens of years) along with large pressure variations on the top boundary artificially increase the importance of Yoldia Sea salinity.

In Figure E-5 the specified time periods for different characteristics of the sea waters are presented. For all parts of the model domain above sea level the recharge waters are of meteoric characteristics. For parts of the model domain where the top boundary is below sea level the main driving force is the density driven mixing due to the salinity in the sea.
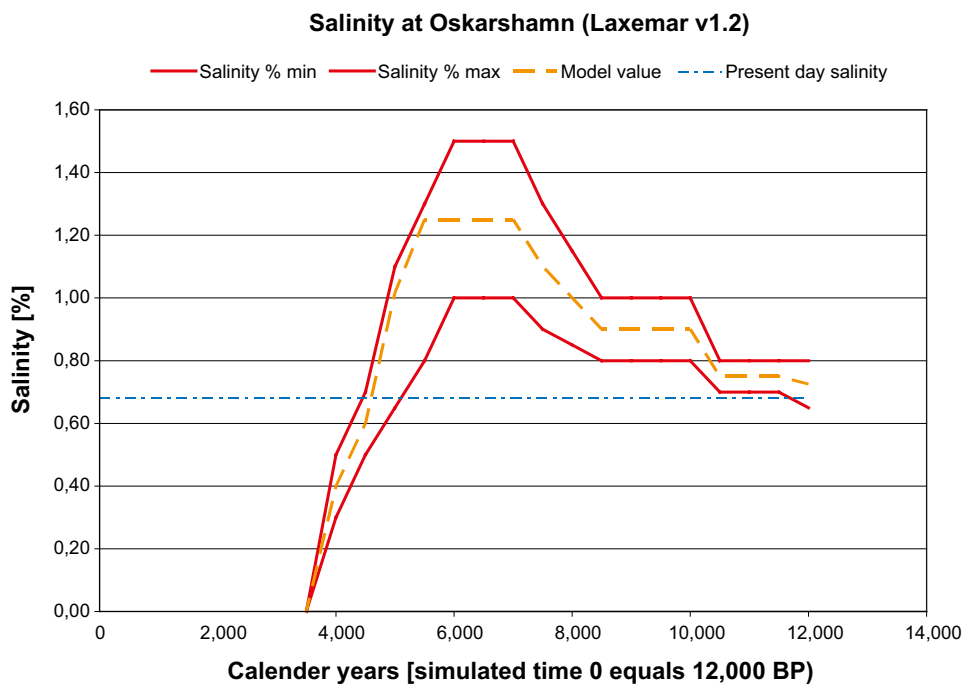
Figure E-4. *Sea salinity development at the location of Oskarshamn during the last 10,000 years used as a transient boundary condition. Based on chart in /SKB 2006/.*
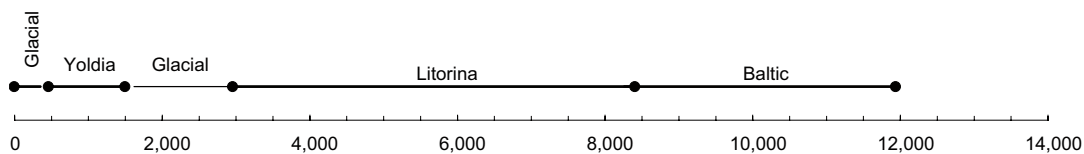
Figure E-5. *Sea water type development since deglaciation as specified in the simulation. Glacial water type refers mainly to fresh water conditions. The Yoldia water is herein assumed to be fresh at the location of Oskarshamn during the entire simulation.*

4   Some comments on the grid and the simulations

The amount of cells in the model domain is approximately 553,000 with a mesh that span from 128 metres in cube down to vertical size of 2 metres in the top surface cells. The central region of the model domain where the Äspö site is located the main cell size is 64 metres in cube.

The simulation is performed as a fully coupled solution of the mass and salt equations. Incorporating 580 time steps with a used time step length of 20 years a full simulation takes approximately 35 hours on a single processor Xeon 3.2 GHz/1 MB Cache/533 MHz computer with 4 GB RAM.

5   Results

Figure E-6 to Figure E-9 illustrate the pressure situation at present day condition, that is after the entire simulation. As expected the results are governed by the top boundary condition of fixed head.

Figure E-10 and Figure E-11 illustrates the salinity situation at present day conditions, that is after the entire simulation.
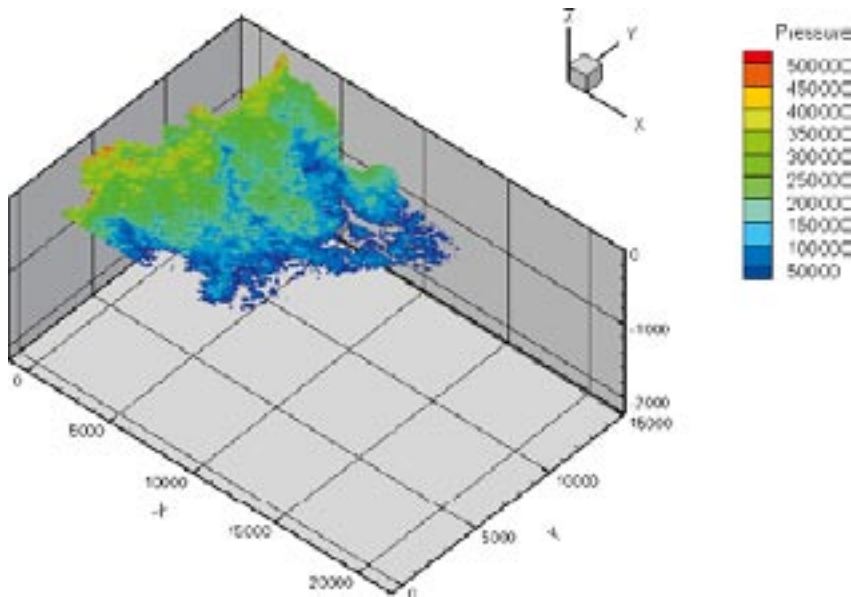
Figure E-6. *Final dynamic pressure, in Pa, situation at ground surface, that is the groundwater table. A simple transformation from pressure to fresh water heads can be done by removing four zeros. The pressure result is governed by the boundary condition and is hence a perfect image of the topographical elevation given in Figure E-1. Axles are in metres.*
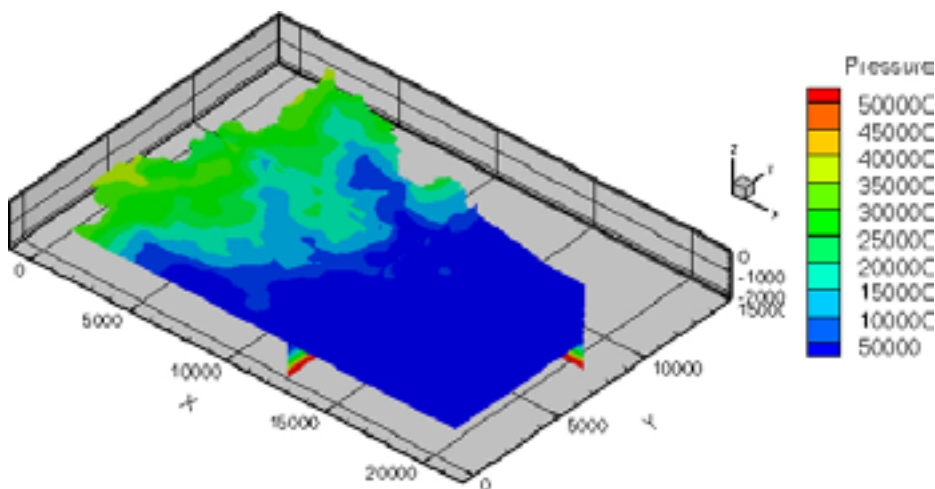
Figure E-7. *Final dynamic pressure, in Pa, situation at the –450 metre elevation. A simple transformation from pressure to fresh water heads can be done by removing four zeros. The pressure result is a smooth reflection of the topographical elevation. Axles are in metres.*
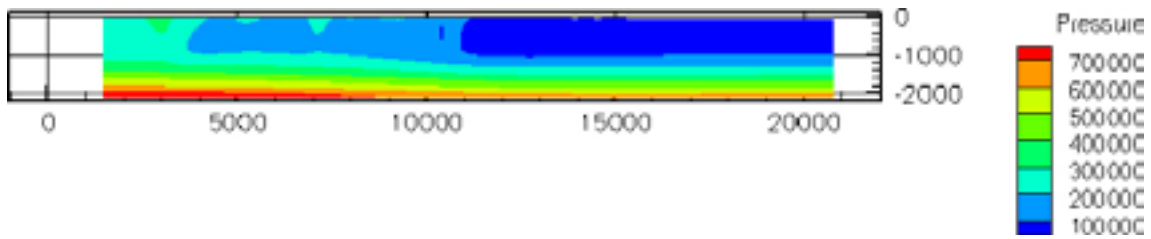
Figure E-8. *Final dynamic pressure, in Pa, situation on a plane along a transect at the y-coordinate of 8,000 metres, west-east. A simple transformation from pressure to fresh water heads can be done by removing four zeros. The pressure result is a smooth reflection of the topographical elevation. Axles are in metres.*
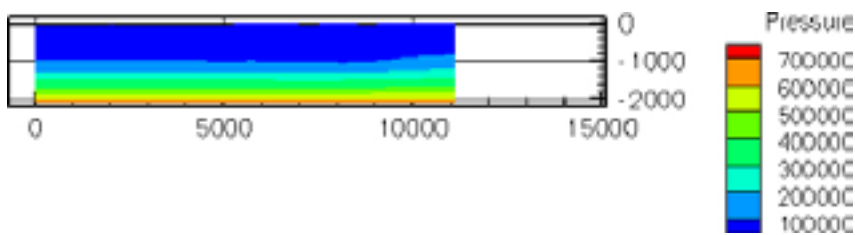
Figure E-9. *Final dynamic pressure, in Pa, situation on a plane along a transect at the x-coordinate of 12,300 metres, south-north. A simple transformation from pressure to fresh water heads can be done by removing four zeros. The illustrated location is located in the sea region and the small topography is clearly illustrated. Axles are in metres.*
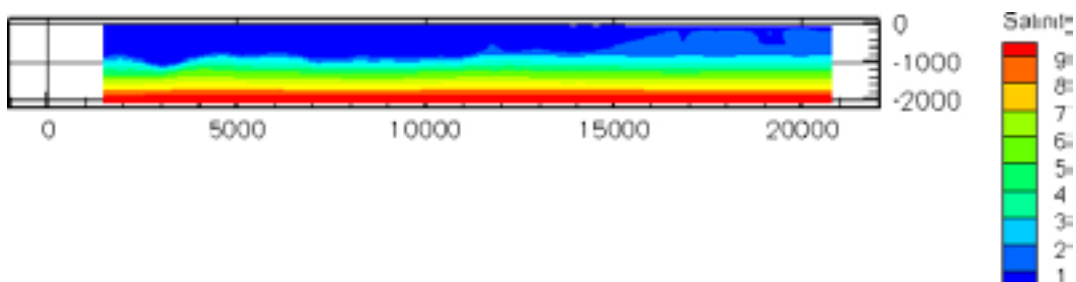
Figure E-10. *Final salinity situation on a plane along a transect at the y-coordinate of 8,000 metres, west-east. Salinity in percentage by weight. The land influence is seen in the smaller salinity in west, the main land region. Axles are in metres.*
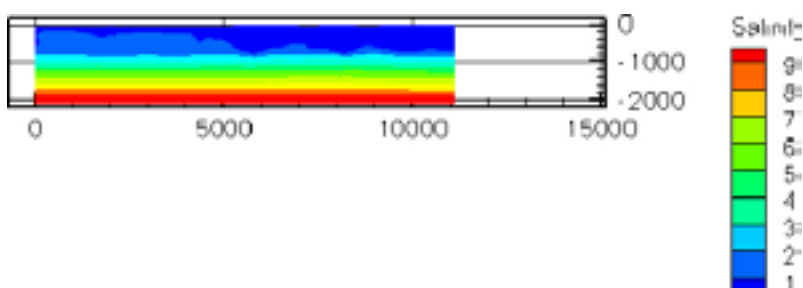
Figure E-11. *Final salinity situation on a plane along a transect at the x-coordinate of 12,300 metres, south-north. Salinity in percentage by weight. The illustrated location is located in the sea region and the land influence is seen in the smaller salinity in north, more land. Axles are in metres.*

154

Figure E-12 to Figure E-16 illustrate the development of Rain water (meteoric) in the model domain. The penetration of rain depends on the topographical differences and distance to the main area of discharge. In the beginning of the simulation small flow cells develop with recharge on the high summits. However, when the sea level sinks the results indicate that a regional flow cell develops, this flow cell controls the deep groundwater flow and flushing of Rain water from the surface water divide all the way out into the Baltic Sea.

In Figure E-14 and Figure E-15 the local flow cells within the archipelago is apparent and in Figure E-16 the local recharge and discharge areas on the ground surface are reflected in deeper and shallower penetration depth for the Rain water. In the simulation the fresh water bubble beneath Äspö reach depths of at least 500 metres, as is indicated in Figure E-16.

In no part of this simulation were effects of the Äspö HRL tunnel accounted for, and the illustration of the tunnel in Figure E-16 is only on behalf of orientation.
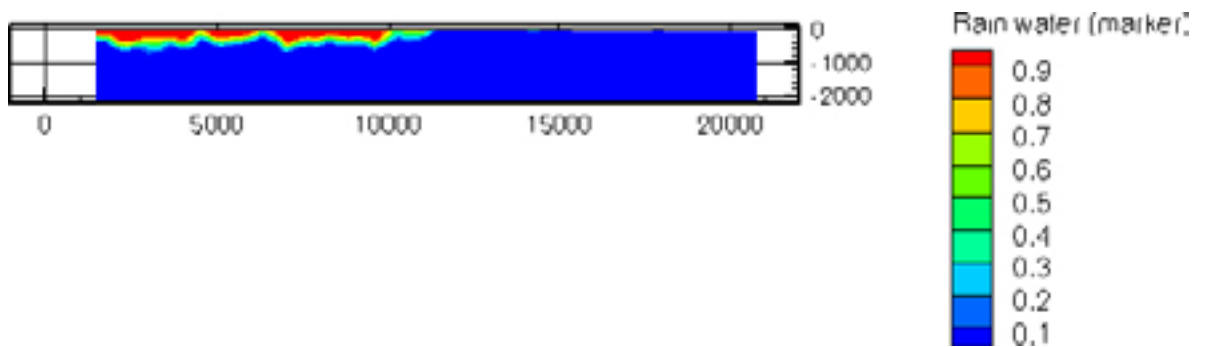
Figure E-12. *Distribution of Rain water after 3,000 simulation years just before the beginning of the Litorina Sea phase on a plane along a transect at the y-coordinate of 8,000 metres, west-east. The sea level stands approximately 18 metres above present day level and the Rain water have replaced the Glacial water at land The undulation is a smooth representation of the topographical elevation, illustrating localised flow cells. Axles are in metres.*
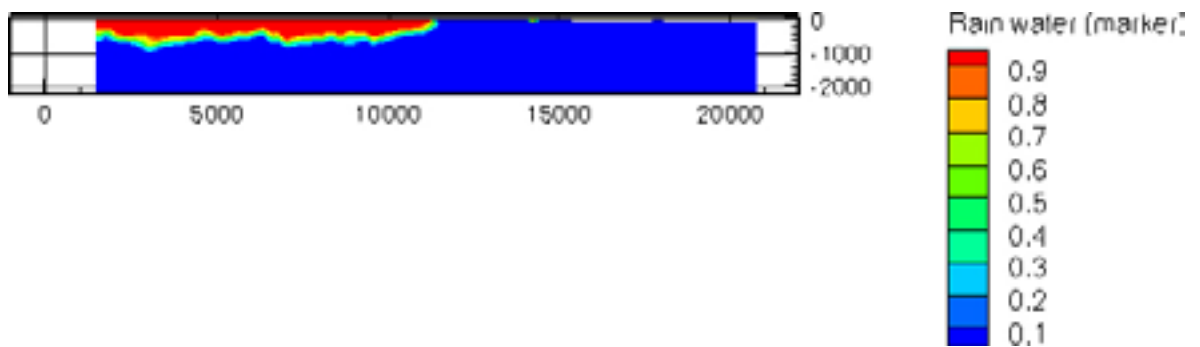
Figure E-13. *Distribution of Rain water after 8,500 simulation years just at the end of the Litorina Sea phase on a plane along a transect at the y-coordinate of 8,000 metres, west-east. The sea level stands approximately 7 metres above present day level and the Rain water have replaced the Glacial water under the ground surface. The undulation is less pronounced and the representation of the topographical elevation not so clear as compared to Figure E-13. Deep groundwater flow in the main land is becoming part of a regional flow cell. Axles are in metres.*
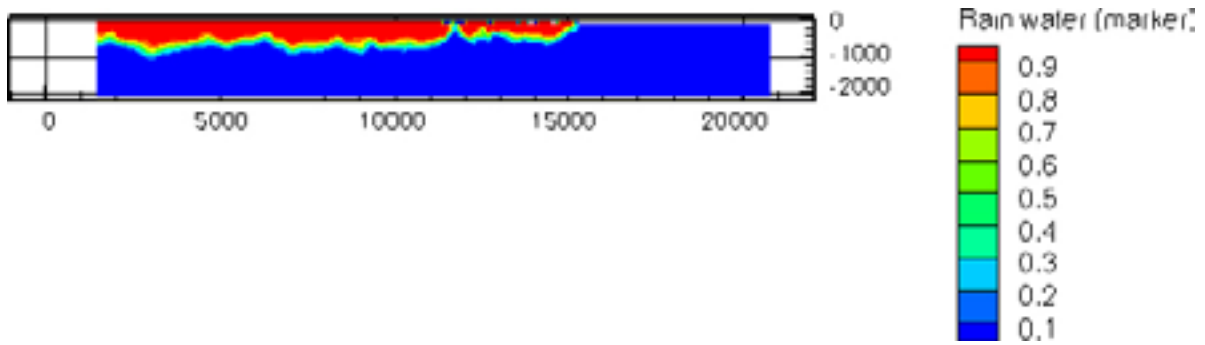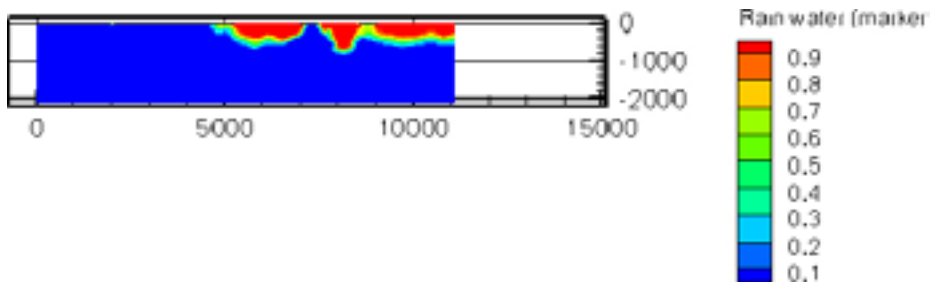
Figure E-14. *Distribution of Rain water after the entire simulation on a plane along a transect at the y-coordinate of 8,000 metres, west-east. The sea level stands at present day level and the Rain water have replaced the Glacial water under the entire ground surface. The undulation in the main land is less pronounced and the representation of the topographical elevation not so clear. Deep groundwater flow in the main land is becoming part of a regional flow cell. The part between 12,000 metres and 15,000 metres illustrate the archipelago with its localised flow cells. Axles are in metres.*

Figure E-15. *Distribution of Rain water after the entire simulation on a plane along a transect at the x-coordinate of 12,300 metres, south-north. The sea level stands at present day level and the Rain water have replaced the Glacial water under the entire ground surface. The northern part illustrates the archipelago with its localised flow cells. Axles are in metres.*
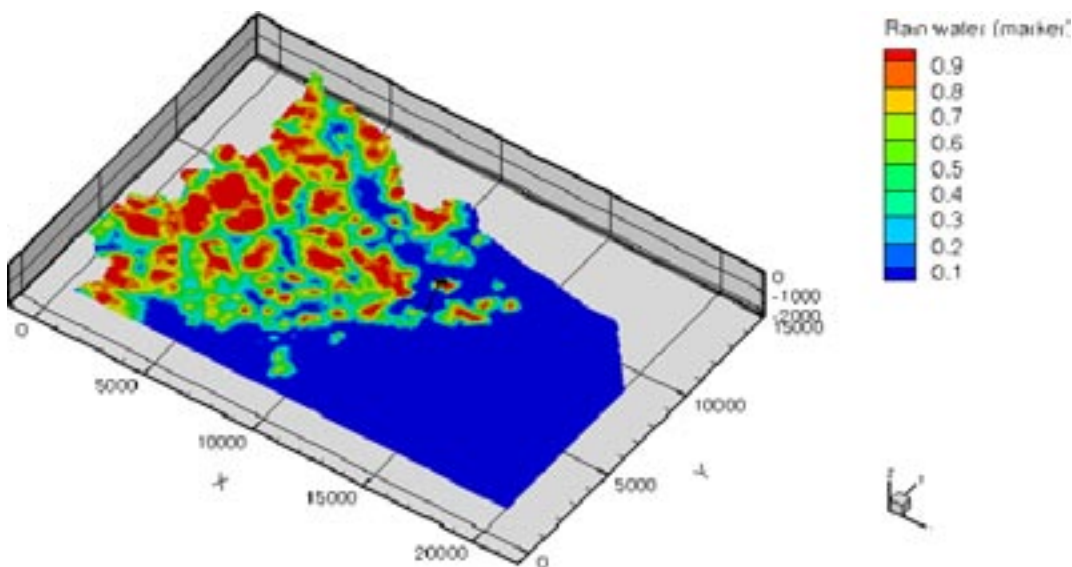
Figure E-16. *Distribution of Rain water after the entire simulation on a plane at the –450 metres elevation. The sea level stands at present day level and the Rain water have replaced the Glacial water under the entire ground surface. Effects of the topography are observed through less penetration depth in regions of low lands acting as discharge areas for the rain water and vice versa for the high summits. The Äspö HRL tunnel is illustrated in the figure, the simulation however has not included any effects of the tunnel. Axles are in metres.*

Figure E-17 to Figure E-19 illustrate the development of the artificial water type noted Mixed water. It is observed that some small perturbation exists in areas where little or no driving force has acted (beneath sea). The only "force" is the pressure transient on the top boundary and these perturbations are likely the effect of the time step length being still somewhat too large. However, the final perturbations seen in Figure E-19 are small and therefore it is believed that the used time step was small enough to capture the essential behaviour and the result is believed accurate in regards to the possible up-lift due to the pressure transient on the top boundary.

Figure E-20 to Figure E-23 illustrate the development of the Glacial water. Since the Glacial water is the initial conditions in the top 500 metres nothing except the flushing due to recharge of Rain water is expected to happen during the first simulation years when the sea water also is of Glacial/fresh type.
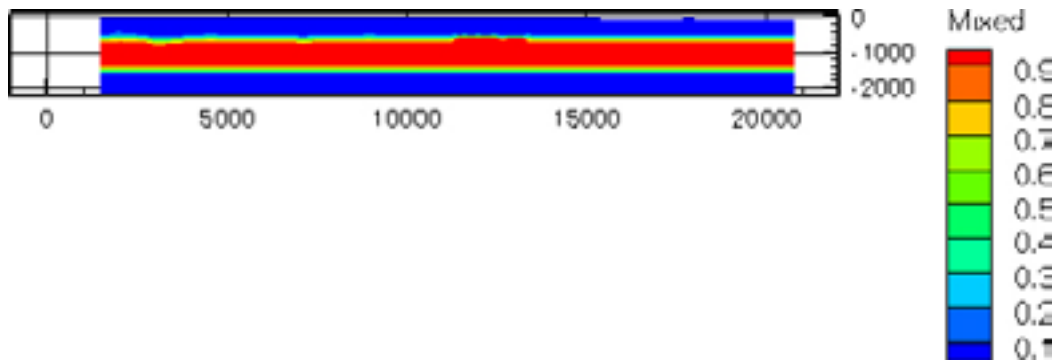
Figure E-17. *The distribution of the artificial water type noted Mixed water after 3,000 years of simulation just before the beginning of the Litorina Sea phase on a plane along a transect at the y-coordinate of 8,000 metres, west-east. The small undulations are mainly found under areas of the deepest penetration of Rain water at the time. Some small perturbations are seen in the finer grid region of the domain, this region is still under sea and relatively far from any recharge area of Rain water. These perturbations are therefore likely an effect of the up-lift effect caused by too large time steps and the imposed large pressure transients on the top boundary. This effect is in these simulations small and as a consequence it is assumed that the simulations are performed with a sufficient time step to account for the pressure transients needed to be accounted for. Axles are in metres.*
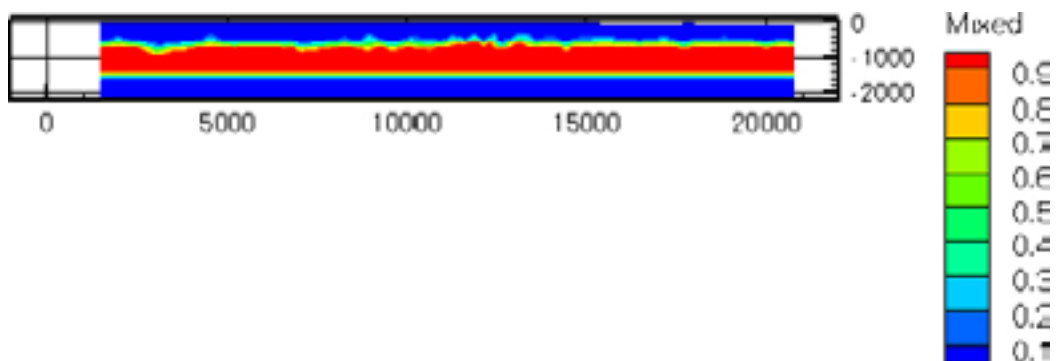
Figure E-18. *The distribution of the artificial water type noted Mixed water after 8,500 years of simulation just at the end of the Litorina Sea phase on a plane along a transect at the y-coordinate of 8,000 metres, west-east. The undulations are found in relation to areas of the deepest penetration of Rain water at the time. Axles are in metres.*
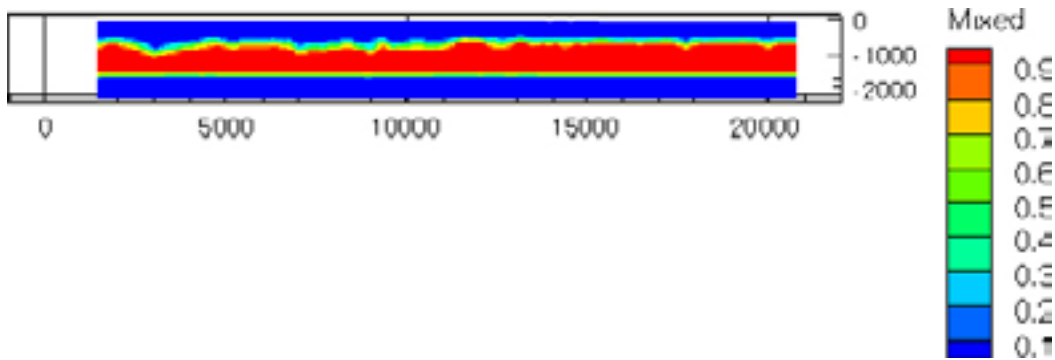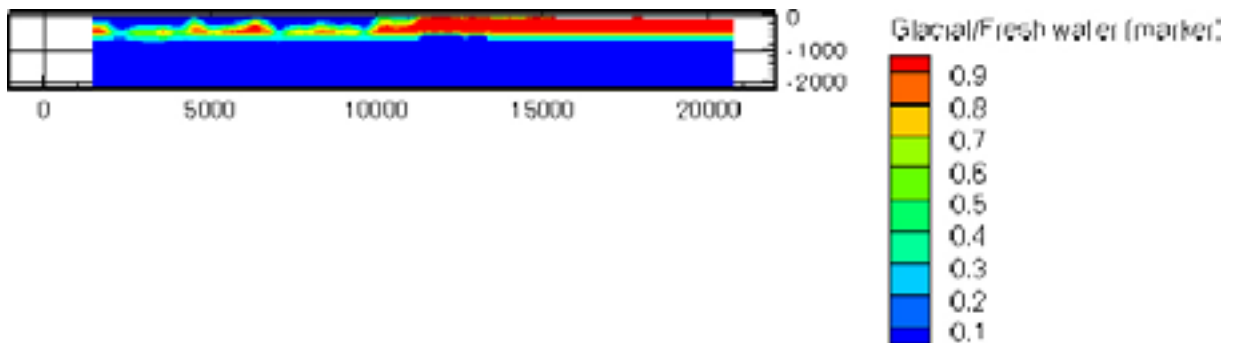
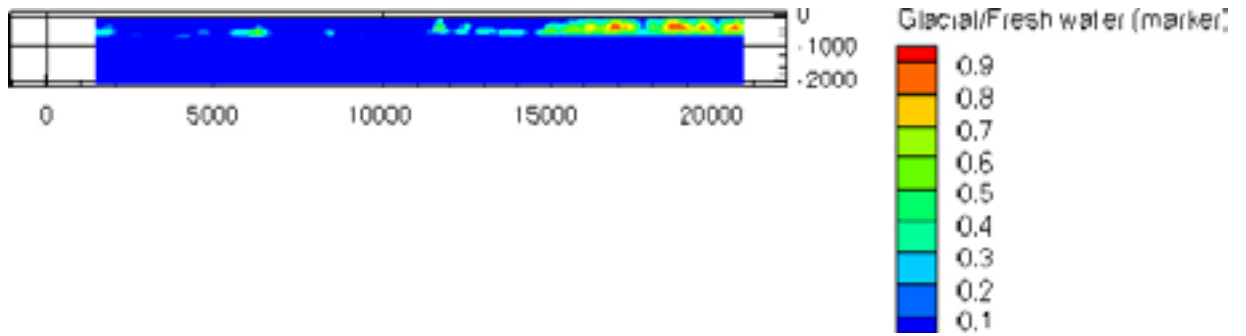***Figure E-19.*** *The distribution of the artificial water type noted Mixed water after the entire simulation on a plane along a transect at the y-coordinate of 8,000 metres, west-east. The undulations are found in relation to areas of the deepest penetration of Rain water at the time. Some perturbations are seen in the region of the domain far out in the Baltic Sea. These perturbations are likely the final effect of the up-lift effect caused by too large time steps and to large pressure transients on the top boundary. This effect is in these simulations small and as a consequence it is assumed that the simulations are performed with a sufficient time step to account for the pressure transients needed to be accounted for. Axles are in metres.*

Figure E-20. *The distribution of the Glacial water after 3,000 simulation years just before the Litorina Sea phase on a plane along a transect at the y-coordinate of 8,000 metres, west-east. Up to this time the only driving force has been the flushing due to recharge of Rain water on the main land. The undulation reflects the local recharge and discharge areas within the exposed model domain. Axles are in metres.*
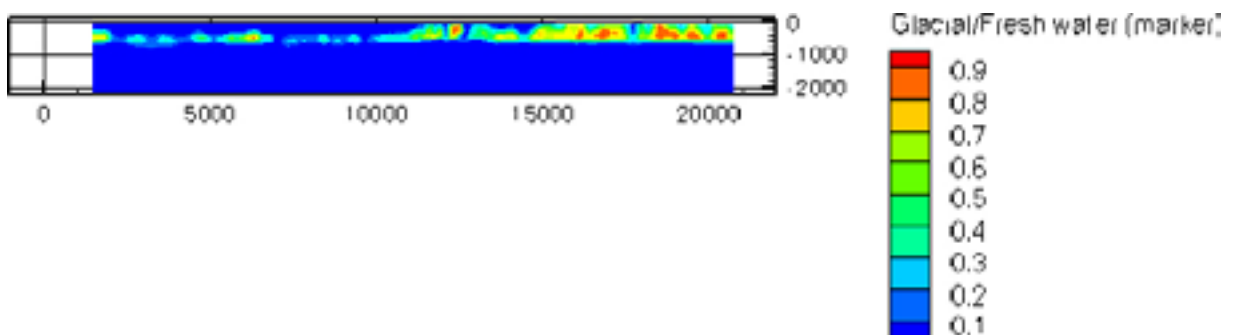
Figure E-21. *The distribution of the Glacial water after 8,500 simulation years at the end of the Litorina Sea phase on a plane along a transect at the y-coordinate of 8,000 metres, west-east. During the Litorina Sea phase the density driven mixing has had its maximum and the flushing due to recharge of rain has increased with increasing land area. Below the exposed main land only small pockets of residual Glacial water is trapped within blocks of rock mass. Hereafter the sea density is always less than during the Litorina Sea maximum and hence only the flushing continue to drive the water exchange. Axles are in metres.*

Figure E-22. *The distribution of the Glacial water after the entire simulation on a plane along a transect at the y-coordinate of 8,000 metres, west-east. Below the exposed main land only small pockets of residual Glacial water is trapped within blocks of rock mass. Out in the Baltic Sea far from the recharge areas little have happened with the residual Glacial water during the last 3,000 years. Axles are in metres.*

In Figure E-20 it is seen that in the parts of the model domain where no recharge has happen the initial conditions are still stable. During the Litorina Sea phase the salinity of the sea increases and a density driven mixing initiates, and the Glacial water is replaced even out under the sea. In Figure E-21 the situation after the Litorina Sea phase is illustrated. Scoping comparisons with the results presented in /Follin et al. 2004/ yields that the general trend of residual Glacial waters are apparent in both simulations. However, in our simulations more pockets of residual glacial waters are found beneath the exposed land areas. But, on the other hand, out beneath the sea our simulation yields a more even distribution of residual Glacial water, where the results in /Follin et al. 2004/ indicate a stronger dependence on flow within the hydraulic conductors defined by the Geological structural model.

Figure E-24 to Figure E-27 illustrate the development of the Litorina water. Figure E-25 illustrates the situation after the end of the Litorina Sea phase which happened approximately 2,000 years after the maximum salinity of the Litorina Sea phase. The Litorina water is mainly found in or within the vicinity of hydraulic conductors defined by the Geological structural model. However, in scoping comparison with the results by /Follin et al. 2004/ our results indicate a more even distribution also affecting the blocks of rock mass in-between the more permeable structures.

After the Litorina Sea phase the Litorina water is diluted with time but the general characteristics are preserved.
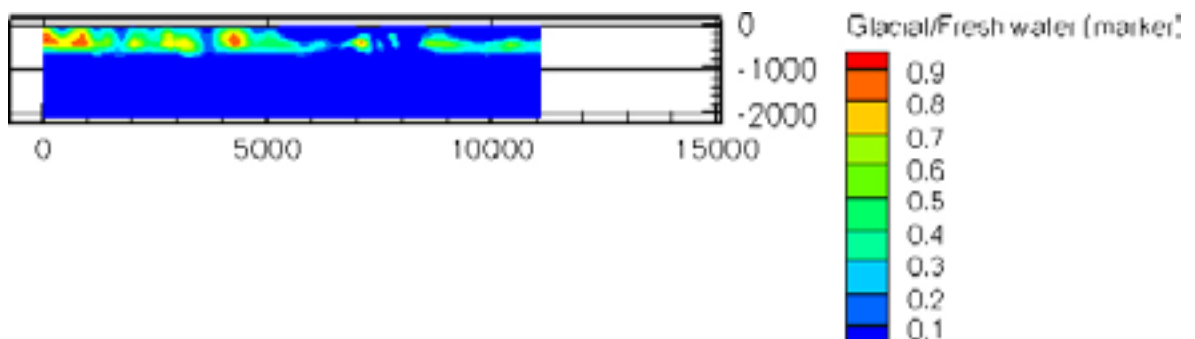

Figure E-23. *The distribution of the Glacial water after the entire simulation on a plane along a transect at the x-coordinate of 12,300 metres, south-north. Below the exposed main land only small pockets of residual Glacial water is trapped within blocks of rock mass. Axles are in metres.*
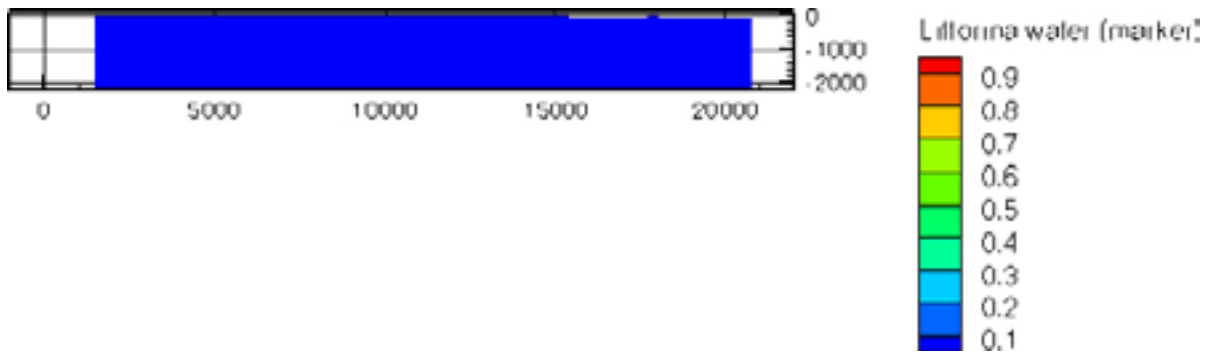
159

Figure E-24. *The initial situation of litorina water after 3,000 simulation years just before the Litorina Sea phase on a plane along a transect at the y-coordinate of 8,000 metres, west-east. No injection of litorina water has happened and hence no litorina water is found within the model domain. Axles are in metres.*
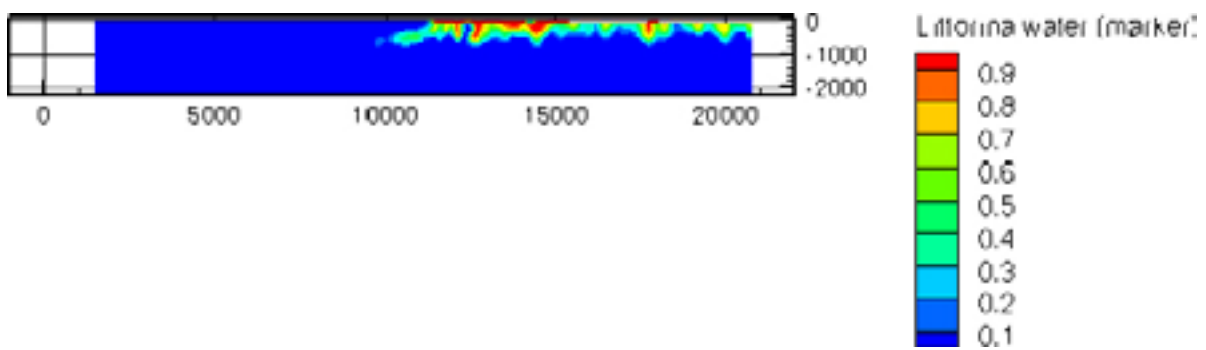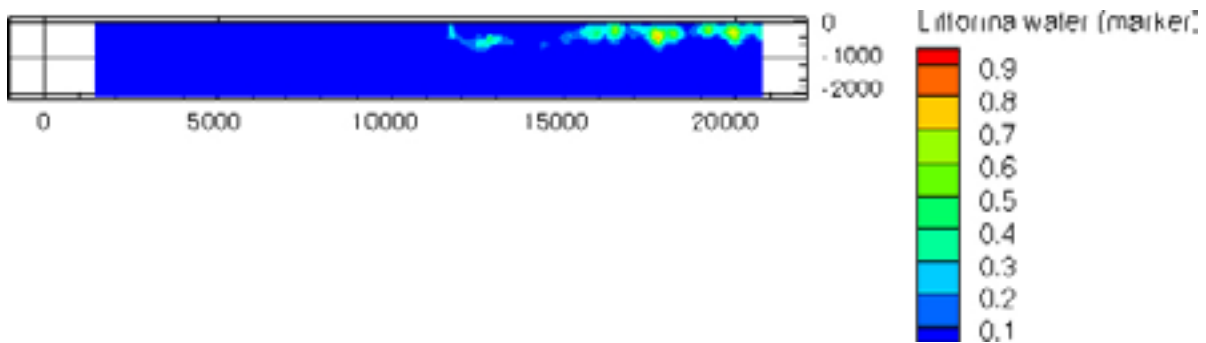

Figure E-25. *The distribution of Litorina water after 8,500 simulation years at the end of the Litorina Sea phase on a plane along a transect at the y-coordinate of 8,000 metres, west-east. Below the exposed main land no Litorina water has been injected and hence the Litorina water can only be found beneath sea or in the vicinity of the present-day shore line. The majority of the Litorina water has found its way down along hydraulic conductors defined by the Geological structural model, however also blocks of rock mass have experienced an exchange of the older water with the Litorina water. Axles are in metres.*

Figure E-26. *The distribution of the Litorina water after the entire simulation on a plane along a transect at the y-coordinate of 8,000 metres, west-east. Below the exposed main land no Litorina water has been injected and hence the Litorina water can only be found beneath sea or in the vicinity of the present day shore line. Out in the Baltic Sea far from the recharge areas the Litorina water has been diluted during the last 3,000 years. Axles are in metres.*
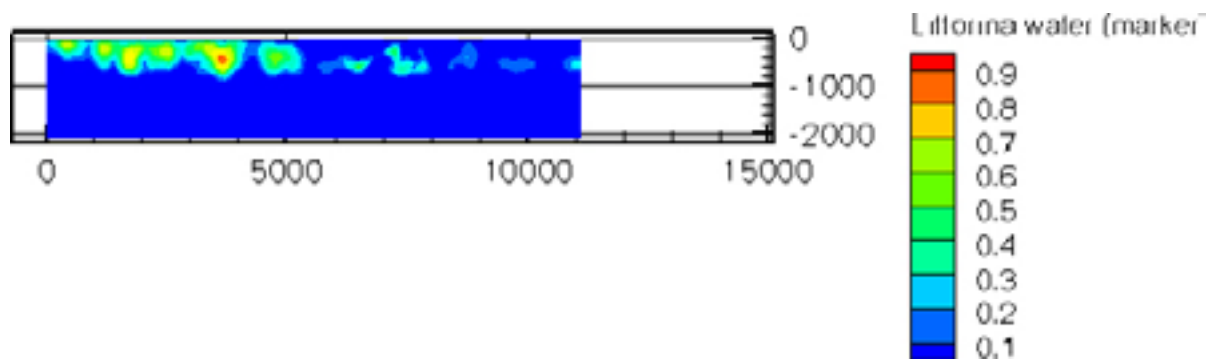
Figure E-27. *The distribution of the Litorina water after the entire simulation on a plane along a transect at the x-coordinate of 12,300 metres, south-north. Below the exposed land areas of the archipelago only small pockets of Litorina water is trapped within blocks of rock mass. Axles are in metres.*

6   Remarks

The simulations performed represent a Base Case and in order to be fully understood some results need to be subjected to some sensitivity studies.

The simulation however proved to be a satisfying set up with plausible results that easily could be used as initial conditions for a tunnel simulation.

The necessary simulation time is reasonable to work with.

7   References

Berglund J, Curtis P, Eliasson T, Olsson T, Starzec P, Tullborg E-L, 2003. Äspö Hard Rock Laboratory, Update of the geological model 2002. SKB IPR-03-34, Svensk Kärnbränslehantering AB.

Follin S, Stigsson M, Berglund S, Svensson U, 2004. Variable-density groundwater flow simulations and particle tracking – Numerical modelling using DarcyTools. Preliminary site description of the Simpevarp area – version 1.1. SKB R-04-65, Svensk Kärnbränslehantering AB.

Laaksoharju M, Gurban I, 2003. Äspö Hard Rock Laboratory, Update of the hydrogeochemical model 2002, SKB IPR-03-36, Svensk Kärnbränslehantering AB.

Påsse T, 1996. A mathematical model of the shore level displacement in Fennoscandia. SKB TR-96-24, Svensk Kärnbränslehantering AB.

Vidstrand P, 2003. Äspö Hard Rock Laboratory, Update of the hydrogeological model 2002, SKB IPR-03-35, Svensk Kärnbränslehantering AB.

Groundwater flow simulations of the Äspö HRL

Regional steady-state situation

Patrik Vidstrand, Bergab

August 2007

Contents

1 Introduction

The tunnel model is incorporated in the regional model of Äspö. However, in order to simulate the effects of the tunnel the discretisation within the model domain incorporate cells of the regional scale of 128 metres in cube down to 1 metre in cube along the tunnel. The simulation incorporates a simplistic surface hydrology model, which accounts for flow in rivers and a more conductive top 20 metres layer. The recharge of water is specified and firstly a present day steady-state situation is established. Starting in this situation the tunnel is introduced, with a stepwise approach – through a successively increasing tunnel wall permeability – so that the full drawdown effect with a tunnel wall permeability (grouted) of $1\cdot10^{-15}$ m^2, is approached after a couple of simulations.

Some minor calibration studies of inflow to the tunnel segments along with an additional study of eight alternative locations for a new tunnel have also been incorporated in the report.

The model properties are defined through the geological structural model and the DFN model (cf Appendix A).

The scope and objectives of this numerical model study was to set up a working model of Äspö HRL as described in the GeoMod project /Berglund et al. 2003, Laaksoharju and Gurban 2003, Vidstrand 2003/. It was further an objective to test the newly developed numerical code DarcyTools v3.0.

It has not been within the scope of this study to provide a fully calibrated model of Äspö HRL.

The outcome of the study is a numerical set up of Äspö HRL along with some observations of difficulties with the GeoMod and POM specifications.

2   Initial and boundary conditions

The model domain has the approximate volume of $21 \cdot 13 \cdot 2$ km^3, and is geometrically bounded by the topography at the top surface. On this boundary a recharge of 165 mm/year /SKB 2006/ is specified. At the ground surface the hydraulic conductivity is $1 \cdot 10^{-3}$ m/s. This surface value is continuously decreased with a factor of 10 for every 3 metres, the lowest value assigned in this top layer is 10^{-6} m/s, and at 20 metres the bedrock characteristics are the governing. The Baltic Sea bottom has been assigned the same hydraulic conductivity as the bedrock. For the simulations presented herein the Baltic Sea is assigned as a specified head boundary; and as DarcyTools does not contain the option of two groundwater tables a specified head situation makes the omission of a possible low-permeable layer less significant. The treatment of the seabed material and this associated boundary condition is however potentially crucial for getting the correct amount of water into drained bedrock close to the shoreline. No studies have been conducted on this topic.

The topography for present-day conditions is illustrated in Figure F-1. The maximum elevations within the model domain are between 40 and 50 metres above sea level.

The surface hydrology model properties are calibrated so that fluxes in rivers are realistic, lakes develop at correct locations, and so that the groundwater table is realistic in relation to the information available /SKB 2006/.

The lateral boundary to the west is specified by a surface water divide along which a fixed head is specified for the top 500 metres with the groundwater table fixed 3 metres below ground surface. For the same lateral boundary the salinity is specified to zero for the top 500 metres, that is fresh water.

All other boundaries are no flow boundaries and the lateral boundaries that exist below the Baltic Sea have been set as frozen (fixed at initial values). The bottom boundary has a fixed salinity at 10 per cent.

The salinity of the Baltic Sea is 0.73 per cent and the head at the sea bottom is fixed at zero elevation.

Initially all of the model domain water is unmarked. The recharge is marked as Rain water (meteoric) and as a consequence all regions of the model domain that are affected by the recharge can be identified.
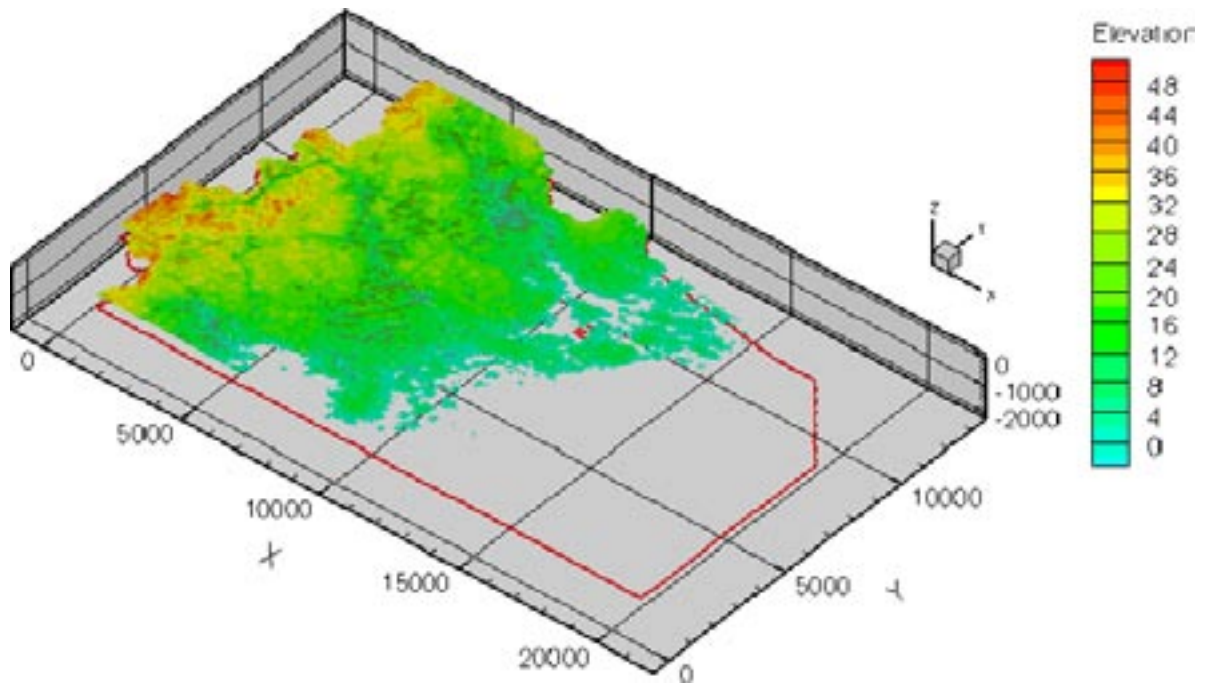
Figure F-1. *Schematic illustration of the elevation (metres above sea level) within the model domain in reference to present-day sea level. The shaded in greyish areas on the land illustrate out-flow of groundwater. Axles are in metres.*

3 Some comments on the grid and the simulations

The amount of cells in the model domain is approximately 1.2 million, with a mesh that span from 128 metres in cube down to 1 metre in cube along the tunnel, as well as a vertical size of 2 metres in the top surface cells. In the central region of the model domain where the Äspö site is located the main cell size is 64 metres in cube, and the laboratory site has a main cell size of 8 metres in cube.

Figure F-2 illustrates the main cell structure of the surface layer. Figure F-3 and Figure F-4 illustrate the finer discretisation down to the tunnel walls.

The simulation is performed as a fully coupled solution of the mass and salt equations. The simulation takes approximately one hour per 40 time steps (one time step represent one half-year); a steady-state solution is reached after approximately 3,000 years for the natural conditions, on a single processor Xeon 3.2 GHz/1 MB Cache/533 MHz computer with 4 GB RAM.
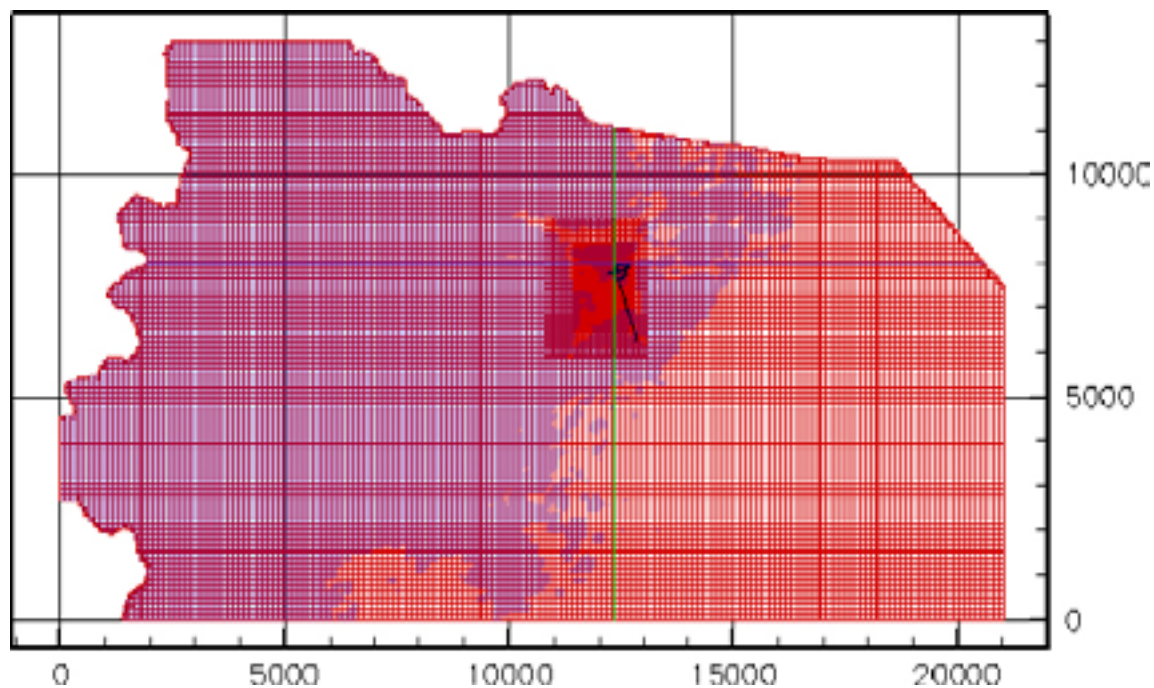
Figure F-2. *Illustration of the main grid. The bluish colour indicates land based surface cells. The larger domain incorporate cells of the size 128 metres in cube; in the first finer discretization around Äspö the cell size is 64 metres and in the second box of finer discretisation the largest cells are 32 metres in cube.*
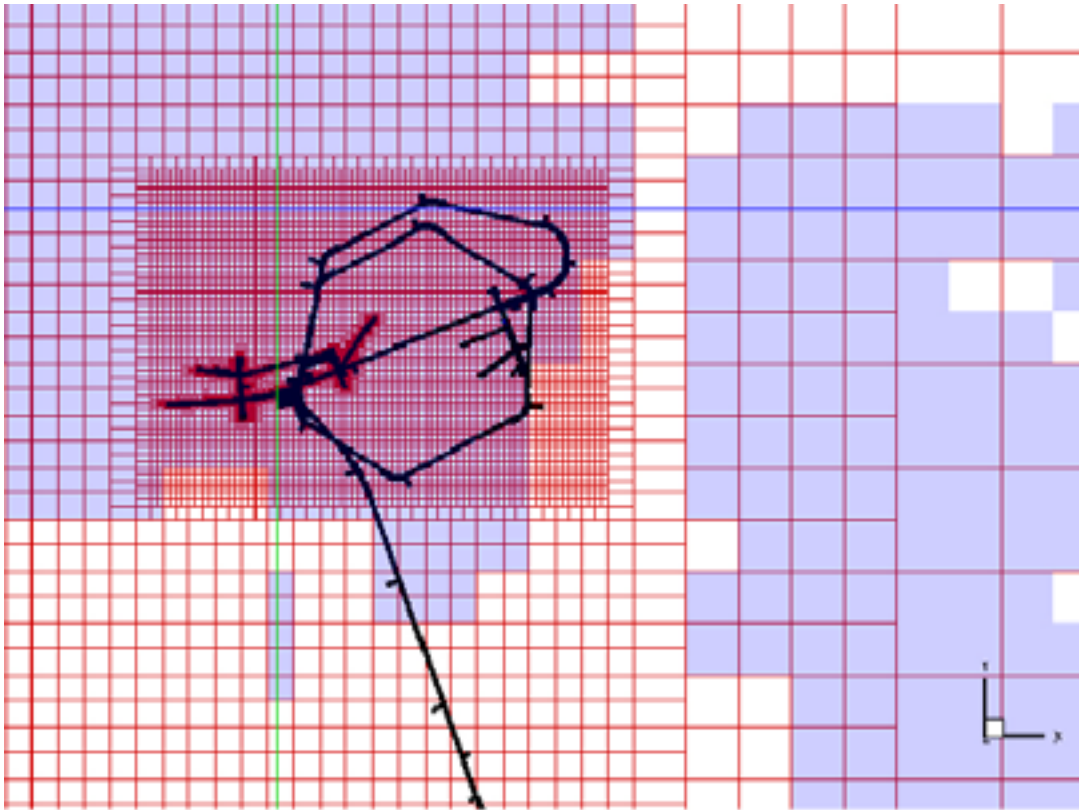
Figure F-3. *Details on the grid at the laboratory scale. The main cell size from right is 128 metres, 64 metres, 32 metres, and 8 metres.*
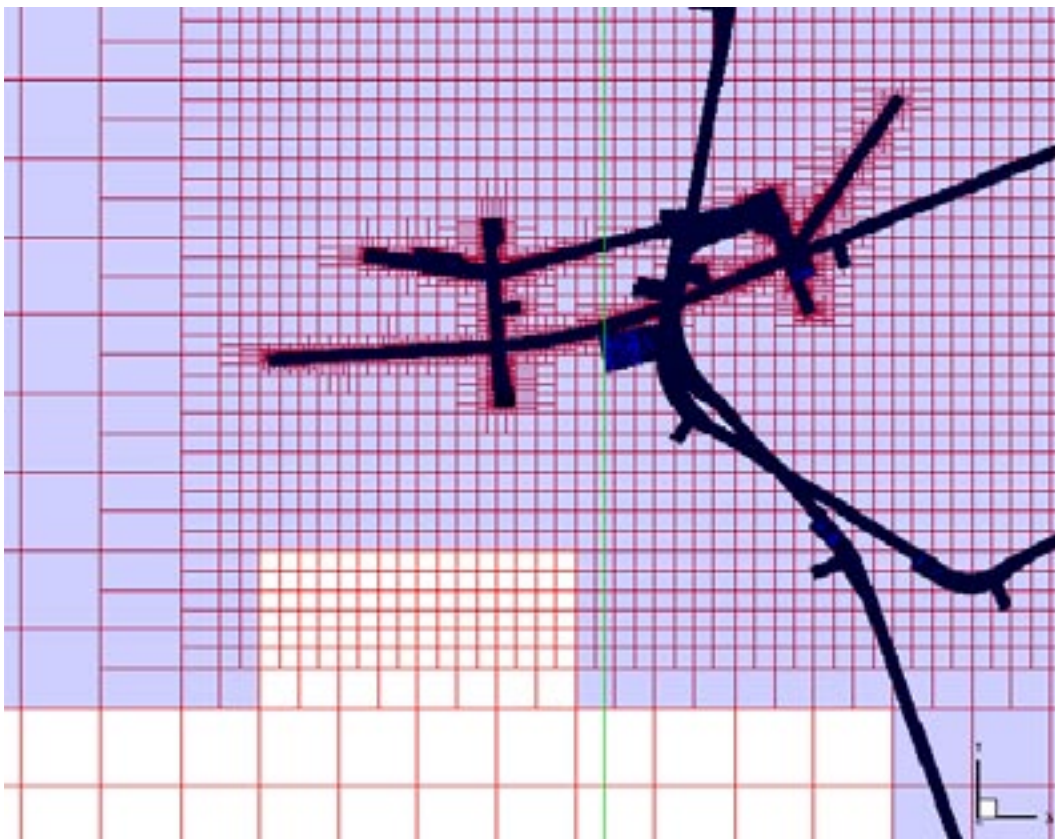

Figure F-4. *Closer details on the grid at the laboratory scale. The main cell size from left is 32 metres, 8 metres, and down to 1 metre along the tunnel.*

4   Results

Figure F-5 to Figure F-9 present the results of a steady-state situation before the tunnel is introduced. Figure F-5 illustrate the groundwater surface which is a smooth reflection of the topography, however as compared to the results from the 10,000 year simulations where the groundwater table was fixed at ground surface this steady-state situation imply a more general flow from west to east and less local flow cells in the top regions of the bedrock. Figure F-6 illustrates the pressure situation at the –450 metre elevation and the results are similar, but still smoother, as the groundwater surface situation. In Figure F-7 the distribution of salt at the –450 metre elevation is illustrated and the results show a good correlation with known recharge and discharge areas in the model domain.

The areas in Figure F-7 with the smallest salinity values match nicely with regions of recharge where the Rain water has a deep penetration also seen in Figure F-8 and Figure F-9 (Rain water). The largest salinity values in Figure F-7 are found along rivers and in the coastal areas where the discharge of water causes a small up-coning of the deeper saline waters.
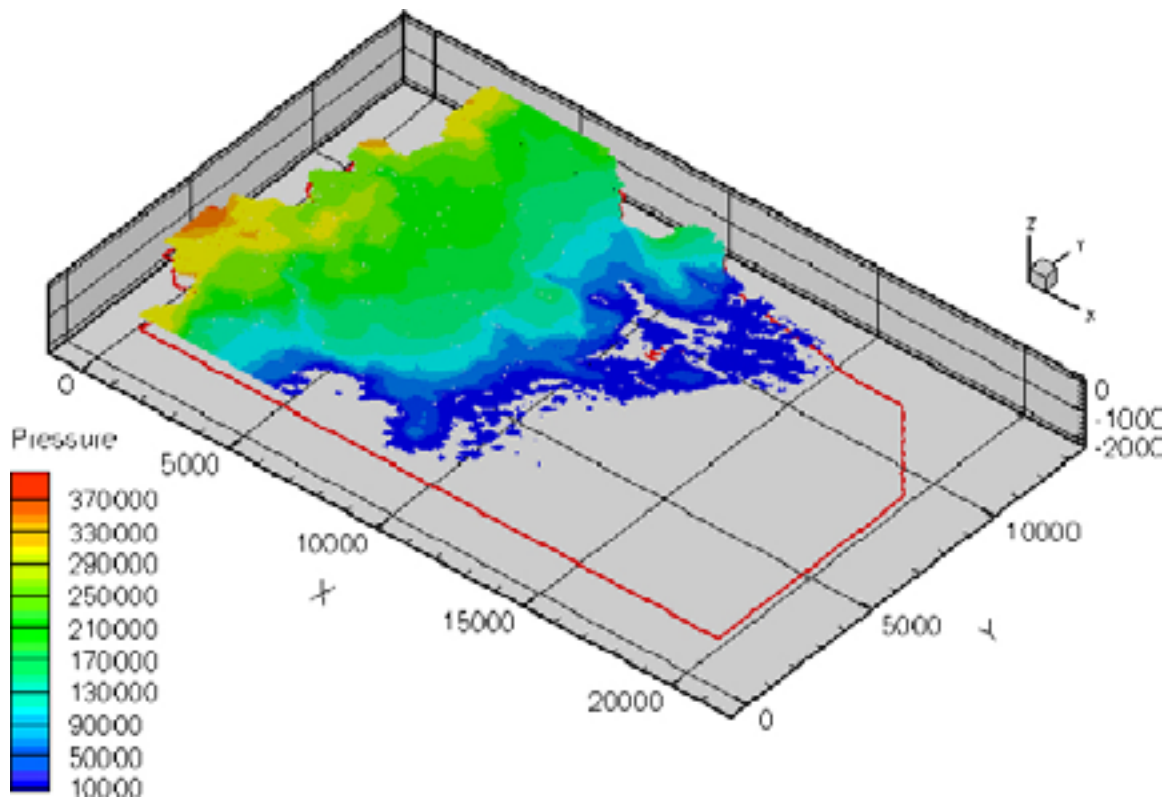
Figure F-5. *The steady-state pressure situation, in Pa, at ground surface (equal to the groundwater table) before the tunnel is introduced. A simple transformation from pressure to fresh water heads can be done by removing four zeros. The pressure result reflects the topography but also a more general west–east flow of groundwater.*
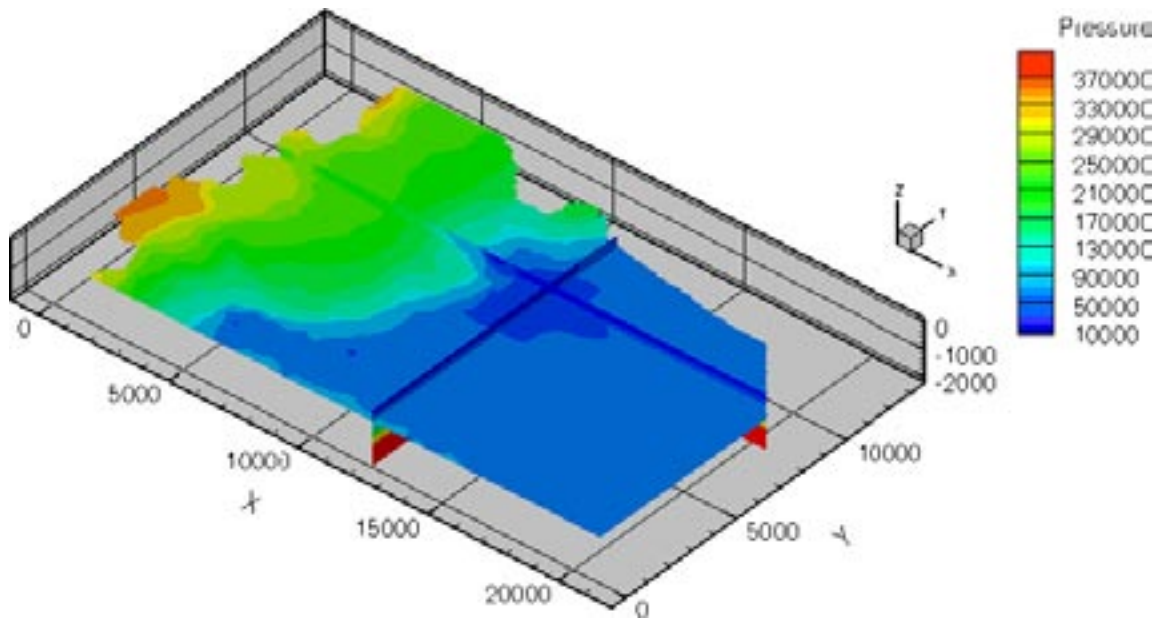
Figure F-6. *The steady-state pressure situation, in Pa, at the –450 metre elevation before the tunnel is introduced. A simple transformation from pressure to fresh water heads can be done by removing four zeros. The pressure result reflects the topography but also a more general west–east flow of groundwater. Äspö is located in the centre (crossing) of the two cross-sections.*
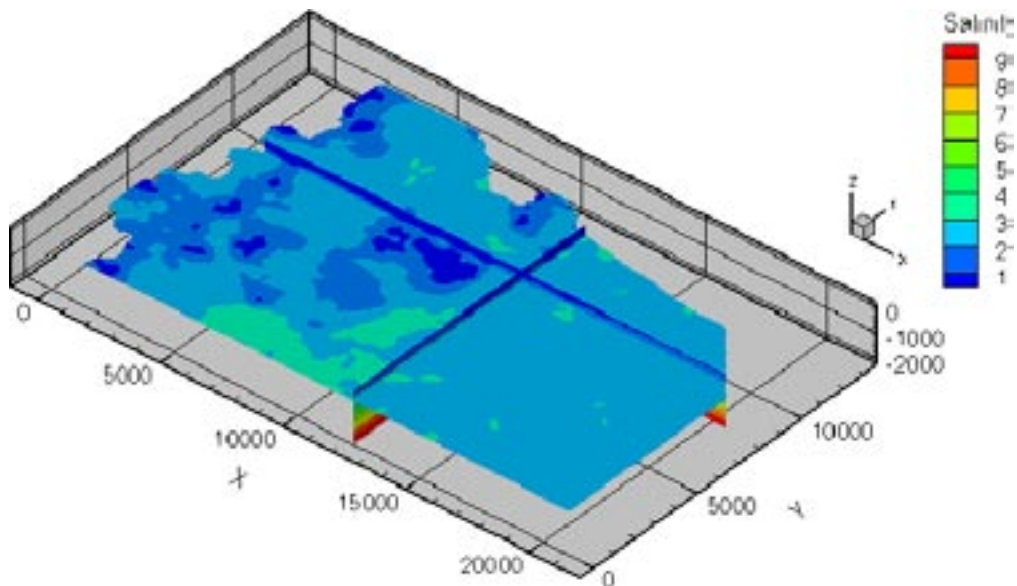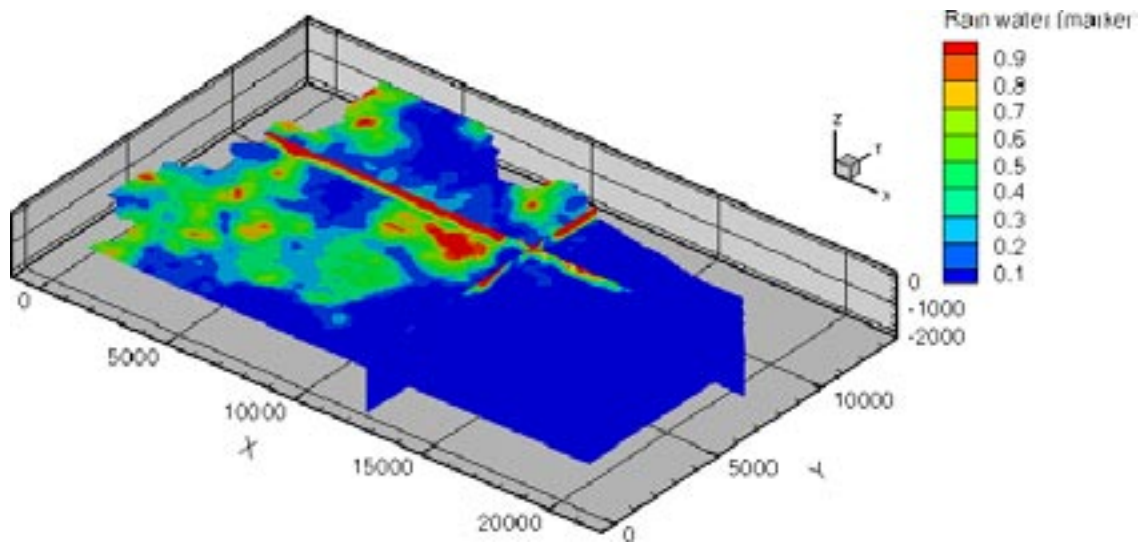

Figure F-7. *The salinity distribution at the –450 metre elevation. Low salinity values are found under recharge areas and the largest salinity values are found along rivers and in the coastal area where the discharge of water cause a small up-coning of deeper saline waters.*

Figure F-8. *Distribution of Rain water in steady-state at the –450 metre elevation before the tunnel is introduced. The results seem plausible and reflect the known information both in the archipelago and on the main land. The deeper penetration of Rain water around the location (10000;7000) represents the Laxemar region which is a bit more elevated than are the surroundings to the south, north, and east. Laxemar is both in the model and in reality a recharge area.*
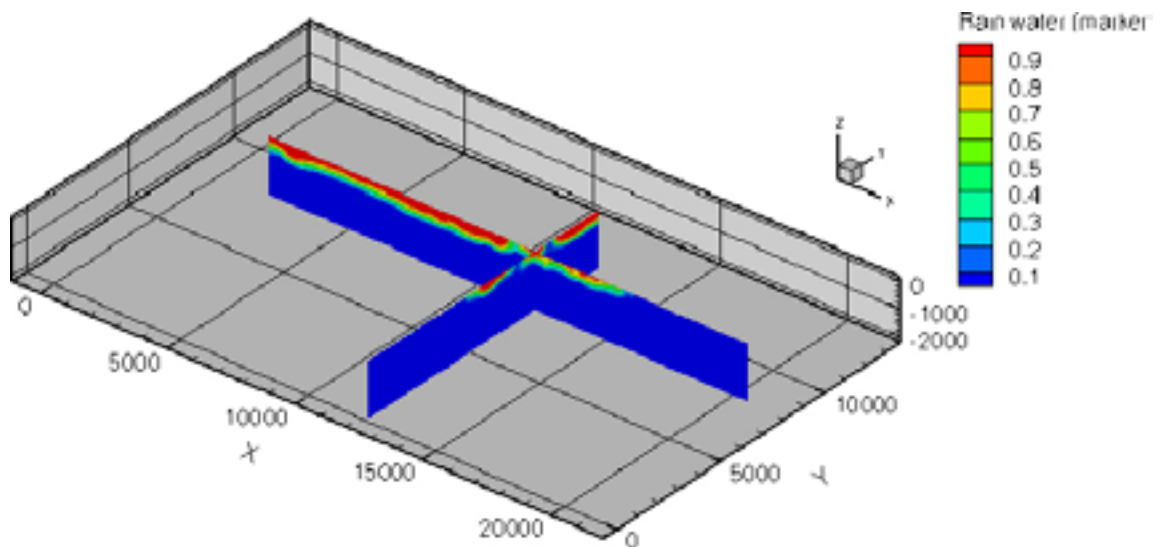

Figure F-9. *Distribution of Rain water in steady-state along two cross-sections before the tunnel is introduced. The crossing corresponds with the Äspö HRL. The results seem plausible and reflect both the archipelago and the main land. The maximum penetration of Rain water is approximately 800 metres.*

179

Figure F-10 to Figure F-20 illustrate the effect caused by the tunnel.

Figure F-10 illustrates the pressure difference at the –450 metre elevation that results when the tunnel is introduced. Except for the valley along Kärrviksån that will be discussed later, the drawdown caused by the tunnel is found below the island of Äspö, in fact most of the drawdown is within the laboratory region. Some smaller drawdown is found beneath the surrounding Baltic Sea, however the drawdown out-side Äspö is very small and may be purely due to created differences in salinity.

Figure F-11 to Figure F-13 illustrate the drawdown on different levels going up-ward. Figure F-13 show the drawdowns of the water table. The results are similar to the results presented in /Svensson 1997/.
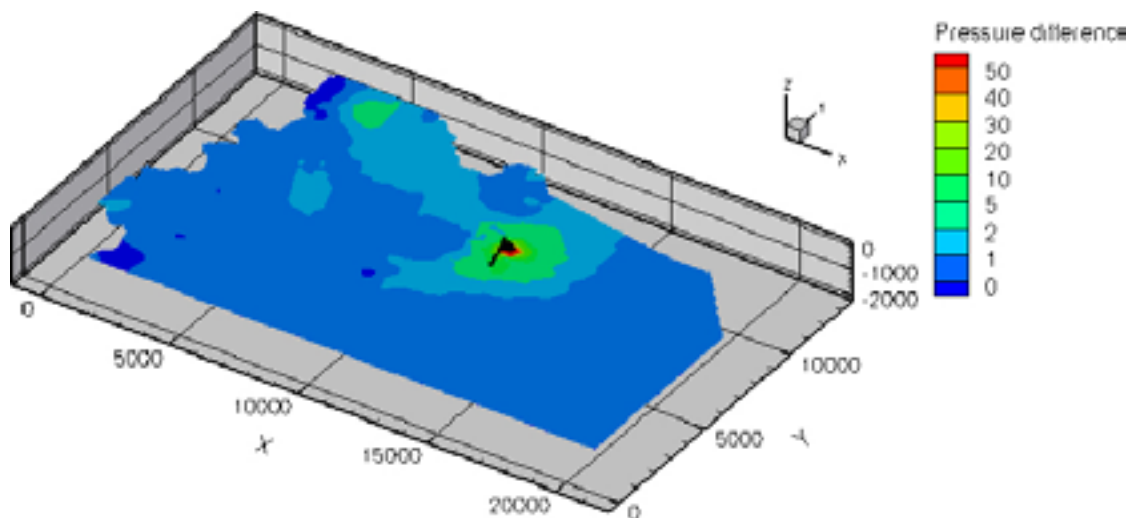

Figure F-10. *The drawdown, in metres of fresh water head, that results when the tunnel is introduced and the model is simulated to a steady-state situation. The illustrated drawdown are on the –450 metre elevation. Except for the valley along Kärrviksån that will be discussed later, the drawdown caused by the tunnel is found below Äspö, in fact the most of the drawdown is within the laboratory region.*
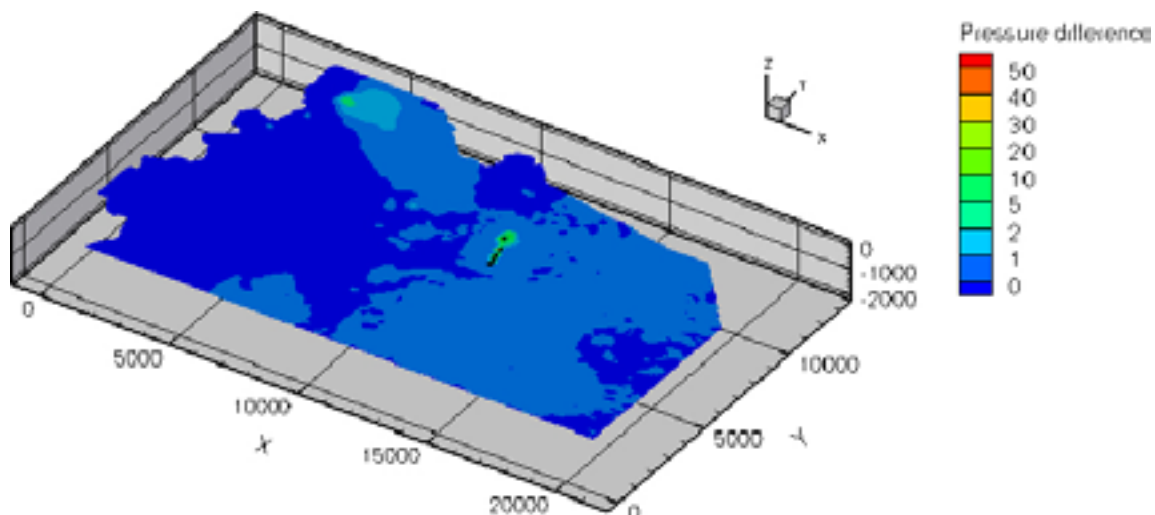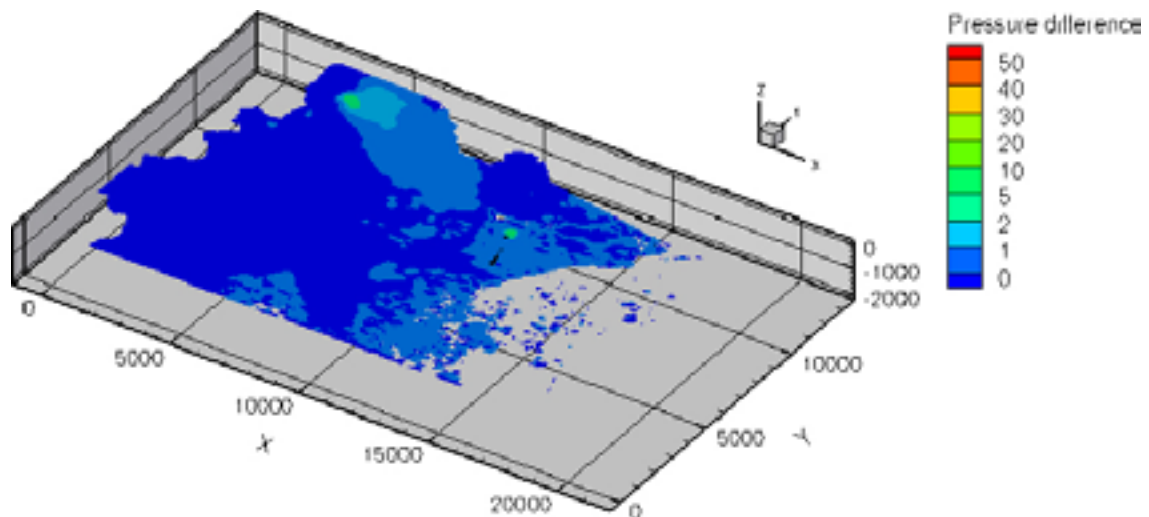

Figure F-11. *The pressure difference, in metres of fresh water head, that results when the tunnel is introduced and the model is simulated to a steady-state situation. The illustrated differences are on the –50 metre elevation. Except for the valley along Kärrviksån that will be discussed later, the drawdown caused by the tunnel is found below Äspö, in fact the most of the drawdown is within the laboratory region.*
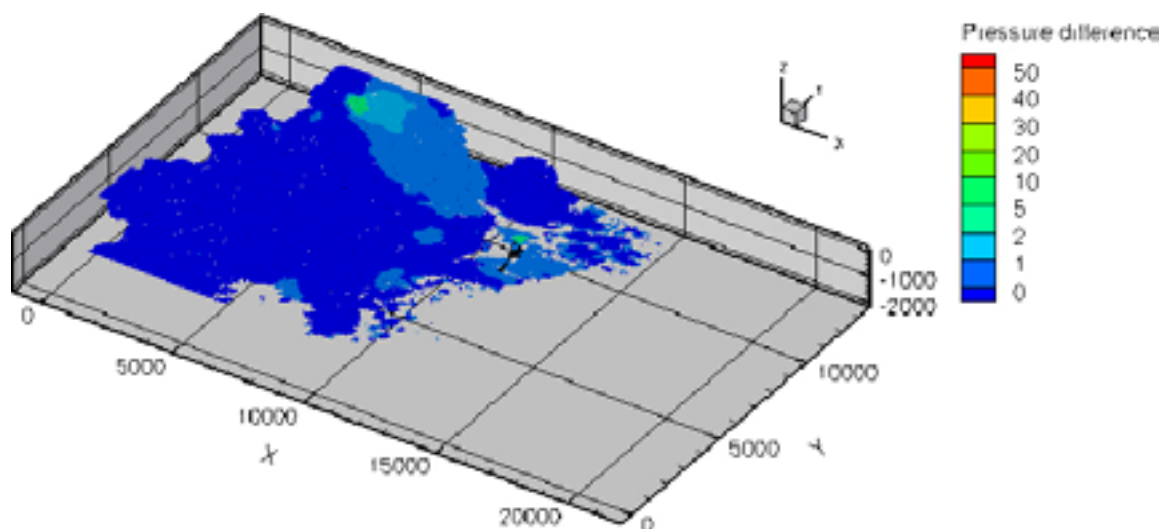
Figure F-12. The pressure difference, in metres of fresh water head, that results when the tunnel is introduced and the model is simulated to a steady-state situation. The illustrated differences are on the –10 metre elevation. Except for the valley along Kärrviksån that will be discussed later, the drawdown caused by the tunnel is found below Äspö, in fact the most of the drawdown is within the laboratory region.

Figure F-13. The pressure difference, in metres of fresh water head, that results when the tunnel is introduced and the model is simulated to a steady-state situation. The illustrated differences are at ground surface hence the illustration is of the drawdown of the groundwater table. Except for the valley along Kärrviksån that will be discussed later, the drawdown caused by the tunnel is found below Äspö and in the area of the tunnel entrance at the Simpevarp peninsula.

The small drawdown found in the northwest corner of the model domain that also connects to the drawdown at Äspö is found in the valley along Kärrviksån. Along this valley some of the hydraulic conductors defined by the Geological Structural model are located; these zones intersect with the Äspö shear zone region and hence have a direct connection with the tunnel (see Figure F-14). This result is somewhat dubious and need further testing, not least since other zones also have a direct connection with the tunnel and they do not indicate the same drawdown. A sensitivity study in which the steady-state situation was simulated for a longer time the same effects raised, hence it is believed that a stable steady-state is reached. As some sort of confirmation on this result some preliminary results of the open repository simulations within the site investigation programme yields similar results /Svensson 2006/. However, the results are not understood, and further investigations of causes are needed.
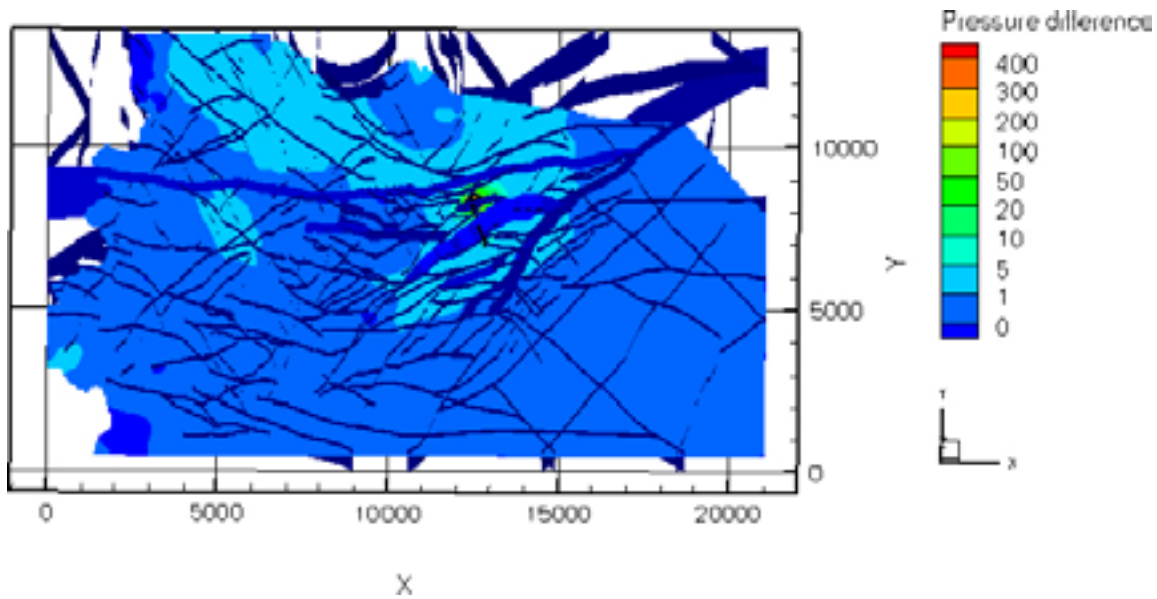
Figure F-14. The pressure difference, in metres of fresh water head, that results when the tunnel is introduced and the model is simulated to a steady-state situation. The illustrated differences are on the −450 metre elevation and the hydraulic conductors defined by the lineament model are superimposed on the figure.

In Figure F-15 the effects on the salinity is illustrated. The results show an effect in the entire land based model domain. The model pulls water from a horizontal layer as seen in Figure F-16. The effect of this selective withdrawal /e.g. Svensson 1997/ is that the recharge areas increase in size and that the local flow cells become smaller and more near-surface or disappears in all. This need more testing and a checking on amount of deep groundwater recharge could increase the understanding of this problem. The DarcyTool code has been developed and this quest is for future simulations an option of the code.
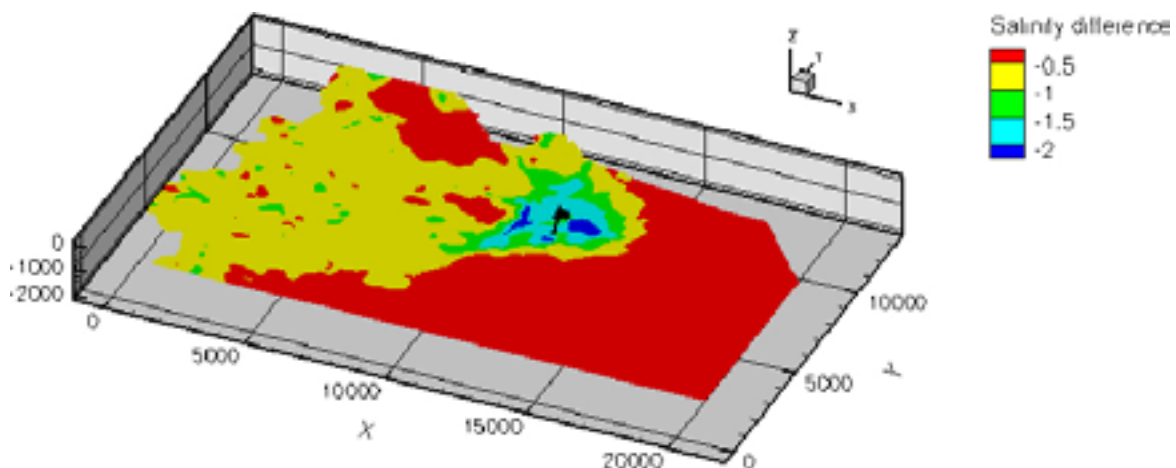

Figure F-15. The salinity difference in per cent that results when the tunnel is introduced and the model is simulated to a steady-state situation. The illustrated differences are on the −450 metre elevation. The tunnel pulls fresh water from a vast area.
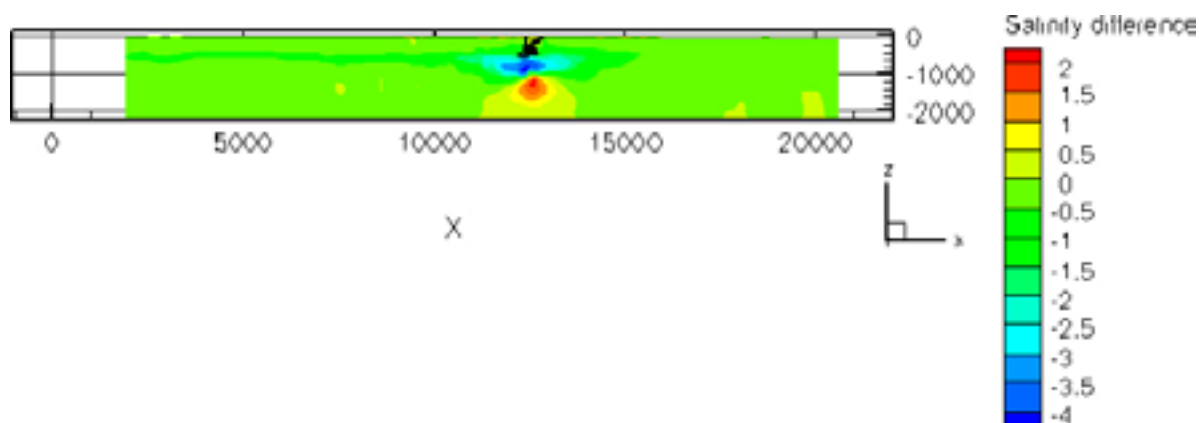
Figure F-16. The salinity difference that results when the tunnel is introduced and the model is simulated to a steady-state situation along a cross-section in the west-east. The tunnel pulls fresh water from a vast area as can be seen through the band of decreased salinity values that goes between the west boundary and the tunnel. Results such as these have been reported in /e.g. Svensson 1997/ and this Figure could be directly compared with the Figure 4-16 in the referred report.

The pressure difference on a cross-section in west-east is illustrated in Figure F-17. These results could be directly compared with the Figure 4-15 in /Svensson 1997/. The images look different but the used colour scale is somewhat different and the no change colour in /Svensson 1997/ goes from –2 to 3.5 (percentage difference). This interval incorporate all vicinity information in Figure F-17 and the main difference between our results and the results in /Svensson 1997/ is that the results presented herein include a large drawdown below the tunnel construction and that the results in /Svensson 1997/ have their largest drawdowns in the close vicinity of the tunnel. Additional differences between the two model set-ups are 1) that our model has a lower permeability towards the deeper regions than was the model in /Svensson 1997/ and 2) the model in /Svensson 1997/ was 3,000 metres deep and hence the tunnel was more distant from the bottom boundary. Further the drawdown is also expressed in fresh water heads which means that the significant change in salinity (e.g. Figure F-16) also yields additional pressure difference as seen in Figure F-17.
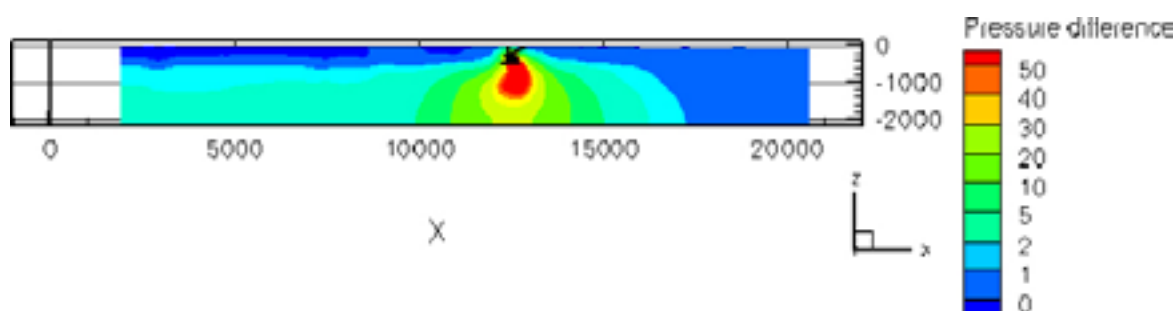

Figure F-17. The pressure difference, expressed in metres of fresh water head, that results when the tunnel is introduced and the model is simulated to a steady-state situation along a cross-section in the west-east. These results could be directly compared with the Figure 4-15 in /Svensson 1997/. The images look different but the used colour scale is somewhat different and the no change colour in /Svensson 1997/ goes from –2 to 3.5. This interval incorporate all vicinity information in Figure F-17 and the main difference between our results and the results in /Svensson 1997/ is that the results presented herein include a large drawdown below the tunnel construction and that the results in /Svensson 1997/ have their largest drawdowns in the close vicinity of the tunnel.

183

Figure F-18 to Figure F-20 show details of the pressure difference that results when the tunnel is introduced. The illustrated differences are on the –450 metre elevation with cross-sections at x-coordinate 12,300 and y-coordinate 8,000. The large drawdown is concentrated close to the tunnel construction and the pressure increases fast when moving away from the tunnel. Already some tens of metres from the tunnel wall the pressure is up with 300 metres of fresh water head.
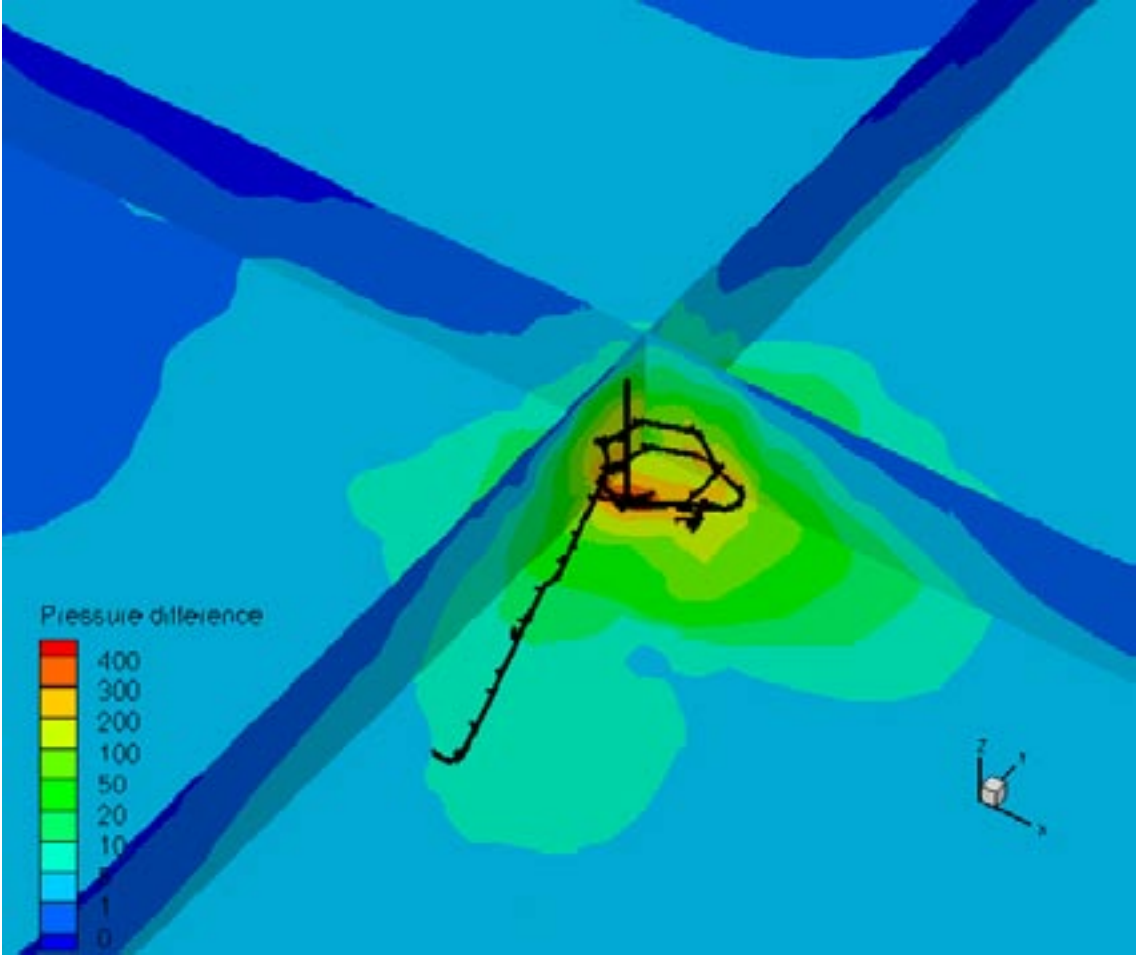

Figure F-18. Details of the pressure difference, in metres of fresh water head, that results when the tunnel is introduced and the model is simulated to a steady-state situation. The illustrated differences on the horizontal plane are on the –450 metre elevation. The large drawdown is concentrated close to the tunnel construction and the pressure increases fast when moving away from the tunnel.
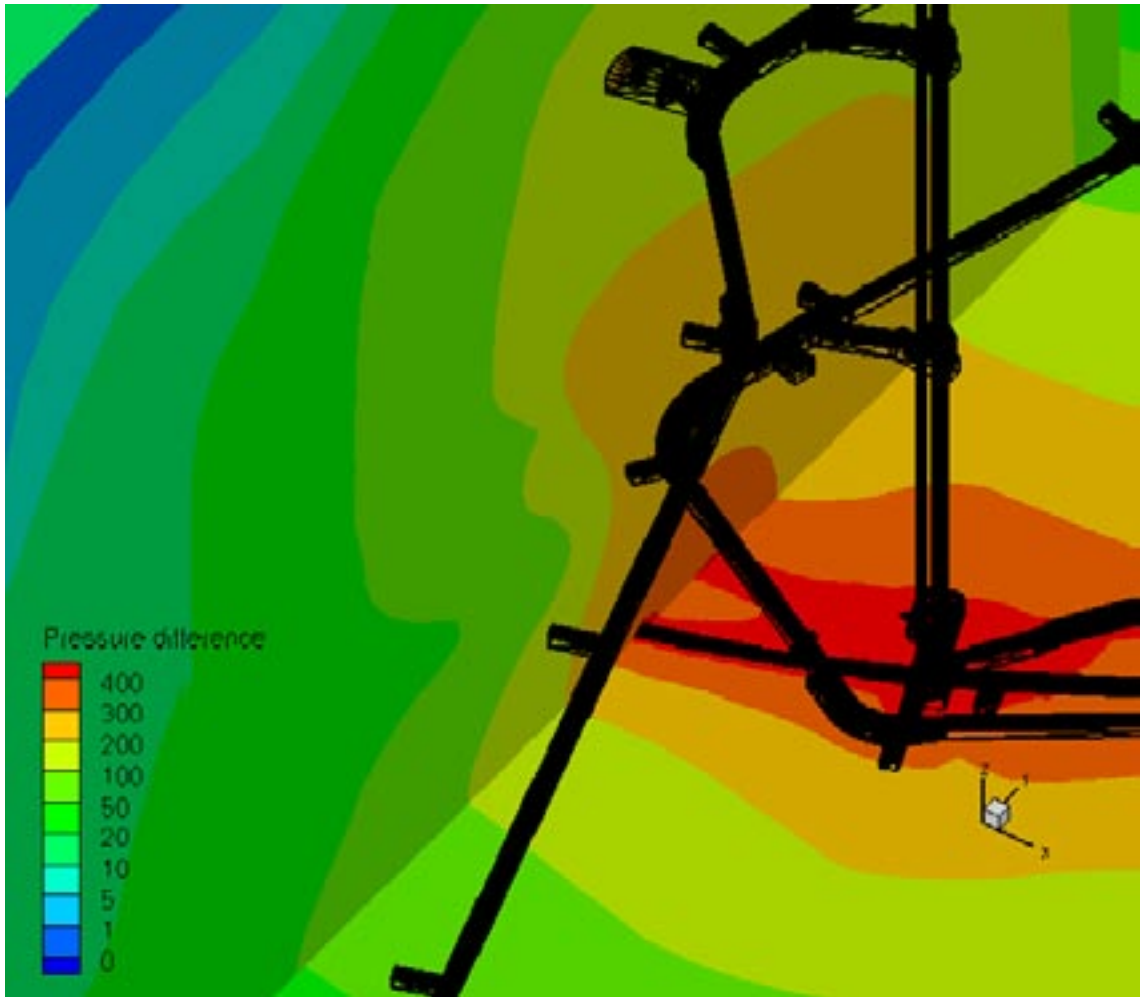
Figure F-19. *Closer details of the pressure difference, in metres of fresh water head, that results when the tunnel is introduced and the model is simulated to a steady-state situation. The illustrated differences on the horizontal plane are on the –450 metre elevation. The large drawdown is concentrated close to the tunnel construction and the pressure increases fast when moving away from the tunnel. As seen the pressure increase some 100 metres of fresh water head only in a couple of metres from the tunnel wall.*
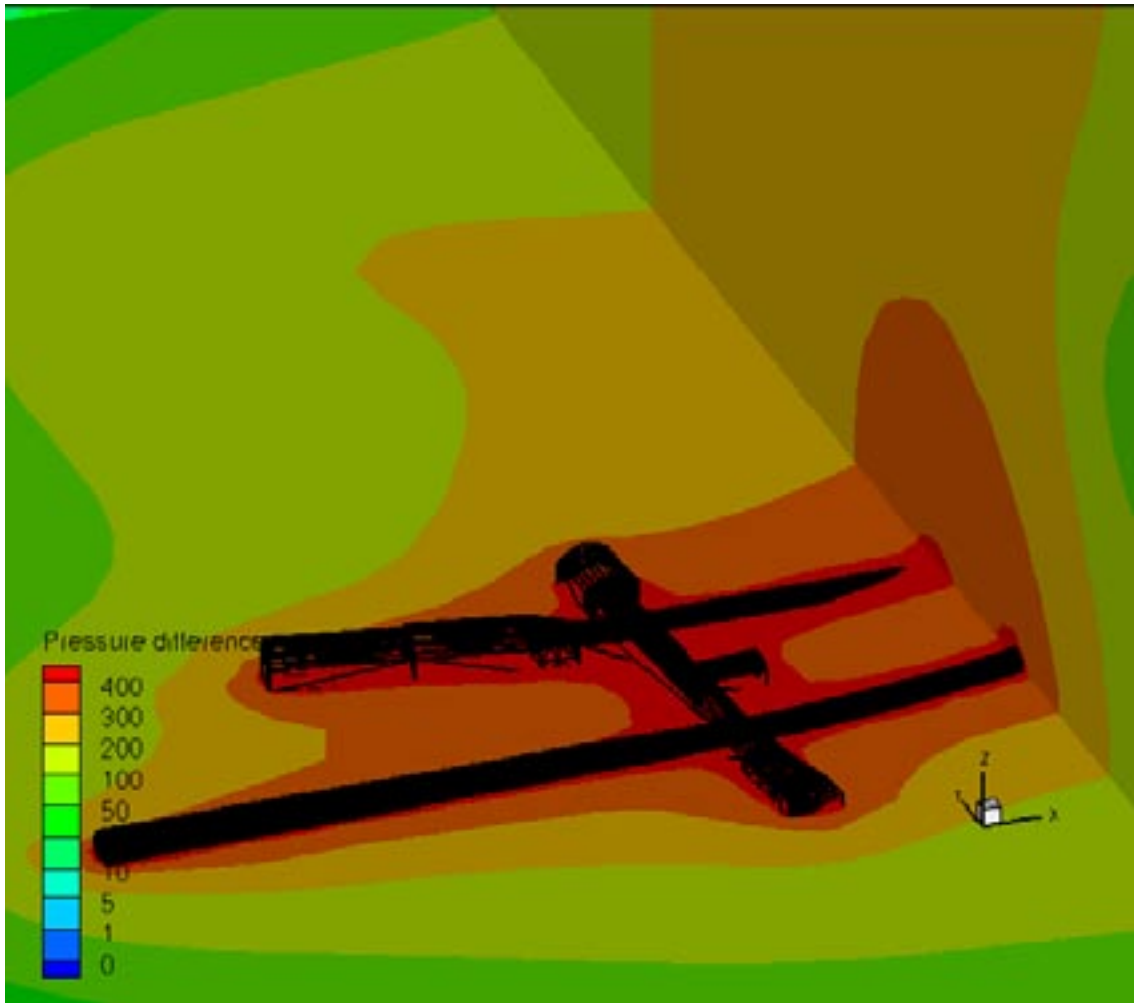
Figure F-20. *Closer details of the pressure difference that results when the tunnel is introduced and the model is simulated to a steady-state situation. The illustrated differences on the horizontal plane are on the –450 metre elevation and on the other side of the cross-section (south-north) also used in Figure F-18 and Figure F-19. The large drawdown is concentrated close to the tunnel construction and the pressure increases fast when moving away from the tunnel. As seen the pressure increases some 300 metres of fresh water head only in tens of metres from the tunnel wall.*

5 Assesment of new tunnels

As an assessment of feasibility of the DarcyTool numerical set up eight alternative positions for a new tunnel were explored by means of predictive simulations. It is essential to bear in mind that the set up of the GeoMod model and Laxemar v1.2 structural geological model is un-calibrated and head, inflows as well as some structure locations are in part erroneous (cf Section 6).

The eight tunnel positions suggested are visualised in Figure F-21. Of the eight three are of a preferred interest namely the tunnel positions denoted TASO, NASA 3384, and TASI. The results presented herein are on these three positions.

The TASO alternative tunnel position is found at an elevation of approximately –415 metres. The position is close by the large-scale structure NE1 which seems to act as a barrier for the drawdown caused by a tunnel at the TASO position. The resulting additional drawdown (Figure F-22) is therefore limited in the southern direction but elongates into the centre of the tunnel spiral within the bedrock area little affected by large geological structures. In Figure F-23 the additional drawdown from a tunnel at the TASO position is visualised at the –445 metres elevation. At this elevation the other two main alternatives are located as visualised in Figure F-24 and Figure F-25. At this deeper elevation a tunnel at the TASO position only affects the low permeable rock mass towards the centre of the tunnel spiral.

The effect of a tunnel at the NASA 3384 position seem to be limited and the pressure gradient towards the NASA 3384 position is predicted to be the greatest of the three main alternatives.

A tunnel at the TASI position is affected by the presence of a medium-scale structure at the far end of the alternative tunnel position. The inflow into the tunnel position is predicted to be by far the largest and also the geological structure affects the pressure and results in a wide-spread influence from a tunnel.
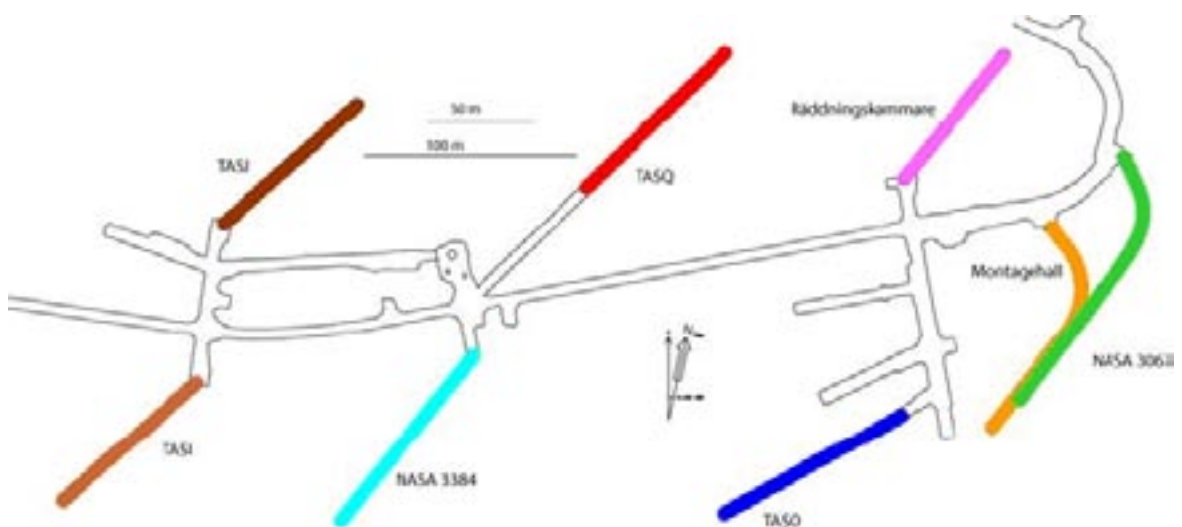

Figure F-21. *Alternative tunnel positions suggested for predictive simulations.*
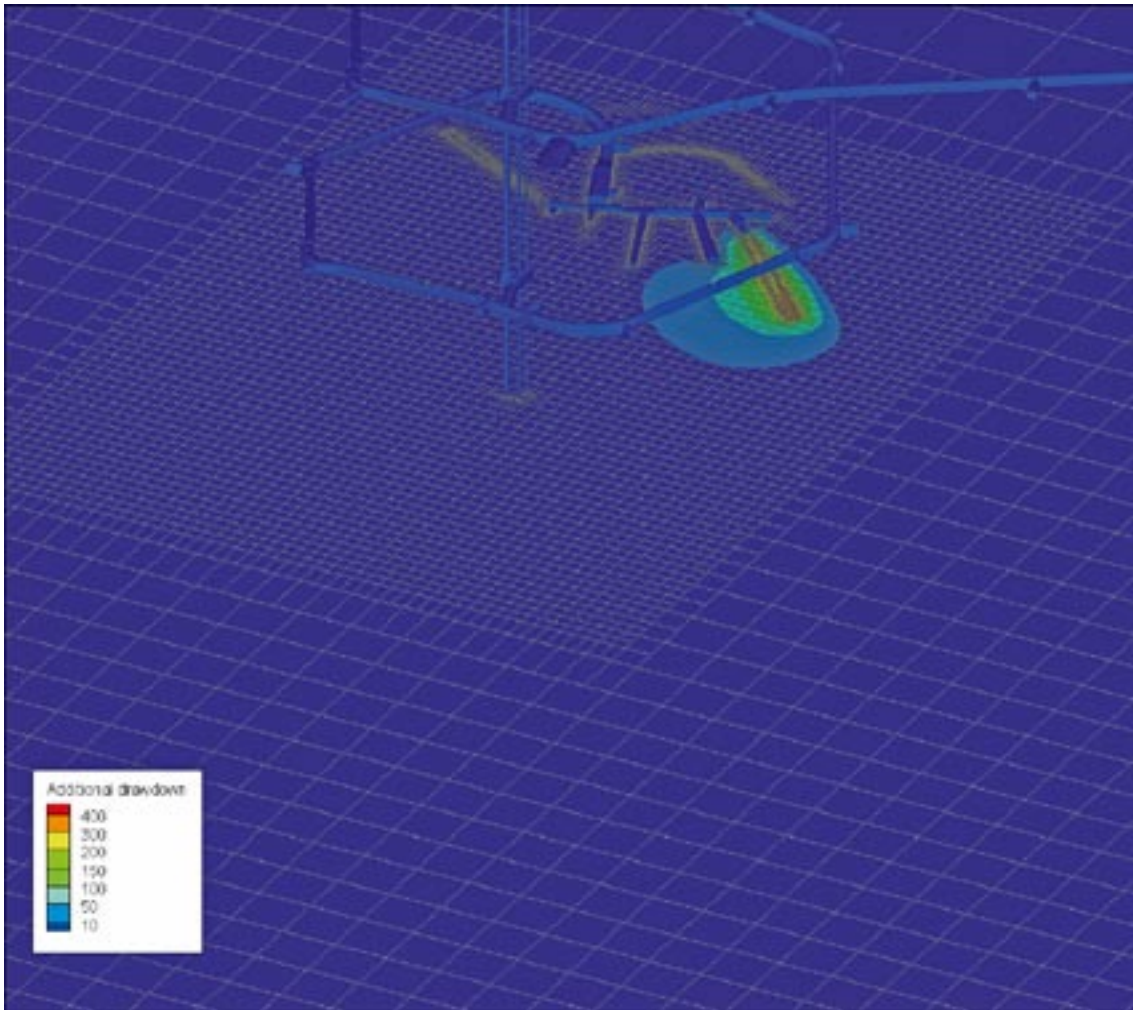
Figure F-22 The TASO alternative tunnel position viewed at the –415 metre elevation. *The additional drawdown caused by a tunnel at this location is concentrated within the rock mass between large geological structures. Towards south the NE1 seem to act as a barrier for the pressure responses.*
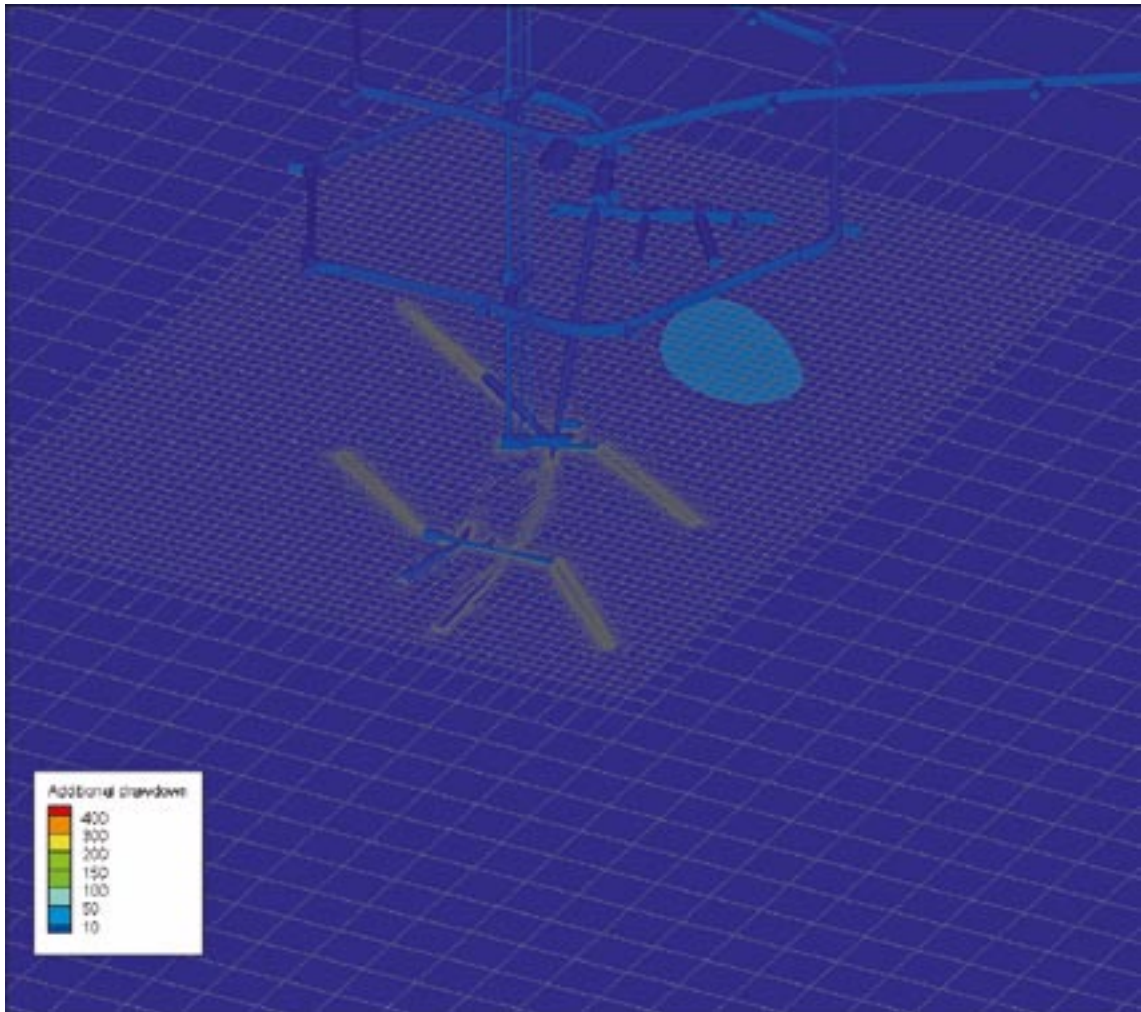
Figure F-23 The TASO alternative tunnel position viewed at the –445 metre elevation. *The additional drawdown caused by a tunnel at this location is concentrated within the rock mass between large geological structures.*
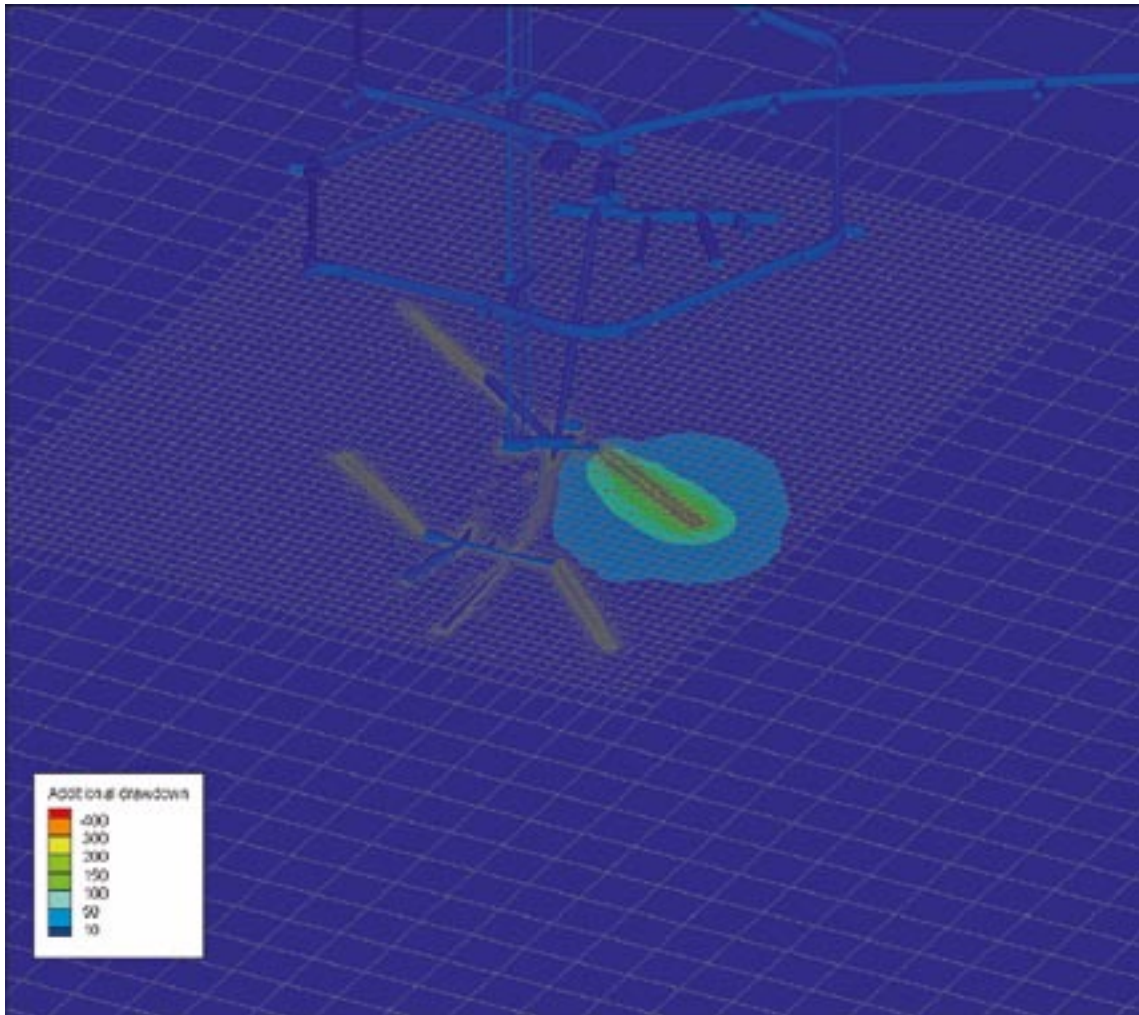
189

Figure F-24 The NASA 3384 alternative tunnel position viewed at the –445 metre elevation. *The additional drawdown caused by a tunnel at this location is concentrated within a relative localised region.*
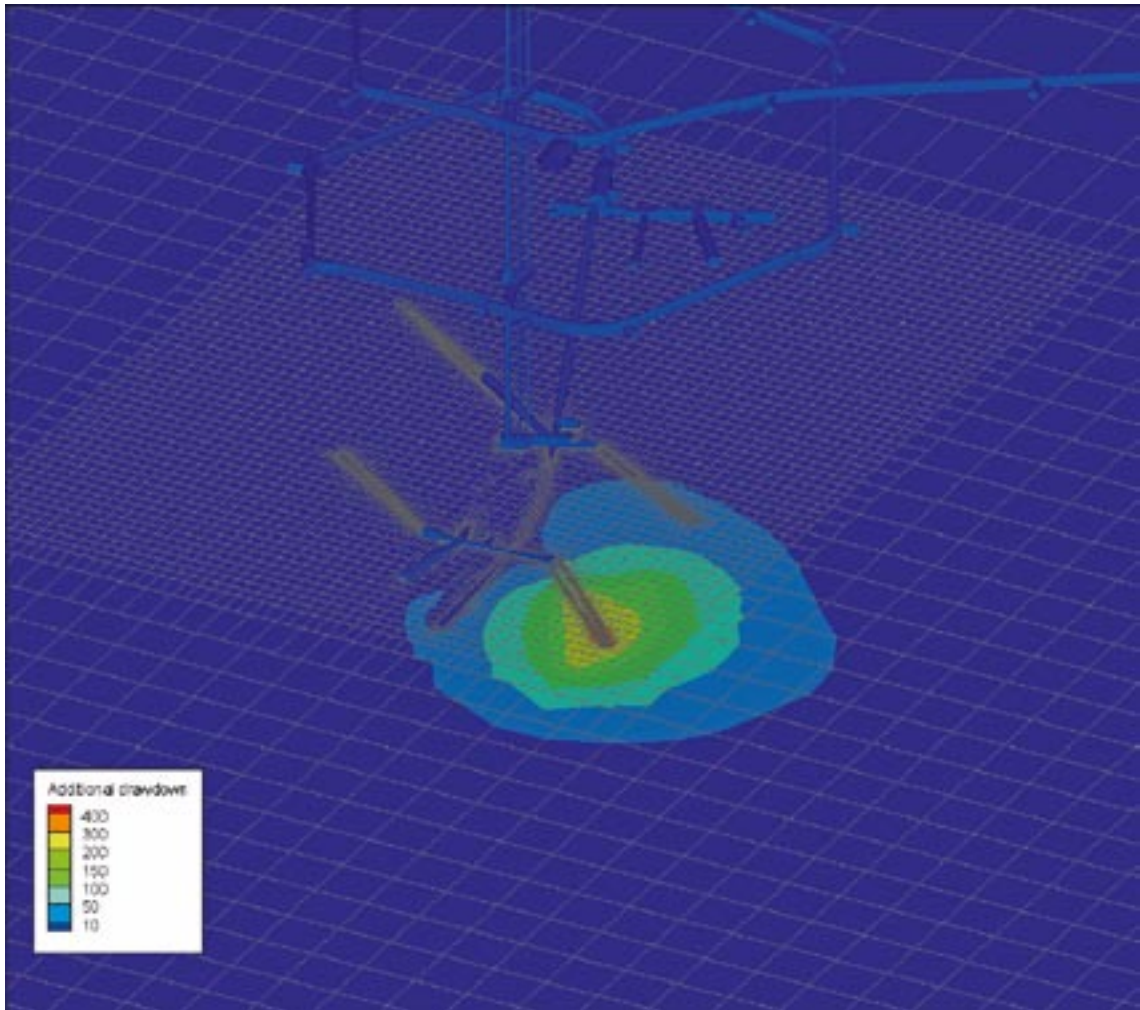
Figure F-25 The TASI alternative tunnel position viewed at the –445 metre elevation. *The additional drawdown caused by a tunnel at this location is affected by the presence of a medium-scale geological structure crossing the tunnel position about three quarters from the starting position.*

6   Discussion

A couple of sensitivity simulations have addressed the grid size. Due to the unstructured grid feature of DarcyTools v3.0 it is possible to simulate detailed cell size also within a regional model. The resolution of the Äspö site has been performed with cell size of 33 metres and smaller for the Base Case described. As one sensitivity study the cell size was decreased to 9 metres and smaller.

The sensitivity study of grid size indicates a significant influence on the results. Hence the resolution used in the Base Case is far from grid independent. This sensitivity result is in part surprising since the cell sizes of the Base Case is in agreement with most cell size criterions used in previously conducted numerical studies /e.g. Svensson 1997/. The grid size dependence is not only due to size criteria's but also affected by different properties etc.; this may be one explanation for the strong influence of grid size on the results. Since the models developed for POM have somewhat different depth dependence as compared to earlier studies of Äspö HRL.

A simple sensitivity study with assigned different depth dependence has been conducted with the result that this has a significant impact on pressure responses but also on the resulting chemistry at the site. Additional field investigations are needed along with further sensitivity studies in order to address the issues of size and depth dependence as correct as possible.

The omitting of the NNW structures from the Äspö97 model is likely to affect the inflow to the tunnel. This could most likely be dealt with through an incorporation of the known water conductive structures along the tunnel.

In addition to the large-scale structures considered in the GeoMod project /Berglund et al. 2003/ also compiled and visualised a number of medium-scale structures extracted from the Fracture Classification and Characterisation project (FCC) and the Äspö Tunnel Mapping System (TMS) database and the SICADA database. /Berglund et al. 2003/ visualised all water-bearing fractures longer than the tunnel width or five metres as narrow discs with a centre located at the tunnel centre-line. Within our work these discs have been expanded to squares with a uniform side size of 144 metres[4]. This size was chosen due to no other reason than to create a possibility to connect over the tunnel spiral. It is recommended that a more geological assessment of these fractures is conducted within the near future. Further two hydraulically active structures[5] not previously included in the hydrogeological model from the APSE tunnel were included /Staub et al. 2003/. The hydraulic conductivity of these water-bearing fractures is assigned values based on the reported probe-hole investigations /Markström and Erlström 1996/ performed during the tunnelling. The resulting transmissivity values are only briefly compared with the Äspö97 model parameterisation and found to be roughly similar.

The compilation of inflow to different tunnel segments in /Vidstrand 2003/ was compared with the out-come of the present DarcyTools simulations. In the conducted simulations only a brief calibration as regard of changed tunnel wall conductivity values has been conducted along the ramp. In Figure F-26 the omission of the NNW structures is clearly seen in the segments where DarcyTools under-predicts the inflow but also in the segments where DarcyTools over-estimates the inflow.

---

[4] Äspö_2005_Hydro (available in SIMONE)

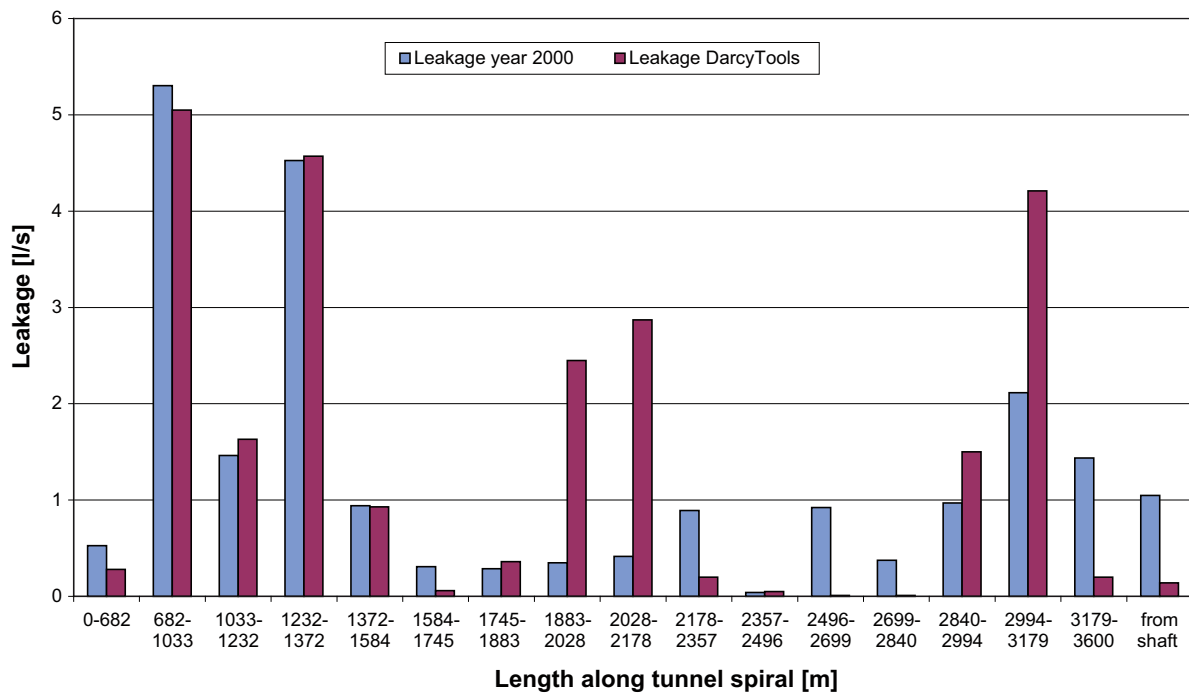[5] Apse-selected-hydro (available in SIMONE)

Figure F-26. *Comparison of measured and calculated inflow to different tunnel segment.*

In tunnel segments 1,584–1,745, 2,178–2,357, 2,496–2,699, and 2,699–2,840 fracture intersections occur that in the earlier Äspö97 model /Rhén et al. 1997/ were interpretated as hydraulic structures of En Echelons characteristics, namely NNW1, NNW2, and NNW7. Even if our numerical set up contains the fracture intersections our selected method to interconnect these fractures under-estimates the true connectivity of these structures. This fact stresses the importance of a good geological interpretation of the water-bearing fractures that crosses over the tunnel.

The leakage into the tunnel segments discussed above does also support depletion of the water pressure in the area of the tunnel spiral. The fact that the pressure in parts of our model hence is a bit too high further support the too high inflow in tunnel segments 1,883–2,028, 2,028–2,178, 2,840–2,994, and 2,994–3,179. These segments do all contain the structure NNW4 that is a well-defined structure and the conductive properties are well-known. Although some further influences on the inflow is believed to result from the connection between NNW4 and NE1 where the latter is found closer to the tunnel spiral in the Laxemar v1.2 geological structure model as compared with the Äspö97 model.

As discussed above both depth dependence and grid size affects the up-coning of Brines. However, also the assigned deterministic large-scale structures influence the up-coning. It is a measured reality that saline water enters the tunnel in the northeast corner of the tunnel spiral. At this location the tunnel is believed to intersect at least a segment of the regional structure EW1. In numerical groundwater simulations based on the Äspö97 model the result also supported a hypothesis of Brine up-coning along this structure. In our results the EW1 structure as defined in Laxemar v1.2 is too far north of the tunnel and not affected in the same manner as measurement and also earlier models suggested.

194

7   Remarks

The simulations performed represent a Base Case and in order to be fully understood some results need to be subjected to further sensitivity studies.

For example the effect of the depth-dependency needs to be further investigated. It seems that our model will pull less saline water into the tunnel construction than did the model by /Svensson 1997/. This and the relatively large pressure drop below the tunnel may be an effect of the less permeable bedrock at depth.

Many of the results are dependent on the geological models available. It is of course a fact that in hydrogeology the geology governs the properties. But here measured as well as simulations of groundwater suggest that something not presently incorporated is present at tunnel segments 1,584–1,745, 2,178–2,357, 2,496–2,699, and 2,699–2,840. The earlier Äspö97 model did incorporate a couple of En Echelon structures at these positions. If not this suggestion is supported by geology an alternative is needed in order to model the groundwater situation of Äspö HRL.

The simulation however proved to be a satisfying set-up with plausible results.

The necessary simulation time is reasonable to work with.

8 References

Berglund J, Curtis P, Eliasson T, Olsson T, Starzec P, Tullborg E-L, 2003. Äspö Hard Rock Laboratory, Update of the geological model 2002. SKB IPR-03-34, Svensk Kärnbränslehantering AB.

Laaksoharju M, Gurban I, 2003. Äspö Hard Rock Laboratory, Update of the hydrogeo-chemical model 2002. SKB IPR-03-36, Svensk Kärnbränslehantering AB.

Markström I, Erlström M, 1996. Overview of documentation of tunnel, niches and core boreholes. SKB Progress Report HRL-96-19, Svensk Kärnbränslehantering AB.

Rhén I, Gustafsson G, Stanfors R, Wikberg P, 1997. Äspö HRL – Geoscientific evaluation 1997/5. Models based on site characterization 1986-1995. SKB TR 97-06, Svensk Kärnbränslehantering AB.

SKB 2006. Preliminary site description. Laxemar subarea version 1.2. SKB R-06-10, Svensk Kärnbränslehantering AB.

Staub I, Jansson T, Fredriksson A, 2003. Äspö Pillar Stability Experiment, Geology and properties of the rock mass around the experiment volume. SKB IPR-03-02, Svensk Kärnbränslehantering AB.

Svensson U, 1997. A regional analysis of groundwater and salinity distribution in the Äspö area. SKB TR-97-09, Svensk Kärnbränslehantering AB.

Svensson U, 2006. The Laxemar repository Modelling changes in the flow, pressure and salinity fields, due to a repository for spent nuclear fuel. SKB R-06-57, Svensk Kärnbränslehantering AB.

Vidstrand P, 2003. Äspö Hard Rock Laboratory, Update of the hydrogeological model 2002. SKB IPR-03-35, Svensk Kärnbränslehantering AB.